EFFECTS OF NUCLEAR RADIATION ON THE OPTICAL PROPERTIES OF Al_2O_3+SiO_2 MIRRORS IN THE ULTRAVIOLET REGION

by

GARY WAYNE SCRONCE

B.S., Kansas State University, 1984

A MASTER'S THESIS

submitted in partial fulfillment of the

requirements for the degree

MASTER OF SCIENCE

Department of Nuclear Engineering

KANSAS STATE UNIVERSITY
Manhattan, Kansas

1987

Approved by:

Hermann Domert

Major Professor

Table of Contents

List of Figures

List of Tables

1. INTRODUCTION

With the onset of the Strategic Defense Initiative, in the scope of defensive laser systems, the need to know the effects of various types of nuclear radiation on laser optical components is becoming of great importance. Knowledge of damage thresholds must be obtained if laser systems are to be designed which will survive the potentially hazardous radiation environments which may be encountered in anti-missile defense applications. An understanding of the damage mechanisms and damage thresholds, for particular optical components, may also prove to be of importance in laser fusion systems.

In the short term, a quantitative understanding is certainly needed, so that sufficient protection for vulnerable optical components may be provided. If these components fail, the entire laser system fails. In addition to the fact that a component failure will render the system inoperable, repair and/or replacement costs warrant sufficient protection against this failure. In the long term, a qualitative understanding of the damage mechanisms may provide the means to design components with an inherently high damage threshold, thus eliminating a weak link in the system.

From solid-state physics, it is known that the absorption of nuclear radiation in a solid, and the subsequent charged particles released in this absorption, can cause a variety of defects. These defects can affect various physical properties of the solid

material, such as electrical conductivity and optical absorptance. Clearly, it is realized that ionizing radiation will cause defects in a solid material. The question is whether or not the magnitude of the damage for a given dose and dose rate is sufficient to cause an optical component to fail.

Some previous work in this area has been done by various authors. Included are: Dr. Hermann J. Donnert,[1] Mark Ferrel,[2] and Kevin Zook at FJSRL, and researchers at Sandia National Laboratories. However, this work has been done for particular optical materials and thus cannot be readily used to infer the effects of different types of nuclear radiation on other such materials. For the time being, until sufficient data have been gathered to allow a broad theoretical, or empirical model to be formed, the effects of these irradiations must be explored on an individual basis.

The purpose of this particular research can be divided into several parts:

1) To determine, experimentally, the optical properties of the three different kinds of mirrors to be investigated in their virgin state. These are: Al_2O_3+SiO_2 multilayer dielectrics, thin-layer aluminum, and double-layered with Ag on top of a Cu layer.

2) To develop, where possible, theoretical models describing the ideal variation of the mirrors' optical properties with wavelength. Thus may the design of the mirror be compared to the properties actually imparted to the mirrors in their construction.

3) To irradiate the mirrors with ionizing radiation, in this case high-energy electrons to simulate the effect of gamma radiation, varing the doses and dose rates. After a period of time, the optical properties of the mirrors were to be measured again and compared with the original ones to determine the extent of any damage.

4) To determine statistically the dose or dose rate dependence of any damage imparted to the mirrors.

2. THEORY

2.1 Definition of Terms

Before entering into a more in depth discussion of the material involved in this study, a definition of the terms involved may help the reader to better understand the work to be shown later.

Index of refraction (n): Simply put, it is defined as the ratio of the speed of an electromagnetic wave in a vacuum to that in matter. For dielectrics, n is a real constant. For metallics, n is often a complex quantity and must be dealt with accordingly.

Transmittance (T): The ratio of the intensity of light transmitted through an interface to that of the light incident on the interface. Since intensity is a real variable, so too is the transmittance. Also termed as *transmission* in this report, not to be confused with the transmission coefficient (t).

Reflectance (R): The ratio of the intensity of light reflected at a material interface to that of the light incident on the interface. R must also be a real quantity. In this text, R is also referred to as the reflectivity.

Absorptance (A): The ratio of the intensity of light absorbed in an optical component to that of the light incident upon it. In an undamaged transparent dielectric medium, the absorptance is theoretically zero for all wavelengths.

Dielectric Material: In this context a dielectric material is one in which the electrical conductivity of the material is effectively zero as far as Maxwell's equations are concerned.

2.2 Dielectric Multilayer Mirror Theory

Before any other analysis dealing with the optical characteristics of the mirrors could be made, it was first necessary that those characteristics were known for a mirror in its 'virgin' state. The optical properties of primary importance in this study were the reflectivity and transmission (or transmissivity) as they varied with the wavelength of the incident light.

Using these two properties, one can also infer the absorption profile for the mirrors. This is allowed through the use of a simple relation;

$$R + T + A = 1 \ , \qquad (2.1)$$

where R = Reflectivity of device,

T = Transmissivity, and

A = Absorption.

Assuming that the mirrors are to be used in a high-energy laser system, a small change in the fraction of incident light absorbed by the mirror could be of critical importance concerning the survival of the mirror. Thus, having no direct means available to measure the absorptance of the mirrors, it becomes important that the reflectivity and transmission are known.

To insure that the measured reflectivity and transmission profiles for the mirrors, specifically the dielectric mirrors, were in accordance with the parameters used in their design, a theoretical model was developed which would generate these profiles.

The main reference used to aid in constructing this model was Born and Wolf.[3] The basic differential equations governing the behavior of electromagnetic waves in different media are Maxwell's equations. These equations can be found in a variety of texts including Born and Wolf. For our purposes there are some simplifying assumptions that were made with relation to Maxwell's equations that makes the problem easier to solve.

The assumptions that are made in this case are as follows:

1) The plane of incidence is the yz-plane. Therefore the z-direction is the direction in which the mirrors are layered.

2) The incoming electromagnetic wave is linearly polarized with it's electric field vector perpendicular to the plane of incidence, i.e. we will deal with a "tranverse electric wave", thus $E_y = E_z = 0$.

3) All media the wave travels through will be non-magnetic. Using these assumptions, Maxwell's equations reduce to six scalar equations.

$$\frac{\partial H_z}{\partial y} - \frac{\partial H_y}{\partial z} + \frac{i\epsilon\omega}{c} E_x = 0, \tag{2.2}$$

$$\frac{i\omega\mu}{c} H_x = 0, \tag{2.3}$$

$$\frac{\partial H_x}{\partial z} - \frac{\partial H_x}{\partial x} = 0, \tag{2.4}$$

$$\frac{\partial E_x}{\partial z} - \frac{i\omega\mu}{c} H_y = 0, \tag{2.5}$$

$$\frac{\partial H_y}{\partial x} - \frac{\partial H_x}{\partial y} = 0, \tag{2.6}$$

$$\frac{\partial E_x}{\partial y} + \frac{i\omega\mu}{c} H_z = 0. \tag{2.7}$$

where E_x = the x-component of the electric field vector,

H_j = the j-component of magnetizing force vector,

ϵ = the material dependent dielectric constant,

μ = the material dependent magnetic permeability,

and c = speed of light.

We will not endeavor to go through all the in between steps here, but Born and Wolf will provide a more thorough derivation for the interested reader. Through a series of manipulations, one arrives at a pair of simultaneous 1st-order linear differential equations for U and V where $E_x = U(z)\, e^{i(k_o \alpha y - \omega t)}$ and $H_y = V(z)\, e^{i(k_o \alpha y - \omega t)}$. These relations are,

$$\left.\begin{aligned} U' &= ik_o \mu V, \text{ and} \\ V' &= ik_o \left[\epsilon - \frac{\alpha^2}{\mu}\right] U \end{aligned}\right\} \tag{2.8}$$

Elimination between these two equations leads to the following coupled second-order linear differential equations for U and V:

$$\left.\begin{aligned} &\frac{d^2U}{dz^2} - \frac{d(\log\mu)}{dz}\frac{dU}{dz} + k_o^2(n^2-\alpha^2)U = 0 \ , \\ &\\ &\frac{d^2V}{dz^2} - \frac{d[\log(\epsilon - \frac{\alpha^2}{\mu})]}{dz}\frac{dV}{dz} + k_o^2(n^2-\alpha^2)V = 0 \end{aligned}\right\} \quad (2.9)$$

where $$n = \sqrt{\epsilon\mu} \ , \quad (2.10)$$

$$k_o = \frac{\omega}{c} = \frac{2\pi}{\lambda_o} \quad (2.11)$$

For a single homogeneous dielectric film, ϵ, μ, and $n = \sqrt{\epsilon\mu}$ are constants for a given λ_o. Letting θ denote the angle that the incident light makes with the z-axis, we may state that,

$$\alpha = n \sin\theta \quad (2.12)$$

From (2.9),we find the following relations now hold,

$$\left.\begin{aligned} &\frac{d^2U}{dz^2} + (k_o^2 n^2 \cos^2\theta)U=0, \\ &\\ &\frac{d^2V}{dz^2} + (k_o^2 n^2 \cos^2\theta)V = 0 \ . \end{aligned}\right\} \quad (2.13)$$

The solutions to these relations must hold to those from (2.8) and are found to be

$$\left.\begin{aligned} U(z) &= A\cos(k_o nz\cos\theta) + B\sin(k_o nz\cos\theta) \\ V(z) &= \frac{1}{i}\sqrt{\frac{\epsilon}{\mu}}\cos\theta\,\{B\cos(k_o nz\cos\theta) - A\sin(k_o nz\cos\theta)\} \end{aligned}\right\} \quad (2.14)$$

Since U(z) and V(z) are solutions which each satisfy a second-order linear differential equation, U and V may be expressed as a linear combination of two particular solutions, U_1, U_2 and V_1, V_2. Choosing particular solutions in this case, it is easiest to use the following forms

$$\left.\begin{aligned} U_1 &= f(z), \quad U_2 = F(z), \\ V_1 &= g(z), \quad V_2 = G(z), \end{aligned}\right\} \quad (2.15)$$

such that $f(\theta) = G(\theta) = 0$ and $F(0) = g(0) = 1$. (2.16)

Thus applying (2.8) to U(z) and V(z), the particular solutions (2.15) that satisfy the boundary conditions (2.16) are

$$\left.\begin{aligned} U_1 &= f(z) = \frac{i}{\cos\theta}\sqrt{\frac{\mu}{\epsilon}}\sin(k_o nz\cos\theta), \\ V_1 &= g(z) = \cos(k_o nz\cos\theta), \\ U_2 &= F(z) = \cos(k_o nz\cos\theta), \\ V_2 &= G(z) = i\cos\theta\sqrt{\frac{\epsilon}{\mu}}\sin(k_o nz\cos\theta). \end{aligned}\right\} \quad (2.17)$$

If we now take into account that the media of interest are non-magnetic ($\mu \approx 1$) and let h equal the thickness in the z-direction of the dielectric film in question, the "characteristic matrix" of an arbitrary dielectric film may be written as

$$\underline{M}(h) = \begin{bmatrix} m_{11} & m_{12} \\ m_{21} & m_{22} \end{bmatrix} = \begin{bmatrix} \cos\beta_j & -\frac{i}{p_j}\sin\beta_j \\ -ip_j \sin\beta_j & \cos\beta_j \end{bmatrix} , \tag{2.18}$$

where $$\beta_j = \frac{2\pi}{\lambda_o} n_j h_j \cos\theta_j , \tag{2.19}$$

$$p_j = n_j \cos\theta_j , \tag{2.20}$$

$$n = \sqrt{\epsilon} .$$

This is of course the characteristic matrix for only one film, but we may now look to expand this concept to a multilayer dielectric medium. Figure 2.1 illustrates the manner in which the mirrors in this study were constructed. The major portion of the mirror is made up of a periodic structure where a high index of refraction - low index pair is repeated 24 times. Due to that periodicity, we may construct a characteritic matrix that represents the behavior of the entire stack by multiplying the matrices representing each layer in the proper order by using the following relation:

$$\underline{M}(z_N) = \underline{M}_1(z_1)\, \underline{M}_2(z_2 - z_1) \cdots\cdots \underline{M}_N(z_N - z_{N-1}) , \tag{2.21}$$

where z_1 is the thickness of media nearest the point of incidence.

For our case, we will start with the periodic part of the stack and work up from that. From (2.18) and Fig. 2.1, the characteristic matrix for an individual H-layer is given as,

$$\underline{M}_H(h_H) = \begin{bmatrix} \cos\beta_H & -\sin\beta_H/p_H \\ -ip_H\sin\beta_H & \cos\beta_H \end{bmatrix} \tag{2.22}$$

where $$\beta_H = \frac{2\pi}{\lambda_o} n_H h_H \cos\theta_3, \text{ and} \tag{2.23}$$

$$p_H = n_H\cos\theta_3 \ . \tag{2.24}$$

Similarly, the matrix for an individual L-layer is

$$\underline{M}_L(h_L) = \begin{bmatrix} \cos\beta_L & -\sin\beta_L/p_L \\ -ip_L\sin\beta_L & \cos\beta_L \end{bmatrix} \tag{2.25}$$

where $$\beta_L = \frac{2\pi}{\lambda_o} n_L h_L \cos\theta_2, \text{ and} \tag{2.26}$$

$$p_L = n_L\cos\theta_2 \ . \tag{2.27}$$

Making use of (2.21), the matrix for one HL-layer, the L being closest to the incident light, is written as,

$$\underline{M}_{HL}(h) = \begin{bmatrix} m_{11} & im_{12} \\ im_{21} & m_{22} \end{bmatrix} = \underline{M}_L(h_L)\cdot\underline{M}_H(h_H) \ , \tag{2.28}$$

where $h = h_L + h_H$. (2.29)

For the total periodic stack, repeated 24 times, we get the characteristic matrix by multiplying (2.28) by itself 24 times in accordance with (2.21).

$$\underline{M}_{\text{periodic}}(Nh) = (\underline{M}_{HL}(h))^{N}. \tag{2.30}$$

From the theory of matrices, it can be shown that the N^{th} power of a 2 x 2 matrix can be written using Chebyshev Polynomials from a proof by ABELÈS to be:

$$\begin{bmatrix} m_{11} & im_{12} \\ im_{21} & m_{22} \end{bmatrix}^{N} = \begin{bmatrix} m_{11}U_{N-1}(a) - U_{N-2}(a) & im_{12}U_{N-1}(a) \\ im_{21}U_{N-1}(a) & m_{22}U_{N-1}(a) - U_{N-2}(a) \end{bmatrix} , \tag{2.31}$$

where $a = \frac{1}{2}(m_{11} + m_{22})$, and (2.32)

U_N = Chebyshev Polynomials of the second kind.

The values of these polynomials are easy to find once "a" is known. One simply uses the explicit expression for the first two polynomials,[4]

$$U_o(a) = 1 \quad , \tag{2.33}$$

$$U_1(a) = 2a \quad , \tag{2.34}$$

along with the recurrence relation for these polynomials,

$$U_j(a) = 2aU_{j-1}(a) - U_{j-2}(a) \quad . \tag{2.35}$$

With all of this in mind, the characteristic matrix for the periodic stack may be written explicitly:

$$\underline{M}_{periodic}(Nh) = \begin{bmatrix} M_{11} & iM_{12} \\ iM_{21} & M_{22} \end{bmatrix} \tag{2.36}$$

where,

$$\left.\begin{aligned} M_{11} &= [\cos\beta_L\cos\beta_H - \frac{p_H}{p_L}\sin\beta_L\sin\beta_H]\, U_{N-1}(a) - U_{N-2}(a) \,. \\ M_{12} &= -[\frac{1}{p_H}\cos\beta_L\sin\beta_H + \frac{1}{p_L}\sin\beta_L\cos\beta_H]U_{N-1}(a) \,. \\ M_{21} &= -[p_L\sin\beta_L\cos\beta_H + p_3\cos\beta_L\sin\beta_H]\, U_{N-1}(a) \,. \\ M_{22} &= [\cos\beta_L\cos\beta_H - \frac{p_L}{p_H}\sin\beta_L\sin\beta_H]\, U_{N-1}(a) - U_{N-2}(a) \,. \end{aligned}\right\} \tag{2.37}$$

and $$a = \cos\beta_L\cos\beta_H - \frac{1}{2}\left[\frac{p_L}{p_H} + \frac{p_H}{p_L}\right]\sin\beta_L\sin\beta_H \,. \tag{2.38}$$

The reflection and transmission coefficients for the stack could now be computed by the following relations,

$$r = \frac{(M_{11} + iM_{12}p_\ell)p_1 - (iM_{21} + M_{22}p_\ell)}{(M_{11} + iM_{12}p_\ell)p_1 + (iM_{21} + M_{22}p_\ell)}, \tag{2.39}$$

$$t = \frac{2p_1}{(M_{11} + iM_{12}p^\ell)p_1 + (iM_{21} + M_{22}p^\ell)} \,. \tag{2.40}$$

Using the reflection and transmission coefficients, the <u>reflectivity</u> and <u>transmissivity</u> may be calculated,

$$\mathcal{R} = |r|^2 \ , \ \mathcal{T} = \frac{p_\ell}{p_1}|t|^2 \ . \qquad (2.41)$$

It should be noted here that (2.39) and (2.40) are general formulas for the reflection and transmission coefficients and thus, are valid for any optical stack with a chracteristic matrix of the form expressed in (2.36). We will not pursue this calculation until the matrix for the total mirror has been established.

Recall the expression for the characteristic matrix of an individual H-layer from (2.22), and let the matrix elements be represented by the following notation:

$$\underline{M}_H(h_H) = \begin{bmatrix} H_{11} & iH_{12} \\ iH_{21} & H_{22} \end{bmatrix} \ . \qquad (2.42)$$

Also recall (2.25) - (2.27) which represented the matrix for a 1/4-wave L-layer. Since the 1/2-wave L-layer in our system can be treated as two 1/4-wave layers placed on top of one another, the matrix for the 1/2-wave layer is calculated in the following manner:

$$\underline{M}_{L^2}(2h_L) = [\underline{M}_L(h_L)]^2 = \begin{bmatrix} L_{11} & iL_{12} \\ iL_{12} & L_{22} \end{bmatrix} \ . \qquad (2.43)$$

where,

$$\left.\begin{aligned} L_{11} &= \cos^2\beta_L - \sin^2\beta_L \\ L_{12} &= -\frac{2}{p_L}\sin\beta_L\cos\beta_L \\ L_{21} &= -2p_L\sin\beta_L\cos\beta_L \\ L_{22} &= \cos^2\beta_L - \sin^2\beta_L \end{aligned}\right\} \qquad (2.44)$$

NOTE: The L^2-layer matrix could have been constructed without using matrix multiplication, but by this method no new B_i's need to be defined.

With the previous information in hand, the characteristic matrix for the complete stack of dielectric films may now be calculated. From Fig. 2.1 we recall that the order of the stacking is,

$$S(HL)^{24}HL^2Air. \qquad (2.45)$$

Therefore, according to (2.21), the matrix for the total mirror, $\underline{M}_T$, is calculated in the following order:

$$\underline{M}_T = \underline{M}_{L^2} \bullet \underline{M}_H \bullet \underline{M}_{periodic} \qquad (2.46)$$

Carrying out the multiplications one finds

$$M_T = \begin{bmatrix} T_{11} & iT_{12} \\ iT_{21} & T_{22} \end{bmatrix}, \qquad (2.47)$$

where,

$$\left.\begin{aligned} T_{11} &= L_{11}(H_{11}M_{11}-H_{12}M_{21}) - L_{12}(H_{21}M_{11}+H_{22}M_{21}). \\ T_{12} &= L_{11}(H_{11}M_{12}+H_{12}M_{22}) + L_{12}(H_{22}M_{22}-H_{21}M_{12}). \\ T_{21} &= L_{21}(H_{11}M_{11}-H_{12}M_{21}) + L_{22}(H_{21}M_{11}+H_{22}M_{21}). \\ T_{22} &= L_{22}(H_{22}M_{22}-H_{21}M_{12}) - L_{21}(H_{11}M_{12}+H_{12}M_{22}). \end{aligned}\right\} \quad (2.48)$$

The reflectivity of the mirror may now be calculated from (2.39) and (2.41), but since r is a complex quantity, the reflectivity becomes,

$$\mathcal{R} = r \bullet r^{*}, \quad (2.49)$$

where r^{*} is simply the complex conjugate of r. After applying (2.39) to the matrix elements in (2.47) and doing some algebra to collect terms, (2.49) yields,

$$\mathcal{R}_T = \frac{(p_1T_{11} - p_\ell T_{22})^2 + (T_{12}p_\ell p_1 - T_{21})^2}{(p_1T_{11} + p_\ell T_{22})^2 + (T_{12}p_\ell p_1 + T_{21})^2}. \quad (2.50)$$

where $p_1 = n_{air}\cos\theta_1$ and $p_\ell = n_s\cos\theta_\ell$.

Similar arguments hold true in the calculation of the transmissivity, and result in the following expression,

$$\mathcal{T}_T = \frac{4p_1p_\ell}{(p_1T_{11} + p_\ell T_{22})^2 + (T_{12}p_\ell p_1 + T_{21})^2}. \quad (2.51)$$

The expressions for the reflectivity and transmissivity in (2.50) and (2.51) are the basis for the computation of these profiles. For the dielectric mirrors we are concerned with, the only independent variables are the wavelength λ, and the incident angel, θ_1.

The angles, θ_2, θ_3, and θ_ℓ, are related to θ_1 by Snell's Law:

$$n_i \sin\theta_i = n_t \sin\theta_t \ , \qquad (2.52)$$

where, n_i = index of refraction on incident side,

n_t = index of refraction on transmitted side,

θ_i = incident angle,

θ_t = transmitted angle.

For a given wavelength, the index of refraction is treated as a constant and thus the transmitted angles are also constant. However, from the literature, it is found that n varies with wavelength for the solids involved here. This means that θ_2, θ_3, and θ_ℓ also become functions of λ. While this λ dependence in n affects the computations somewhat, since the largest incident angle we are concerned with is 10^o, the angles need only be computed once. At small angles, small changes in n affect a $\Delta\theta$ which is so small that it may be neglected without significant introduction of error.

Figure 2.2 shows the labeling of the angles relative to one another. It can be shown from elementary optics that the

transmission angles in each medium are independent of the order in which the media are stratified. This is the reason that Fig. 2.2 is not needed to show all the individual layers in the mirror. By use of Snell's Law, it can be shown that all of the dependent angles are related to the incident angle (θ_1) by the following equations:

$$\sin\theta_2 = \frac{n_1}{n_L} \sin\theta_1 \ ,$$

$$\sin\theta_3 = \frac{n_1}{n_H} \sin\theta_1 \ , \qquad (2.53)$$

$$\sin\theta_\ell = \frac{n_1}{n_S} \sin\theta_1 \ .$$

Using the equations developed previously, a computer program was written to calculate reflectivity and transmission over a variable range of wavelengths. Profiles were calculated at normal incidence with the constant indices of refraction provided by the mirrors' manufacturers. A listing of the supplied mirror characteristics for each type of mirror is supplied in Tables 2.1 and 2.2. Since no absorption is assumed in the mirrors the reflectivity is simply 1-(transmission) for a given wavelength. This allows comparison of only R or T, not both, to be needed for determining the accuracy of the model.

2.3 Expected Damage Mechanisms

According to Donnert the prime mechanism by which gamma radiation (or high-energy electrons) will affect a material is through the activation or deactivation of color centers. A discussion of this phenomenon follows. References used as guides for this discussion were Azaroff and Brophy,[10] and Kittel.[11]

A color center is a lattice imperfection. Color centers serve to introduce localized states in the forbidden-energy region of an insulator. This effect is similar to that of adding impurities to a semiconductor. In the case of color centers however, the imperfections result in the selective absorption of a portion of the spectrum due to presence of the levels established in the forbidden energy gap. The width of the gap determines the range of wavelengths which might be absorbed. Only those photons with energies smaller than the width of the energy gap for a material can possibly be absorbed.

The simplest type of color center is an F-center. F-centers can be produced by any type of ionizing radiation provided that the proper energy is supplied. X-irradiation is commonly used to produce color centers for most applications, but electron irradaition is equally effective. An F-center is a negative ion vacancy with one excess electron bound at the vacancy.[11] Most other types of centers are variations on this theme or combinations of F-centers localized adjacent to one another in the lattice.

Simple lattice vacancies may also be created by high-energy radiation and may also have an effect in the ultraviolet region.

Table 2.1 Given Design Parameters for Dielectric Mirrors.

Dielectric Mirrors for KrF Eximer Laser (λ = 248 nm)

Mirror Configuration: $S[(HL)^{24} H(L)^{2}]Air$

S ≡ Fused-Silica Substrate, n_{FS} = 1.50

Quarter-Wavelength Dielectric Coatings:

H ≡ High-Refractive Index Material
Al_2O_3, n_H = 1.66, design thickness = 37.3 nm

L ≡ Low-Refractive Index Material
SiO_2, n_L = 1.46, design thickness = 42.5 nm

Half-Wavelength Dielectric Overcoating:

$(L)^2$ ≡ Double Thickness L-Layer
SiO_2, n_L = 1.46, design thickness = 84.9 nm

Table 2.2. Given Design Parameters for Metal Mirrors

MONOCOATED MIRROR

Mirror Configuration: S[Al]Air

S ≡ Fused-Silica Substrate, $n_{FS} = 1.50$

Al ≡ Aluminum coating, design thickness = 200 nm

BICOATED MIRROR

Mirror Configuration: S[CuAg]Air

S ≡ Fused-Silica Substrate

Cu ≡ Copper Coating, thickness = 100 nm

Ag ≡ Silver coating, thickness = 200 nm

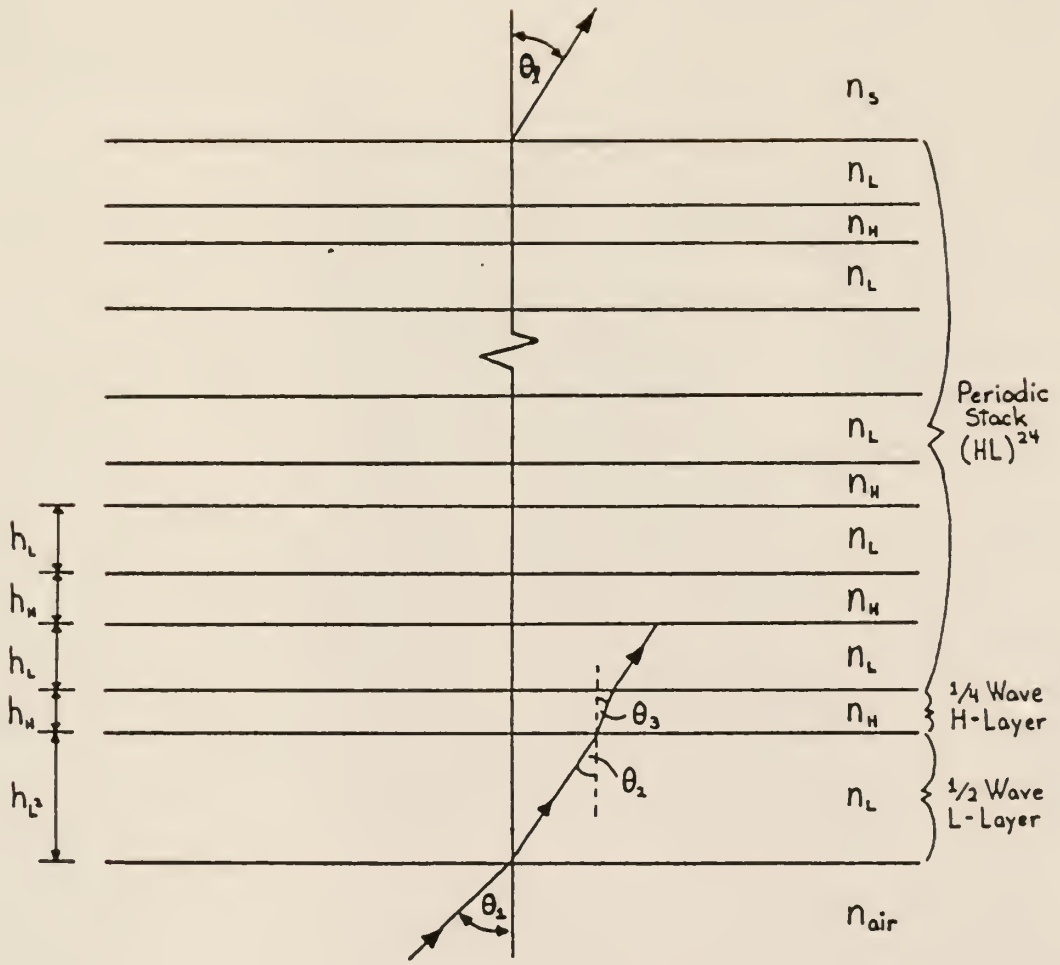

Fig. 2.1 Construction diagram for the dielectric mirrors.

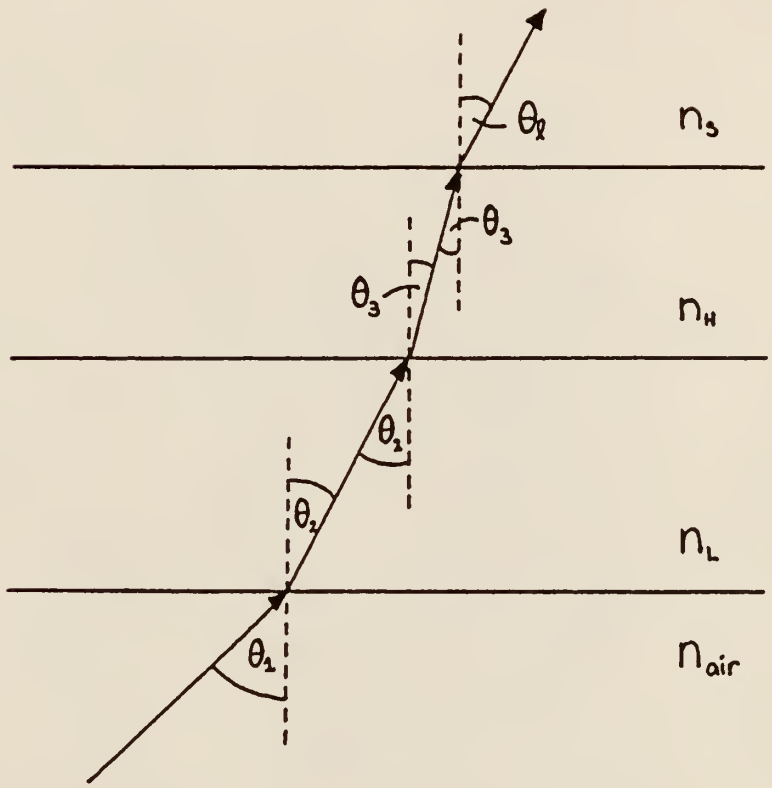

Fig. 2.2 View of stacking arrangement for purposes of calculating angles.

3. EXPERIMENTAL PROCEDURE

3.1 Pre-irradiation Mirror Studies

Before any of the mirrors were irradiated, it was necessary to establish baseline measurements of their optical properties. As mentioned before, the properties of greatest interest are the reflectivity and transmission as they vary with wavelength of incident light.

The measurements were done on a CARY 2300 Spectrophotometer at the Air Force Weapons Laboratory, Kirtland Air Force Base. This machine is capable of basically three types of measurements; optical density, percent transmission, and reflectivity.[2] Due to geometric optical considerations within the machine direct measurements of reflectivity can not be done because the incoming beam bounces off the test sample twice before reception in the detector. Thus the reason R^2 is reflected in the output instead of R. The type of plot produced by the machine is determined by two things; a switch and the type of slide wire used in the plotting mechanism. The difference in the slide wires has to do with different resistance variations built into the wires. In this fashion, various currents cause the pen assembly to move to a different position along the guide. Of course this measurement is only accurately scaled if matched into the proper circuity selected by the switches.

The data can be recorded in several different ways with the CARY 2300. There is a choice of three different lamps to use for wavelength scans. There is an infrared lamp for studies in the infrared and near-infrared regions of the spectrum. One lamp is for

use in the visible region of the spectrum and overlaps slightly at either end of that region with the near-infrared and UV regions. The last lamp, for use in the UV region down to ~200 nm, is a water cooled deuterium lamp. None of these have perfectly flat intensity profiles, but the machine has the ability to compensate for intensity variations by closing and opening an aperature that the light passes through before it reaches the sample.

The other variable wich may be changed is the speed that the machine scans through the wavelength range. Slower scans may be used to look at unknown areas to look for rapid variations in detail. Once the profile behavior for a type of measurement is known then the user can opt for a faster scan speed, especially if variations are fairly smooth. The speed of the chart paper through the system is constant so the scan speed selected is automatically calibrated to the markings on the paper in the directionn of movement away from the machine. Howwever, in the other direction the pen must be manually zeroed (at 100% for %T) without a sample in the chamber.

The Procedures for an individual measurement are as follows:

1. Make sure that the machine is set up for the proper type of measurement, either %T or R^2.

2. Place the power switch on and open the detector shield. Also turn on the water flow if using the deuterium lamp. Turn on the lamp and let it warm up, approximately 3 minutes.

3. Set the pen down on the paper and turn on the paper drive. Using the baseline adjustment knob, slowly move the pen to the baseline value for the measurement being taken. It was found that being able to look at a straight line gave a better indication of whether the pen was zeroed than by looking at a dot on the paper. Zero is the baseline for R^2 measurements, one is the baseline for %T measurements with no sample in the chamber. When done, close the shield, turn off the paper drive.

4. Open the sample chamber and place the sample in, making sure the lid to the chamber is fully seated to prevent overload of the detector.

5. Choose a paper speed calibration that matches the type of profile to be done. In this case, 20 nm/division was used because of time to run considerations and also because this scaling was easy to read on the final profile.

6. With the pen off of the paper and turned off to prevent its movement, set the paper up till the pen will fall on a solid line division. Blocks of five spaces are marked by heavier lines in the direction of paper movement. If the starting wavelength is not a multiple of the scale calibration set the pen on the appropriate corresponding point on the scale.

7. Set the pen down and simultaneously flip the paper drive on and flip the wavelenth scan switch to negative. The starting wavelength was chosen to be the high end of the region so that the profile would read with wavelength increasing from left to right.

8. When the lower end wavelength is reached lift the pen up, turn off the paper drive, turn off the wavelength scan switch, drop the shield, and remove the sample.

To start another measurement of the same type, start over again at the fourth step.

Measurements of %T and R^2 versus wavelength were done for each of the mirrors from 230 nm to 300 nm. Early plots from 200 nm to 400 nm with the UV lamp and from 400 nm to 1500 nm with the visible lamp showed no unpredictable absorption bands present in the mirrors. Thus, since the dielectric mirrors were designed for use around 248 nm with a KrF laser systems the region of interest in this study was narrowed to the range from 230nm to 290 nm.

3.2. Mirror Irradiation

Irradiation of the mirrors was done at the EG&G LINAC Facility in Goleta, CA. Due to the limitations on beam time at EG&G it was necessary to make two different trips there to complete the data included in this report.

At the beginning of each session on the LINAC the operator had to prepare the machine according to the experimental needs. In order to center the beam and to see to adjust the radius of the beam, an aluminum foil piece was placed over the end of the beam port. This foil was marked off with a "bulls-eye" pattern and coated with a phosphor which interacts with the electrons and gives off a visible light, see Fig. 3.1. Through a remote camera system, the operator can see where the beam is contacting the foil. Knowing

the position of the beam and its shape allows the operator to adjust these parameters using different banks of magnets. The electromagnets can be used at different field strengths to shape and focus the beam in a lens-like fashion and other groups to deflect the beam in the vertical or horizontal direction to position its angle of exit from the port. The beam was centered and reduced to a spot approximately 5/8 of an inch in diameter.

With this completed, the optic table was rolled into position in front of the beam port. The optical arrangement used in the first session is shown in Fig. 3.2 and the arrangement for the second set in Fig. 3.3. Alignment of the mirror samples and the Faraday Cup reference detector was done with a low-power HeNe laser placed on the axis of the LINAC for just that purpose. The target area of the mirror is shown in Fig. 3.4.

From there, the current and length of the beam pulse were adjusted by the operator from the console. As a backup to what is read on the console the length and current strength of the pulse was measurable on each shot. This was done by two detectors; one inside the LINAC, and one external "reference" detector directly in line with the outgoing beam. Examples are shown in Fig. 3.5. These signals were sent to separate oscilloscopes with camera attachments that trigger a picture when the beam fires.

At this point this sytem was prepared for irradiation to begin. The procedure followed was fairly lengthy because in addition to the long-term radiation effects that this study is concerned with, data was also being taken to look at the transient effects. However, I

will only include those aspects which directly relate to this study. The procedure was as follows:

1. The mirror was taken into the LINAC room and placed, coating out, into the mirror holder. With a small piece of paper on the front of the mirror, the laser was used to align the target area with the beam axis. An index mark was made on the rim of the mirror radially opposite the target area for referencing the target area later.

2. The operator energized the LINAC and fired the beam pulse.

3. The oscilloscope pictures of the shot from the reference detector and the LINAC's detector were labeled for identification later and studied to insure that the planned pulse was delivered to the mirror.

4. Once the LINAC room was clear another mirror was placed in and the first one placed back in its protective labeled case.

Breaks in this simple procedure occurred whenever the shot paramters were changed. First of all, radiochromic dosimetry was used to determine the spatial distribution of the electron beam density and also as a measure of the dose being delivered by a type of pulse. To take these measurements, a small piece of radiochromic film was placed on a mirror at the point where the beam was aimed at then the beam was fired. The films darken in areas where the electrons strike it, with more bluing where more electrons strike the film. The VAX-11 computer system was used to take data from an optical density scanner that scanned the film in a grid pattern. This was done by EG&G personnel who were familiar with the system.

A sample of the printout given for this analysis is shown in Fig. 3.6. NOTE: Radiochromic film is also sensitive to UV light from any source and care must be taken to lower unintended exposure to UV light.

In addition, the operator had to go through the previously mentioned steps to reset the beam size, current, and length of pulse. Once this was done a sample shot was made without a sample to check the new adjustments on the LINAC detector and reference detector pictures.

The procedures followed for each session at EG&G were the same with the exception of change for long pulses. The information regarding the type of pulse delivered to each mirror in the first experiment is compiled in Table 3.1. In the second experiment the LINAC was fitted with a water cooled extension to the beam port. This allowed the machine to safely deliver longer pulses to the mirrors. No other changes in basic procedure were required. The irradiation information for this second session is presented in Table 3.2.

3.3 Post-irradiation Studies

Upon completion of each session of mirror irradiation the mirrors were once again sent to the AFWL for transmission and reflectivity measurements. This time however, a specially made attachment had to be used in the sample chamber. The attachment is shown in Fig. 3.7. It was designed to align the target spot on the mirror with the optical system of the Cary 2300. The index line on

the mirror was positioned at 12 o'clock to rotationally align the target spot. Previous procedures were followed again.

Two measurements were recorded on top of each other for each reflectivity profile; the post-irradiation profile from the target spot and the profile from an unirradiated area of the mirror. Comparison with pre-irradiation data showed that the profiles from an area of the mirror not directly targeted were identical to the pre-irradiation profiles. The purpose of this "double plot" scheme was to allow easier direct comparisons for damage analysis. The filters used in the optical systems were also measured for transmission versus wavelength at this time using the same procedure.

Table 3.1. Irradiation information for mirrors #1, to #11 for the effects of electron damage on optical components research. Note: electron energy = 16.5 MeV, UV filter in line for all data except for mirror #1. Dose and dose rate are approximate.

Mirror Number	e^- Beam Current (A)	Pulse Width (ns)	Dose (krad)	Dose Rate (krad/ns)
1	4.0	20	40	2.0
2	5.0	20	50	2.5
3	5.0	20	50	2.5
4	5.0	20	50	2.5
5	5.0	20	50	2.5
6	7.0	20	70	3.5
7	7.0	20	70	3.5
8*	7.0	20	70	3.5
9	5.0	45	125	2.8
10	5.0	45	125	2.8
11	5.0	45	125	2.8
3L	5.0	45	125	2.8
4L	7.0	20	70	3.5
5L	4.0	20	40	2.0
8L	5.0	45	125	2.8
9L*	7.0	20	70	3.5
10L	4.0	20	40	2.0

*Mirror #8 was shot twice on the same location under the listed conditions.

Table 3.2. Irradiation information for the mirrors used in the second session of the experiment. Electron energy is 16.5 MeV. Dose information approximate.

Mirror No. and Position	e^- Beam Current (A)	Pulse Width (ns)	Dose (krad)	Dose Rate (krad/ns)
12(A)	.225	500	56.25	.1125
12(B)	.225	500	56.25	.1125
13(A)	.225	200	22.5	.1125
13(B)	.225	200	22.5	.1125
14	5	20	50	2.5
1L	5	20	50	2.5
2L(A)	.225	200	22.5	.1125
2L(B)	.225	200	22.5	.1125
6L	5	20	50	2.5
7L(A)	.225	500	56.25	.1125
7L(B)	.225	500	56.25	.1125

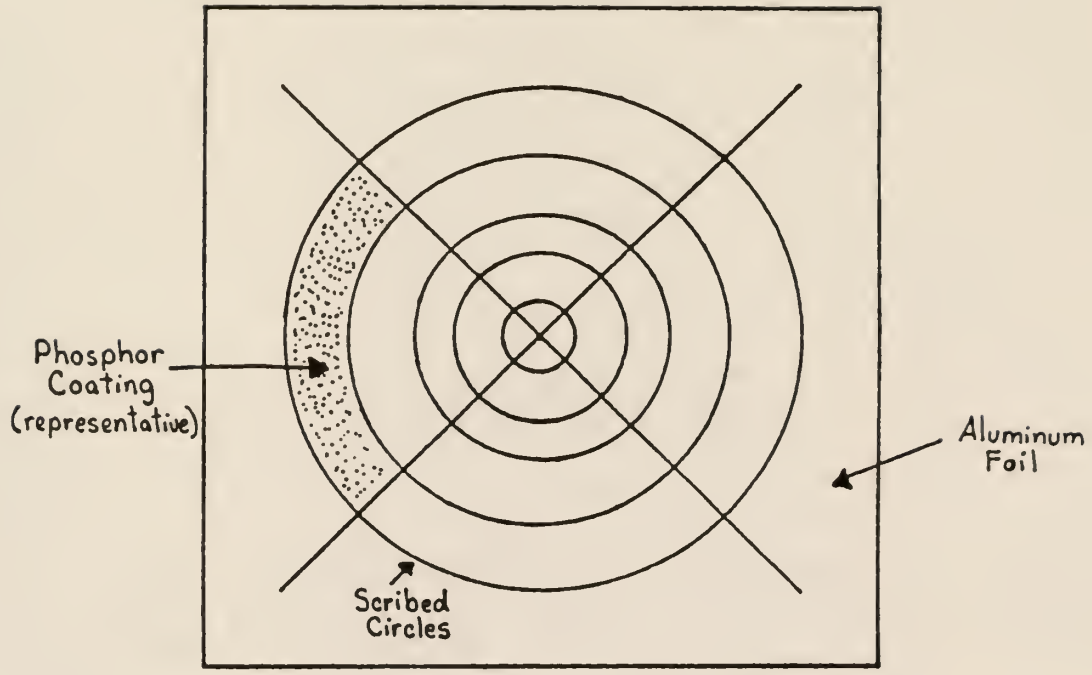

Fig. 3.1 Sketch of beam alignment foil.

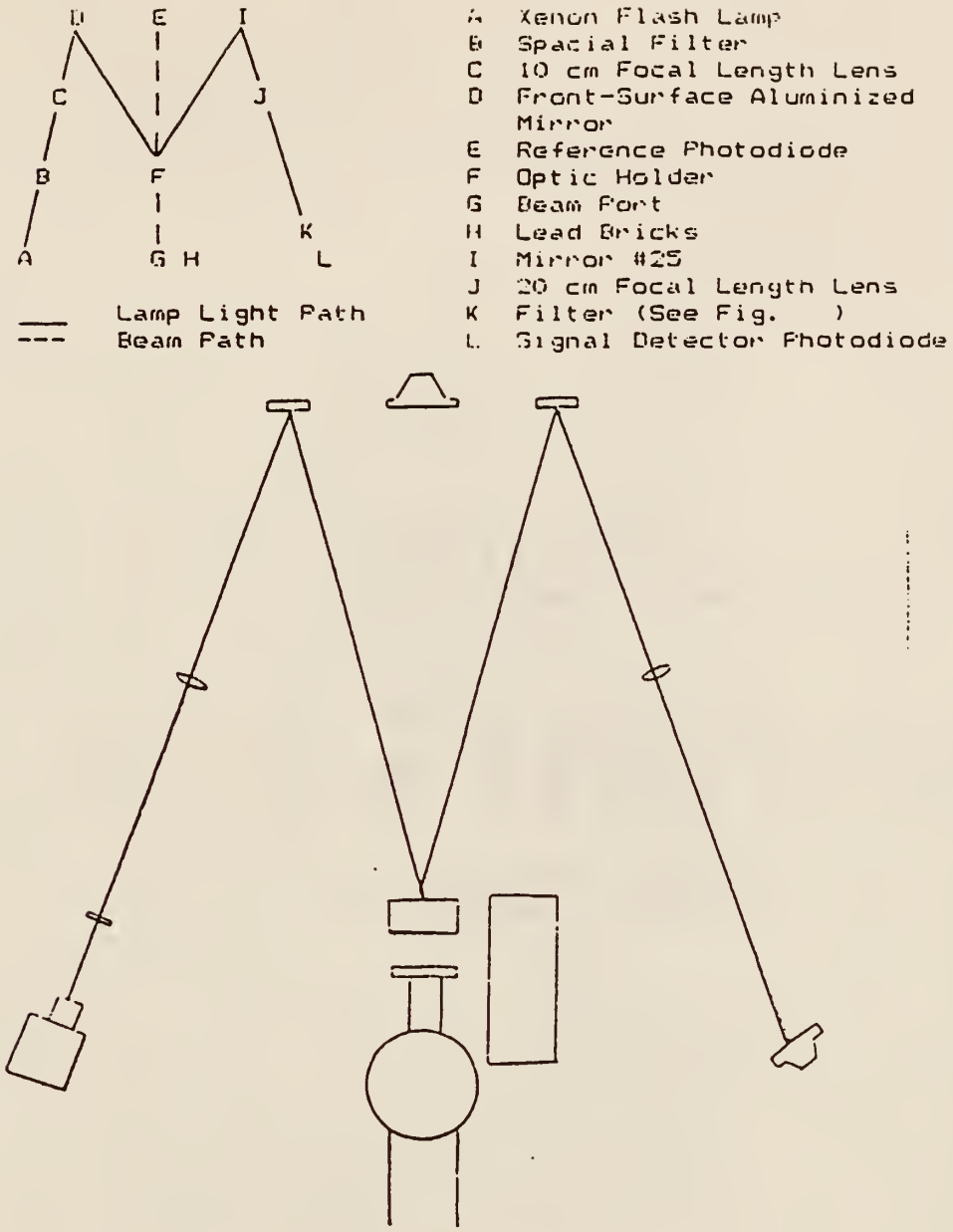

Fig. 3.2 Irradiation geometry for the first mirror set.

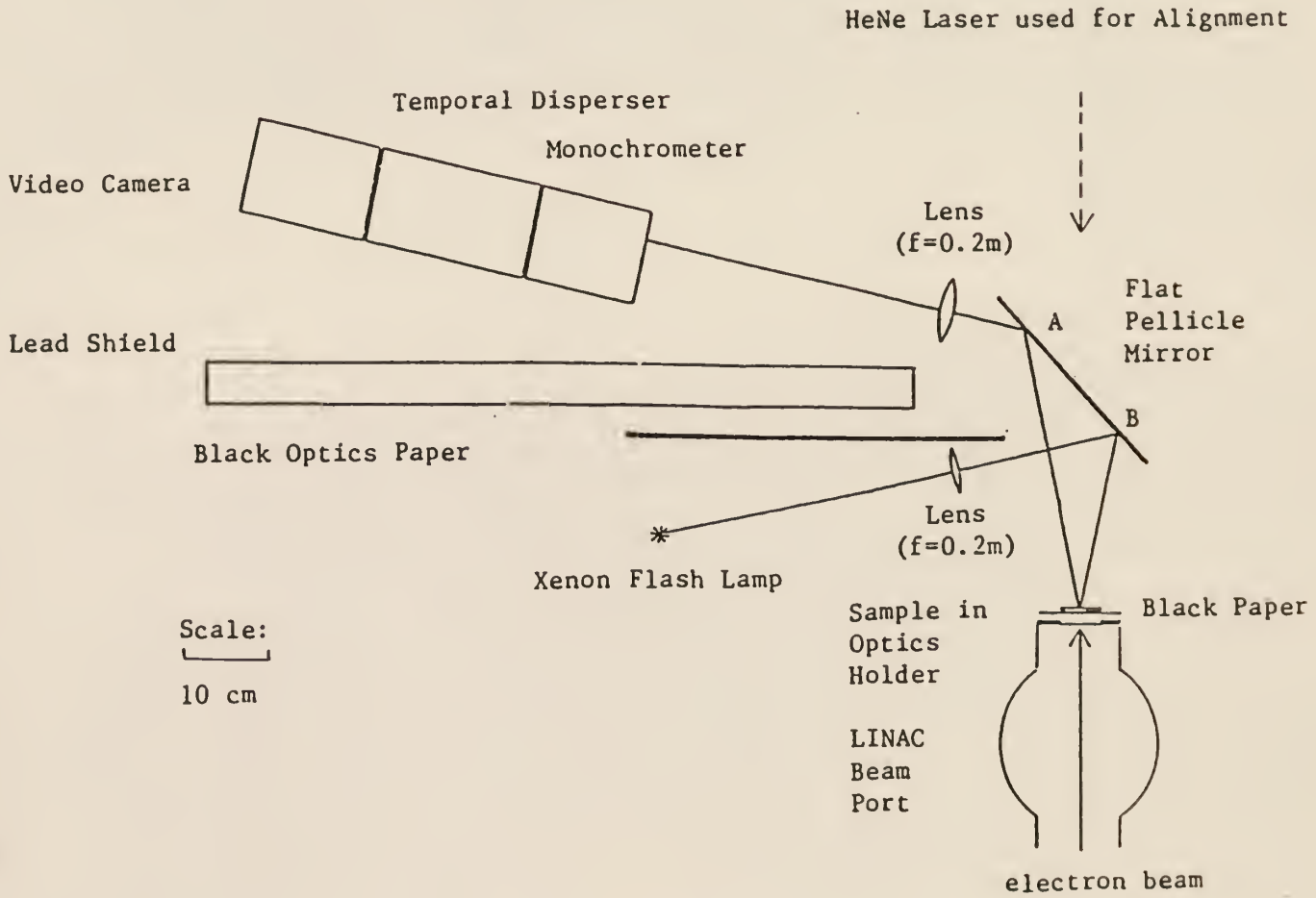

Fig. 3.3 Irradiation geometry for the second mirror set.

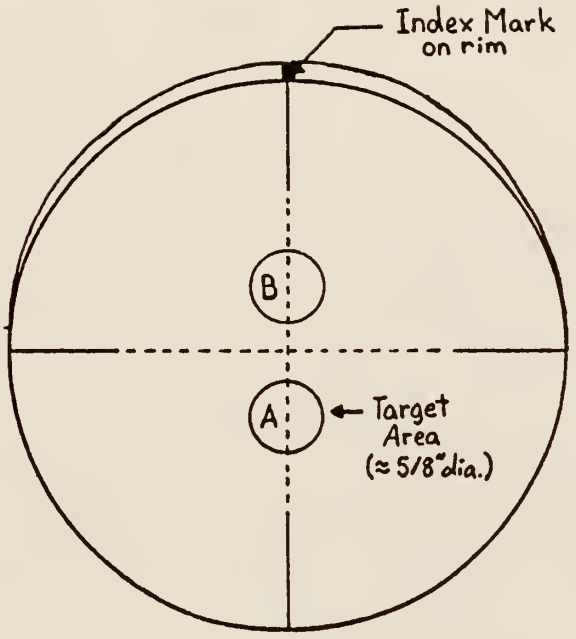

Fig. 3.4 Mirror target areas.

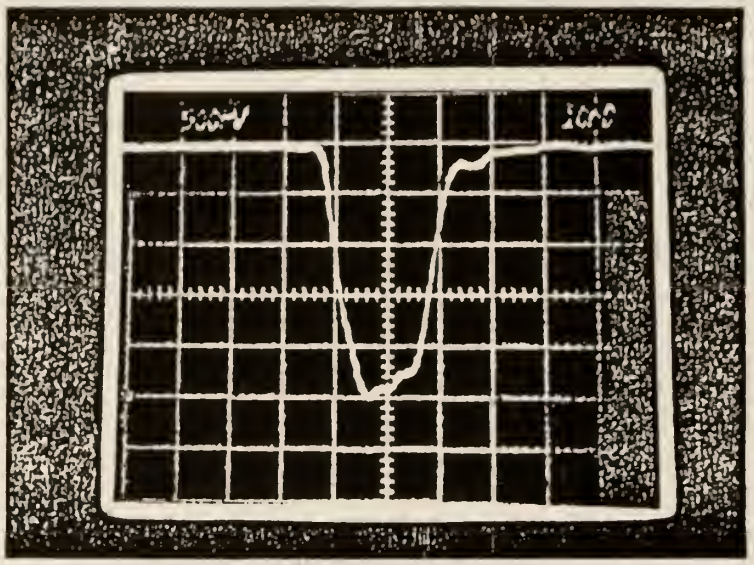

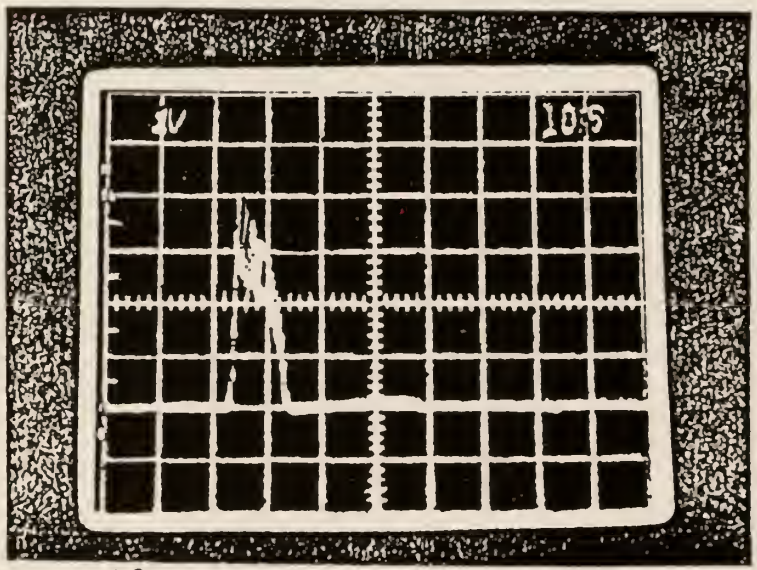

Fig. 3.5 Example of reference and block detector outputs.

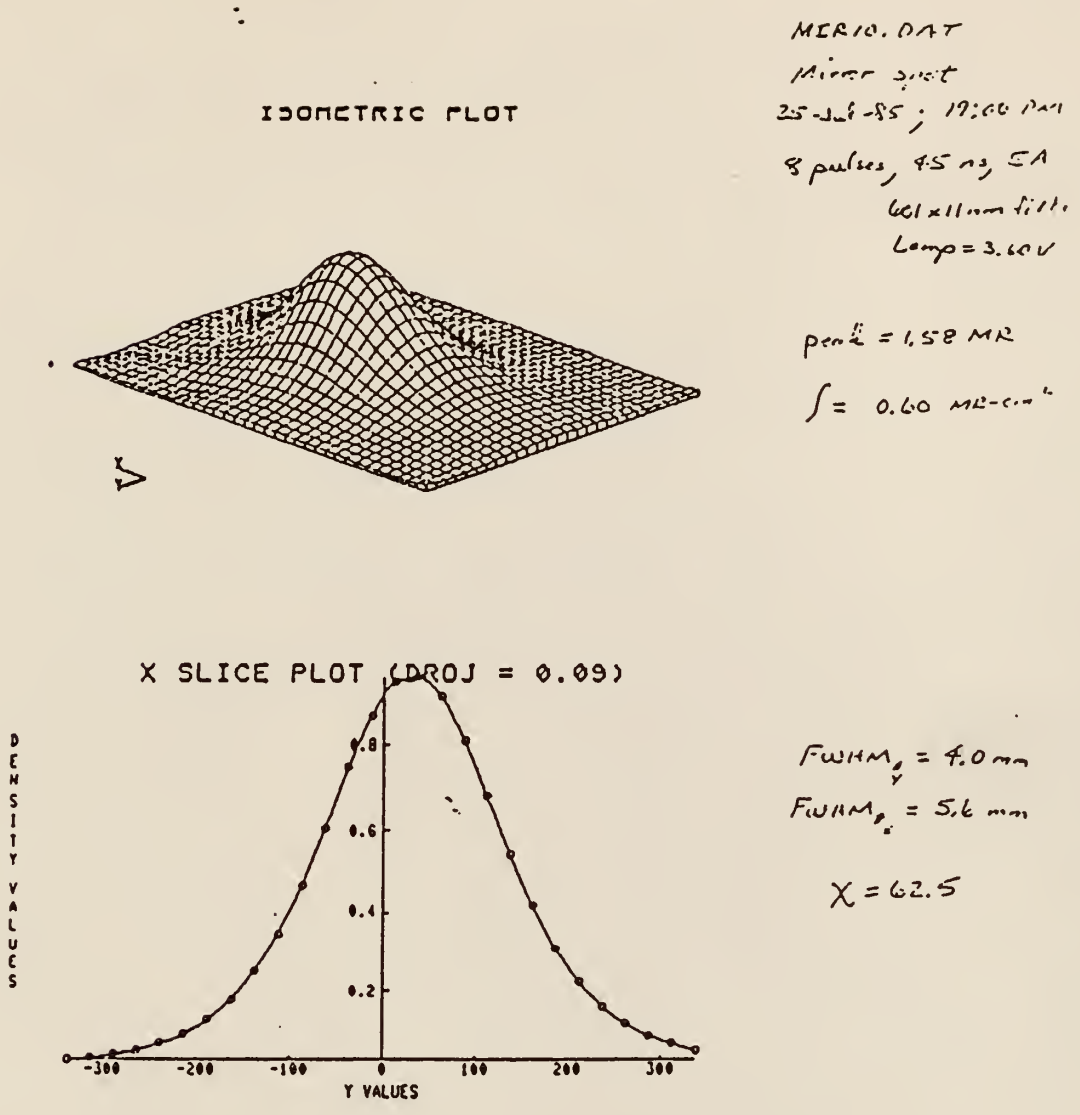

Fig. 3.6 Sample printout from radiochromic dosimetry analysis.

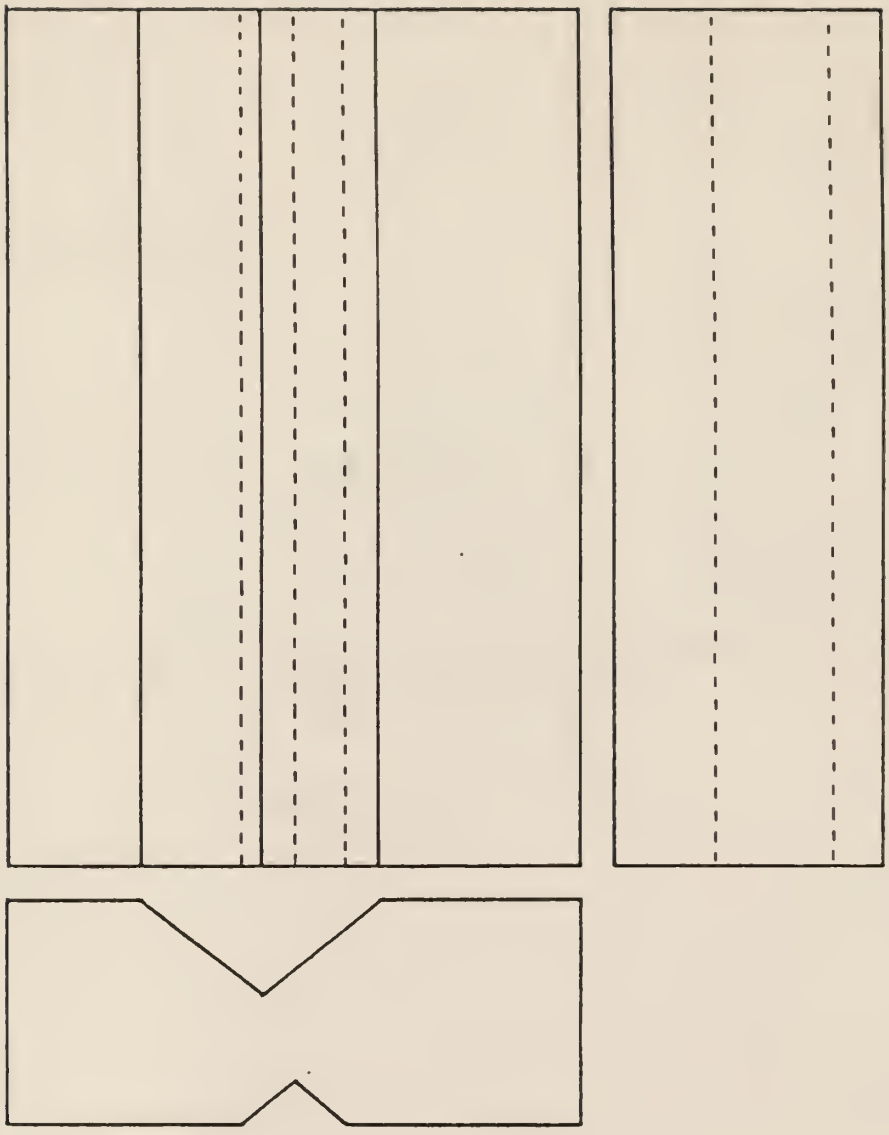

Fig. 3.7 CARY-2300 insert for post-irradiation measurements.

4. COMPARISON OF THEORETICAL EXPERIMENTAL PROFILES

4.1 Dielectric Mirrors

For initial comparison of the theoretical profiles to the experimentally determined ones, a dielectric mirror was chosen at random. The mirror chosen was dielectric mirror #8. The first thing looked at was how the two reflectivity profiles compared to one another.

We are primarily concerned with the optical properties at normal incidence. Using the values of refractive index provided with the mirrors, a reflectivity profile was generated using the program discussed in Appendix A. This profile is plotted with the mirror #8 profile in Fig. 4.1. Comparing these two profiles showed too great a differential to be acceptable. The peak reflectivities compared well to each other, but the theoretical peak was much wider and it's center was shifted to the left. Because of this disparity something was assumed to be missing in the model. Fault was placed on the model because of the sophistication of present fabrication techniques which are known to be very accurate. Two variables were available for change: incident angle and indices of refraction.

Upon recalling how the CARY 2300 measured reflectivity, it was noticed that the angle of incidence used for the measurements was not 0^{o}, but 10^{o}. Figure 4.1 also shows this profile. Obviously, this was not the answer to the problem. Born and Wolf confirm that the peak will shift to shorter wavelengths as the incident angle increases for a multilayer system. Therefore, it was assumed that the constant refractive indices used in the computations were the weak link in the data.

Tables of refractive index versus wavelength can be found for materials under different ambient temperatures in a myriad of references. Due to this multiplicity of conflicting data there was a need to establish a guideline for sorting out the applicable data for our particular use. The guideline used in this case was to assume that the values of n given to us should be matched as closely as possible around the 248 nm central peak. Using this criteria, sources of n vs λ were found for fused silica and aluminum oxide. These listings are shown in Tables 4.1 and 4.2 respectively. Under this critieria it was not possible to find a satisfactory correlation between refractive index and wavelength for silicon dioxide. A possible reason for this failure is the fact that the SiO_2 used in the mirrors was deposited by electron beam and has a final structure unknown to us. It is probable that the silicon dioxide layers in the mirror are devoid of a symmetric lattice structure and the majority of tables presented for SiO_2 are for the crystalline structure.

Since no relationship was found tabulated for silicon dioxide, the information for fused silica was also substituted in for SiO_2. To allow use of the variable indices in the computer program the data in the tables needed to be converted to functional relationships. For both sets of data a linear fit proved to be an accurate representation of the data in the wavelength band from 230 nm to 290 nm. Since we were only concerned with this small wavelength band rather than the entire spectrum it was justifiable

to limit the fits to this range. The dotted line in Figure 4.1 is the theoretical profile generated at normal incidence with the two different variable refractive index fits included in the computer model. By going to variable indices the peak area shifts to the higher wavelength direction and plotting at normal incidence only compounded the problem, but the plot also shows that this change is a step in the right direction.

At this point the decision was made that the function $n_{\text{fused silica}}(\lambda)$ was not an accurate representation of $n_{SiO_2}(\lambda)$ in a direct substitution. One would however suspect that the two functions would have a similar slope due to the SiO_2 make-up of each, the difference being the form of the compound. As refractive index is largely dependent on material polarization at a molecular or atomic level, this argument has a logical basis. On a trial and error basis the intercept portion of the linear fit was changed in the program and the new profiles (at 10^{o} incidence) compared to the measured one.

The final set of fits settled are displayed, with correlation coefficients were applicable, in Table 4.3. The profile generated by this data set is shown in comparison to the measured profile for dielectric mirror #8 in Fig. 4.2. The widths of the primary peaks match up well. At half-maximum the difference in width is 1.690. The peak reflectivities also compare favorably. At 250 nm and ten degrees incidence the difference in reflectivity is 0.5% with the theoretical result slightly higher than the measured result.

There are two noticeable differences between the theoretical profile and the measured one that bear further discussion, both concerning the resonance peaks. The first difference is in the position of the peaks and valleys of the resonance peaks. Because the slope of the central peak is sharper theoretically than the measured peak, the theoretical resonances lag in wavelength behind the measured ones. The most probably reason for this relates to how the measured data is obtained. The CARY 2300 scans for the intensity reaching the detector for different wavelengths on a continuous basis. The recording mechanism is mechanical in nature and this inserts a finite response time to any changes in R^2 or T. The signal information is supplied to the pen assembly which determines it's position from feedback with the current flowing to the assembly along it's slidwire. This process also contributes to the response time. Differences in wavelength correspond to differences in time over the course of conducting a measurement. The finite response time of the CARY 2300 could be a factor in the differences in the positions of the resonance peaks for the two profiles. Of course, it is also possible that there are differences in the actual make-up of the mirror layers and the designed parameters.

The other noteworthy difference is in the magnitude of the reflectivity at each wavelength between the two sets of resonance peaks. The valleys in these resonance areas reach very nearly zero in the theoretical profile. The measured profile shows a monotonic

decreasing trend in which the amplitude of these valleys starts relatively high and goes asymptotically to zero with increasing distance from the peak. Since the photomultiplier tubes in the CARY 2300 are constantly being exposed to a signal it is reasonable to assume that there may be a build up of signal within the tube over a period of time. As the peaks begin to show up and expose the detector on a constant basis there is not time for the P-M tube to relax and discharge the build up of charge within itself. It is suspected that this carryover represents the systematic difference in amplitude between the measured and theoretical resonances.

Comparisons of theoretical transmission profiles with the measured ones show the same differences and thus need not be discussed separately.

4.2 Metal-coated Mirrors

The theoretical spectral reflectance for each of the different types of metal mirror studied was not derived earlier, as this is a straightforward procedure. Guidelines for a treatment of single or double layer metallic film reflectance can be found in a wide variety of optics literature. Among these references, two with good treatments of this subject are Hecht and Zajac[7] and Anders.[8] Both of these sources provide figures which display the spectral reflectance of a number of metallic layer mirrors (single film). Of importance for this study is that aluminum, copper, and silver are included in this list. An outtake of this figure is displayed in Fig. 4.3.

Recall that metal mirrors #1L through 5L are double-layered with copper as the inner layer and silver as the outer layer. In configurations where the top layer is of an absorbing medium, it would be expected that the properties of this layer would dominate the properties of the mirror as a whole. This assumes that the top layer is of sufficient thickness to allow little incident light to be transmitted through it.

Comparison of the spectral reflectivity of this type of metal mirror to Fig. 4.3 bears out this expectation. The shape of the reflectivity profile for the Cu-Ag mirrors reflects strongly the absorption characteristics exhibited by a pure Ag mirror. Most notably, both share the sharp absorption band from approximately 300 nm to 325 nm. In the range of interest for this study the silver layer lessens the effectiveness of this mirror rather than improving it. One would expect this mirror to perform very well in the visible region however.

The other type of metal mirror examined, mirrors #6L through 10L, are single-layered with aluminum as the active reflector. From Fig. 4.3 it is expected that these mirrors will have a fairly uniform spectral reflectance with values slightly decreasing with decreasing wavelength. Measured reflectivity profiles for this type of metallic mirror show that this is the case. The measured profiles show a lower than expected reflectivity when compared to Fig. 4.3 for aluminum but the thicknesses are likely not comparable. It is

reasonable to assume that the thickness of the mirror film in this study is the lesser one and this explains the difference observed.

Table 4.1. Refractive Index at 20°C for Three Specimens of Fused Silica Averaged.[5]

λ (nm)	Computed Index
230.21	1.520081
237.83	1.514729
239.94	1.513367
248.27	1.508398
265.20	1.500029
269.89	1.498047
275.28	1.495913
280.35	1.490990
289.36	1.488734
296.73	1.487194

$$n(\lambda) = 1.6344335 - (5.039218 \times 10^{-4}\ nm^{-1}) * \lambda$$

$$r = 9.883448$$

Table 4.2. Refractive Index for Aluminum Oxide at Wavelengths in the Region of Interest.[6]

λ(nm)	Refractive Index
220	1.692
230	1.685
240	1.679
250	1.672
260	1.666
270	1.661
280	1.656
285	1.653
290	1.651
300	1.645

$$n(\lambda) = 1.8147 - 5.675 \times 10^{-4}\ nm^{-1}) * \lambda$$

Table 4.3. Summary of Refractive Index Fits Developed for the Mirrors.

Silicon Oxide	$n(\lambda) = 1.6094 - (5.039 \times 10^{-4}\ nm^{-1}) * \lambda$
Fused Silica	$n(\lambda) = 1.6344 - (5.039 \times 10^{-4}\ nm^{-1}) * \lambda$
Aluminum Oxide	$n(\lambda) = 1.8147 - (5.675 \times 10^{-4}\ nm^{-1}) * \lambda$

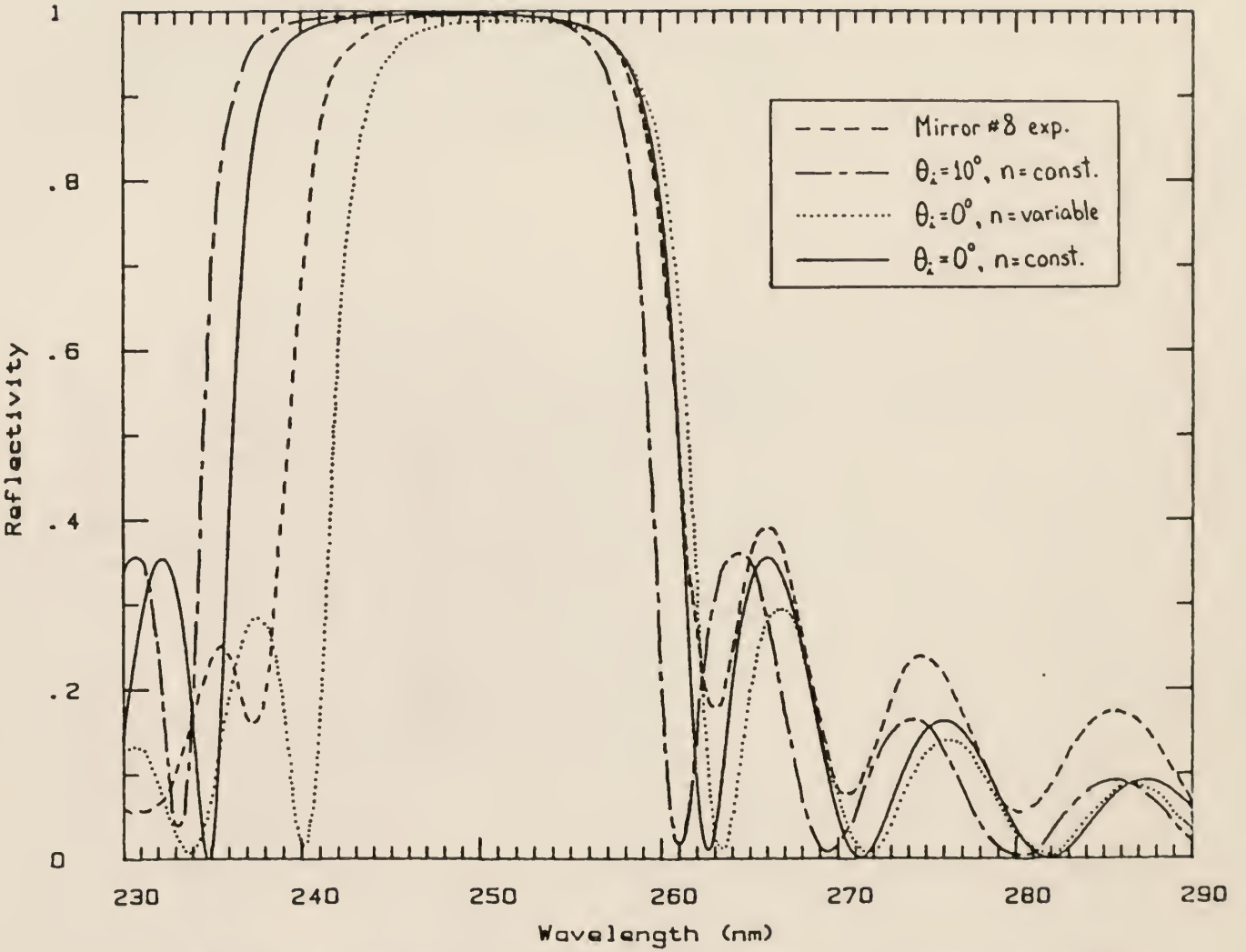

Fig. 4.1 Various computed reflectivity profiles compared to the measured profile for dielectric mirror #8.

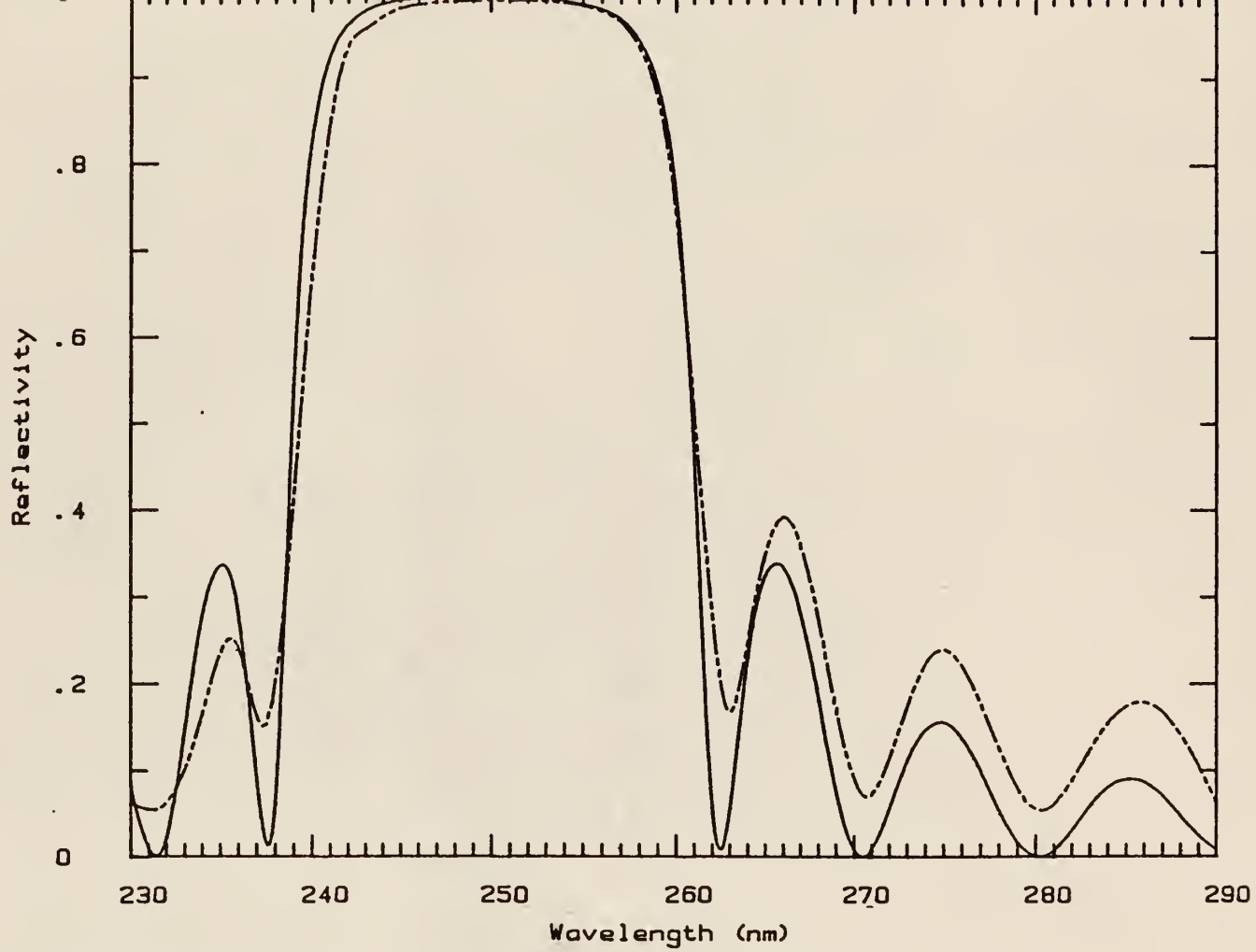

Fig. 4.2 Comparison of final theoretical reflectivity profile for dielectric mirrors and that of a measured profile.

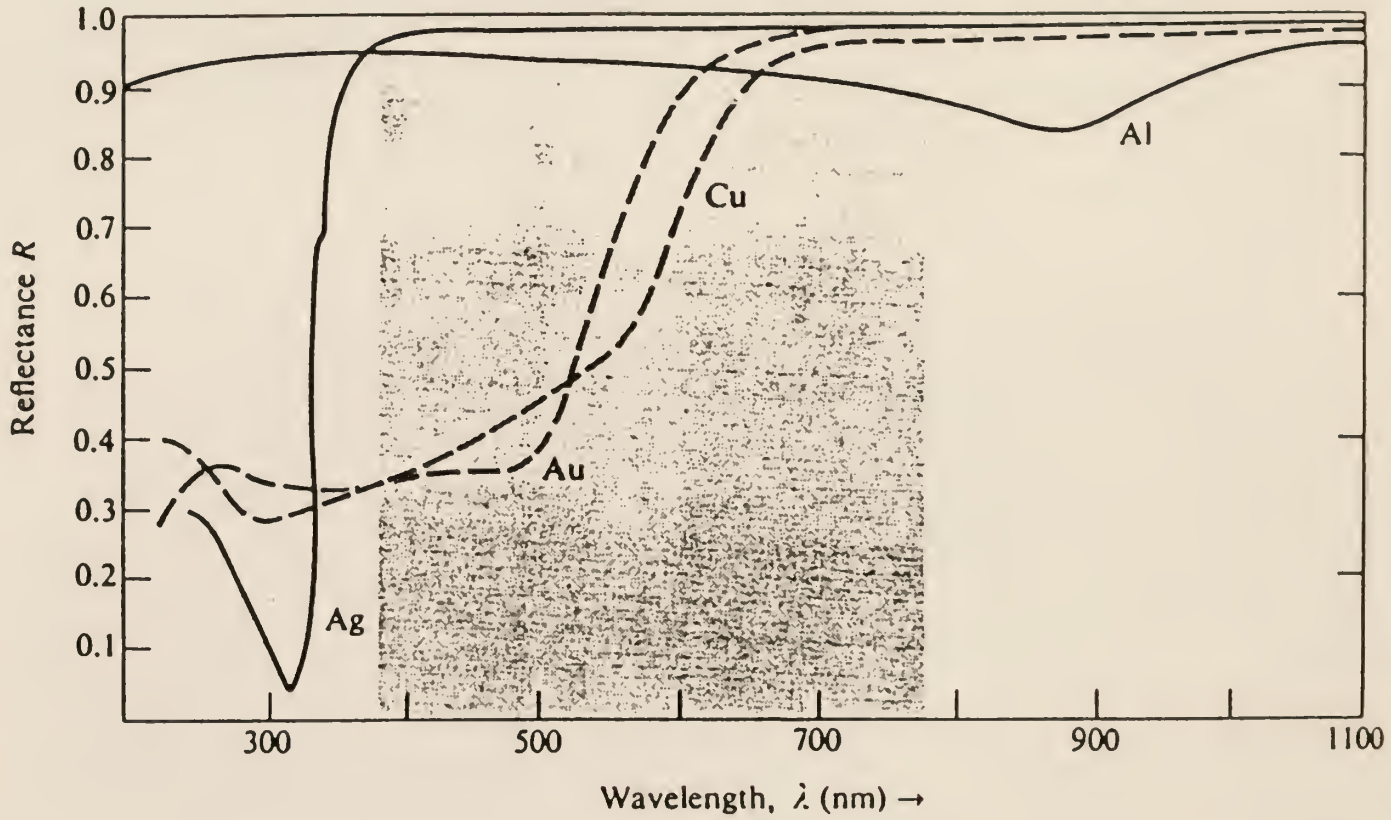

Fig. 4.3 Reflectance versus wavelength for silver, gold, copper, and aluminum. Source: Hect and Zajac.

5. POST-IRRADIATION RESULTS

5.1 Dielectric Mirrors

The pre- and post-irradiation reflectivity and transmission plots were recorded on strip charts as was previously discussed in Section III. All of the data were read off of the charts and re-plotted for presentation here.

As a result of the scale used to print the profiles on the CARY spectrophotometer the original plots were not very smooth using direct plotting of lines from point to point. For this reason, the finished plots have incorporated the use of a cubic spline fit routine by the plotter program used to produce the plots. A discussion of interpolation using cubic spline functions is presented in an easily understandable form by Hornbeck.[9] The finished plots are presented in Figs. 5.1 through 5.29 for the dielectric mirrors.

A comparison of the pre- and post-irradiation profiles show that little or no change in the optical properties of the dielectric mirrors is observed for the doses and dose rates used in this study. Differences in the resonance peaks of several mirrors were observed, but nothing suggesting the activation of an absorption center was noted. The shape of resonance areas doesn't change, just the amplitude of the peaks and valleys. The most plausible explanation for these kinds of differences is a minor lack of continuity in response from the measuring mechanism in the CARY 2300 over these fast varying regions.

The region of interest for damage to the mirrors centers is a tight wavelength band about 248 nm. This is the operating region of the KrF eximer laser system for which the mirrors were designed. The central reflecting peak for the mirrors is fairly flat at its apex. For this reason, damage to the mirror will be defined as a change in the optical properties of the mirror at the center of the primary peak. At ten degrees incidence, this central value is measured at 250 nm. The values of the measured optical properties at this wavelength are summarized in Table 5.1 for both pre- and post-irradiated conditions.

Only three of the fifteen dielectric mirrors irradiated exhibited any change in optical properties in the post-irradiation measurements at the central peak. Each of the three showing any difference show only a small change in peak reflectivity with no change in transmissivity. No in-depth analysis is required to look at the results and ascertain that no systematic pattern of damage has been established. In fact, an error in each reading could readily be assigned which would reasonably negate differences of this magnitude. The width of the lines plotted on the strip charts implies only a .003 unit certainty in any measurement read from the original charts. In other words, this finite line width implies that an error of $\pm$ .003 must be applied to any individual measurement due to this factor only. This factor along with the fact there is no logical pattern in the occurences of change leads to the conclusion that no mirrors were truly damaged.

5.2 Metal-coated Mirrors

The pre- and post-irradiation reflectivity profiles for both types of metal mirror were processed in the same manner as the profiles for the dielectric mirrors. Transmission profiles for the metal mirrors were not measured and displayed here. Because of the absorption inherent in the use of metallic layers as the active reflectors, a measure of transmissivity of the mirror was not determined to be needed for a determination of damage imparted to the mirrors. The creation of any absorption centers should be directly indicated by a change in the reflectivity profiles.

Notice was made before of the fact that neither type of metal mirror showed the necessary reflectiveness at the 248 nm band operating region of the KrF eximer laser system. A higher efficiency reflector is needed to survive the expected high power levels the laser would be operated at. For this reason, the damage criteria defined for the dielectric mirror will not apply to the metal mirrors. A specific damage critiera will not be designated for this type of mirror. Instead a comparison of the pre- and post-irradiation spectral reflectivities will be scrutinized over the measured region.

The results for the reflectivity measurements on the metal mirrors are shown as Figs. 5.30 through 5.35. The only mirror showing any possibility of damage imparted is the Cu-Ag mirror #2L. The data for this mirror are plotted in Fig. 5.31. As with the dielectric mirrors, this change is not duplicated in other mirrors

of the same type. Also worth noting is the fact that of the Cu-Ag mirrors irradiated, #2L received the lowest dose at the lowest dose rate. In light of these facts one must assume that this difference between pre- and post-irradiated reflectivities is not indicative of damage to the mirror, but the result of an error in the spectral reflecitvity measurements.

Table 5.1. Compilation of Dielectric Mirror Properties Before and After Irradiation, with Their Respective Doses Received at 250 nm.

Mirror No.	Dose (krad)	Dose Rate (krad/ns)	Reflectivity		Transmissivity	
			Pre-irradiation	Post-irradiation	Pre-irradiation	Post-irradiation
1	40	2.0	.990	.990	.006	.006
2	50	2.5	.990	.990	.007	.007
3	50	2.5	.990	.990	.006	.006
4	50	2.5	.991	.991	.006	.006
5	50	2.5	.988	.990	.006	.006
6	70	3.5	.991	.991	.006	.006
7	70	3.5	.991	.991	.008	.008
8	140	3.5	.989	.989	.006	.006
9	125	2.8	.991	.991	.007	.007
10	125	2.8	.992	.992	.007	.007
11	125	2.8	.991	.991	.006	.006
12	56.25	0.1125	.985	.985	.006	.006
13	22.5	0.1125	.973	.971	.007	.007
14	50	2.5	.971	.971	.004	.004
26	Unknown*	Unknown	.984	.985	.006	.006

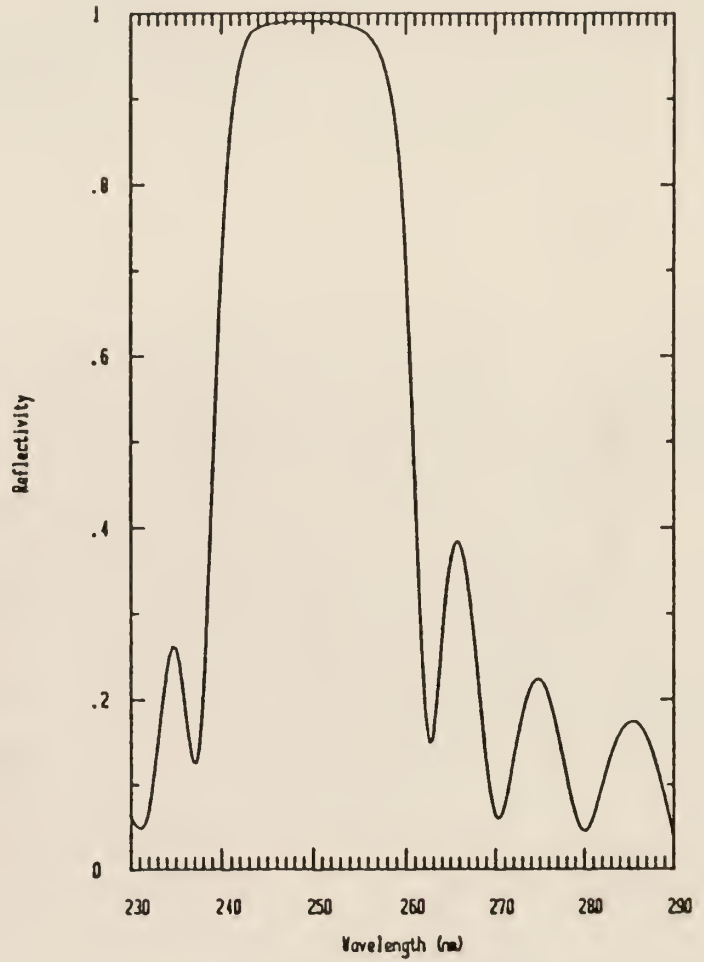

Fig. 5.1 Pre- and post-irradiation reflectivity profiles for dielectric mirror #1.

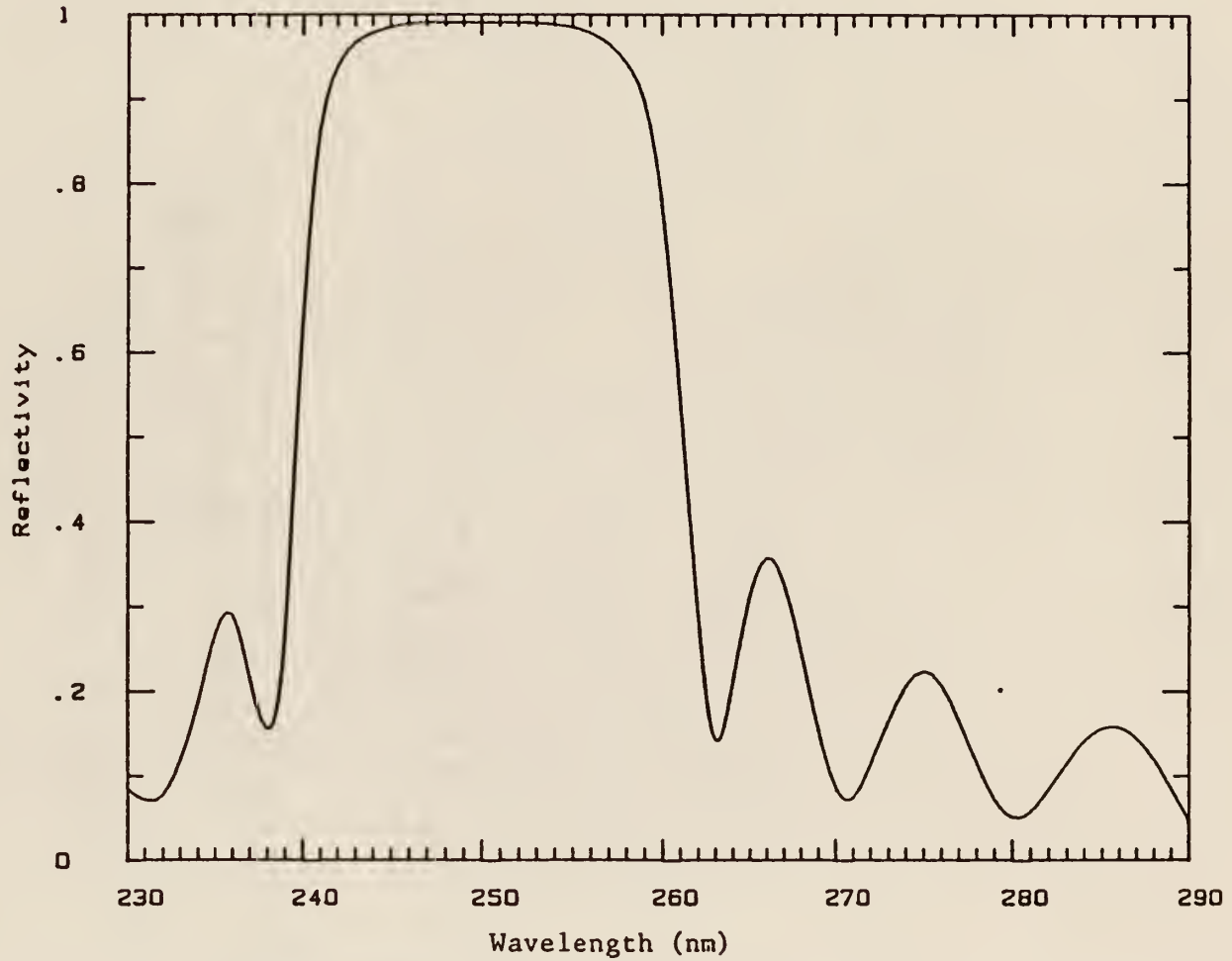

Fig. 5.2 Pre- and post-irradiation reflectivity profiles for dielectric mirror #2.

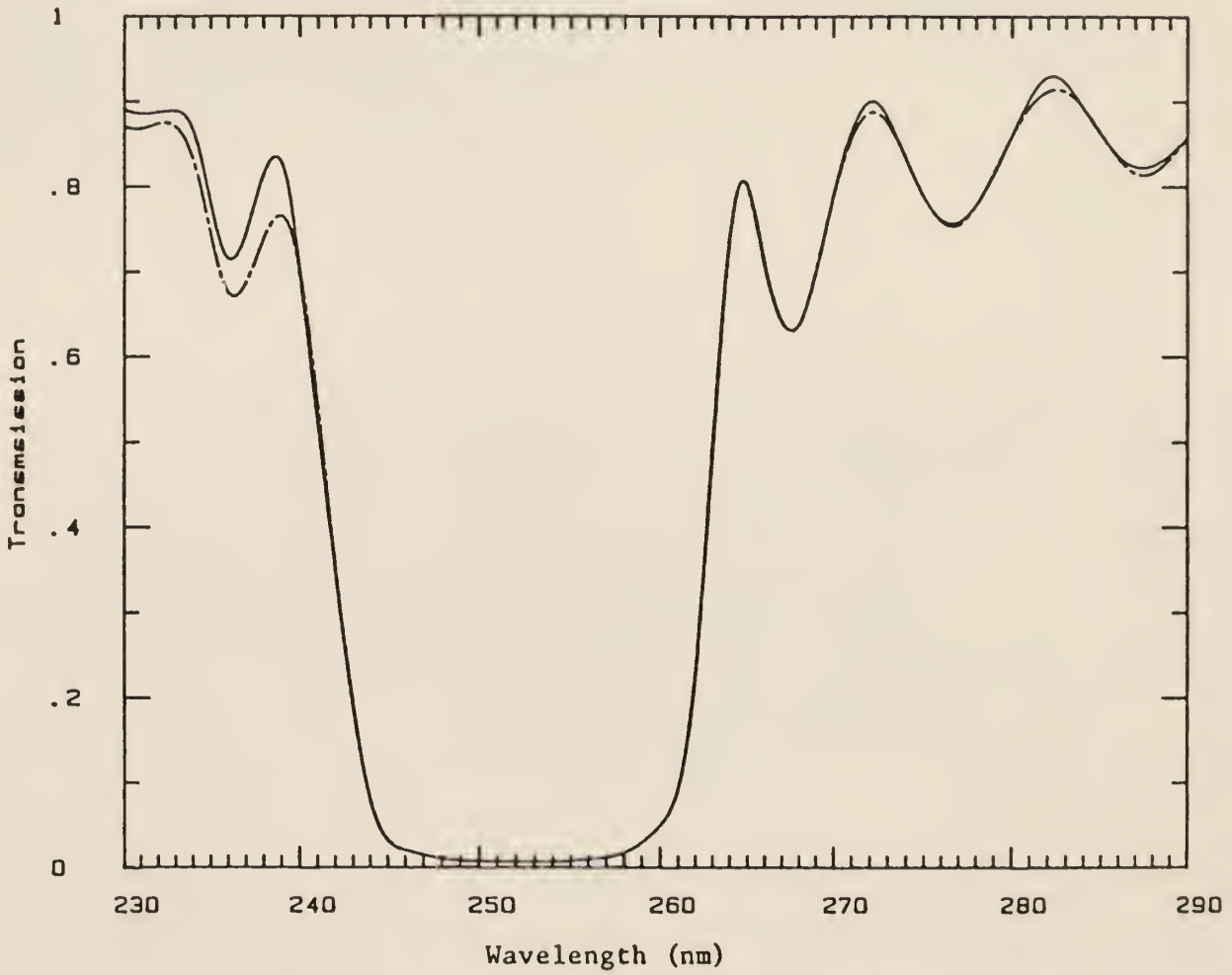

Fig. 5.3 Pre- and post-irradiation transmission profiles for dielectric mirror #2.

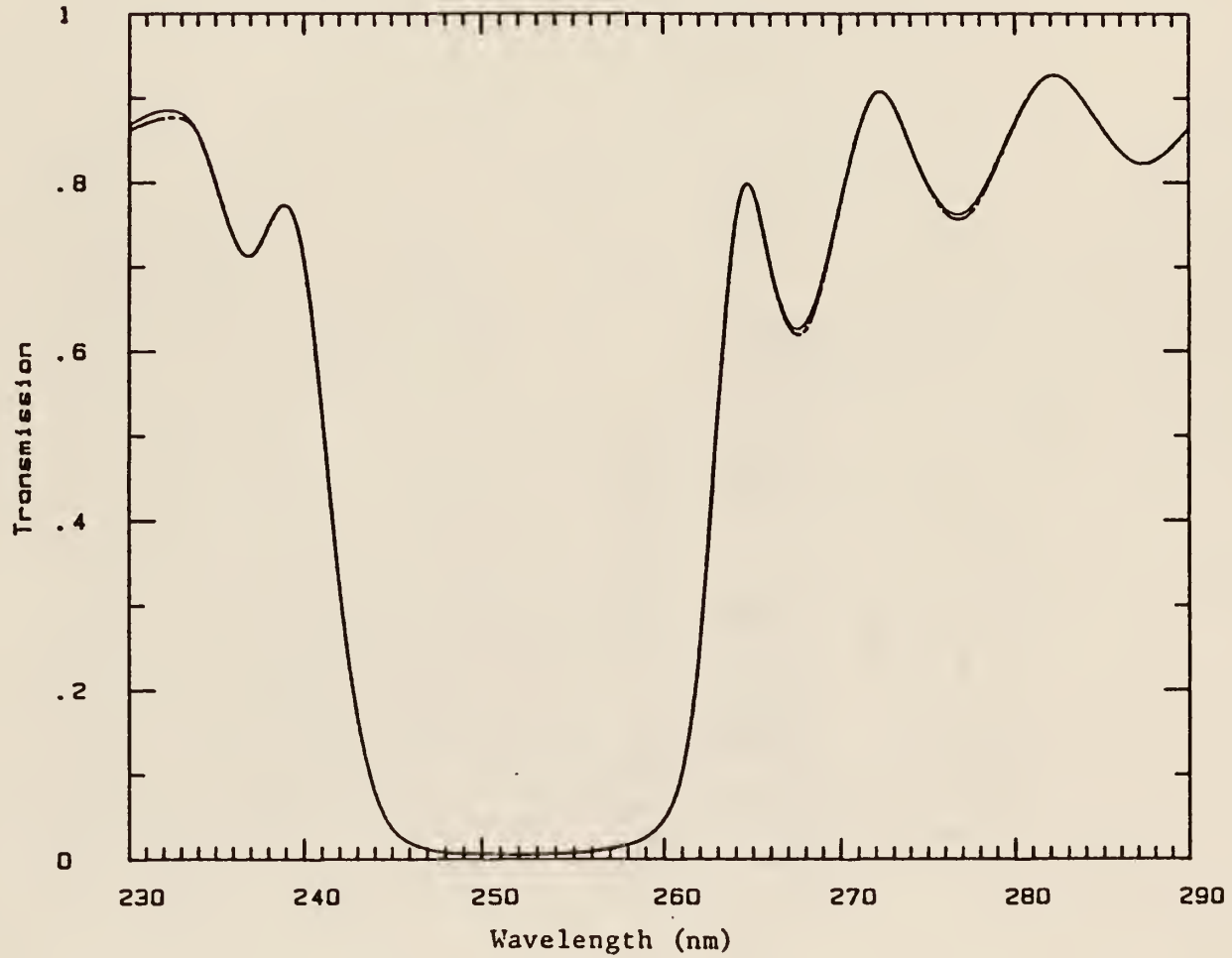

Fig. 5.4 Pre- and post-irradiation transmission profiles for dielectric mirror # 3.

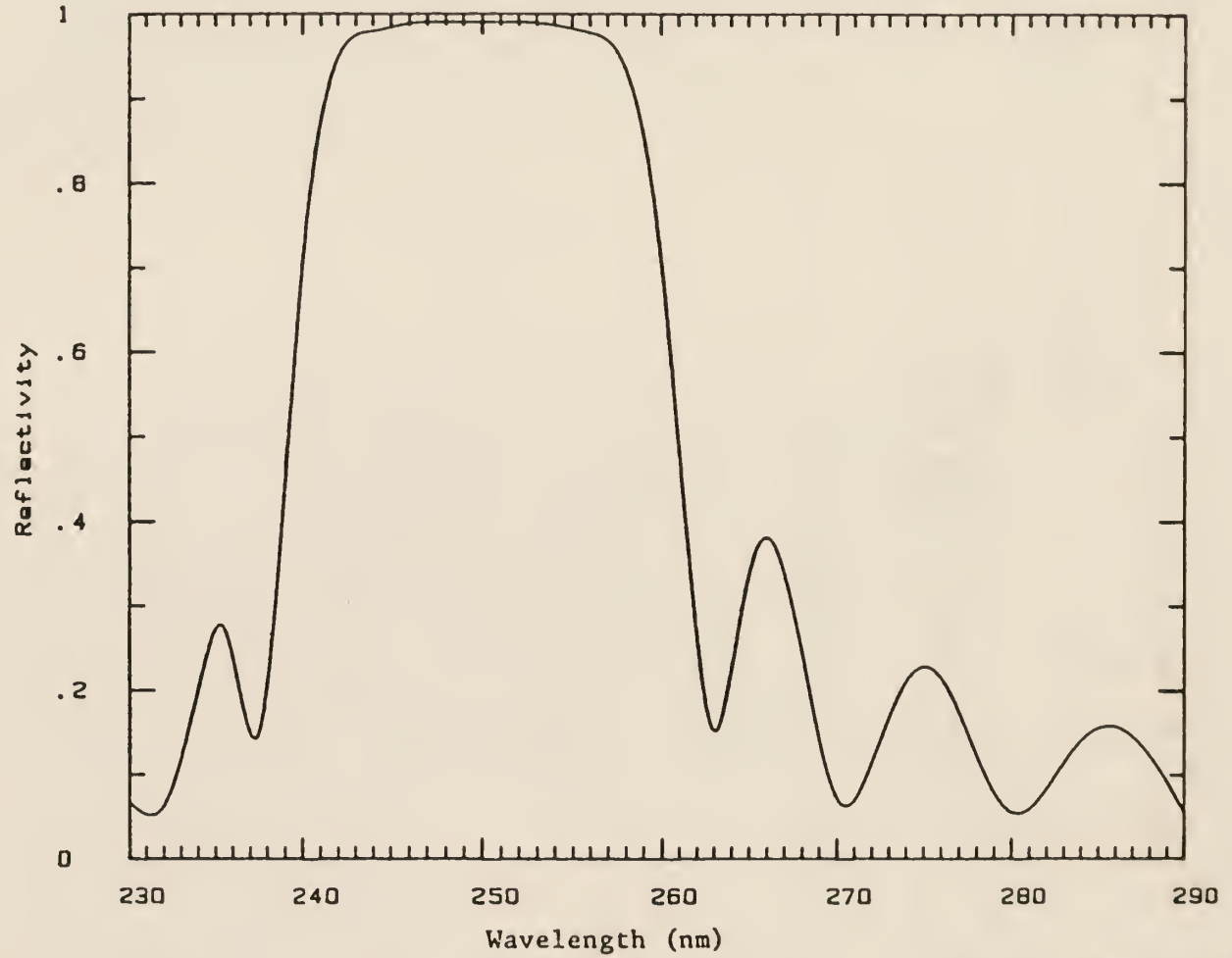

Fig. 5.5 Pre- and post-irradiation reflectivity profiles for dielectric mirror # 3.

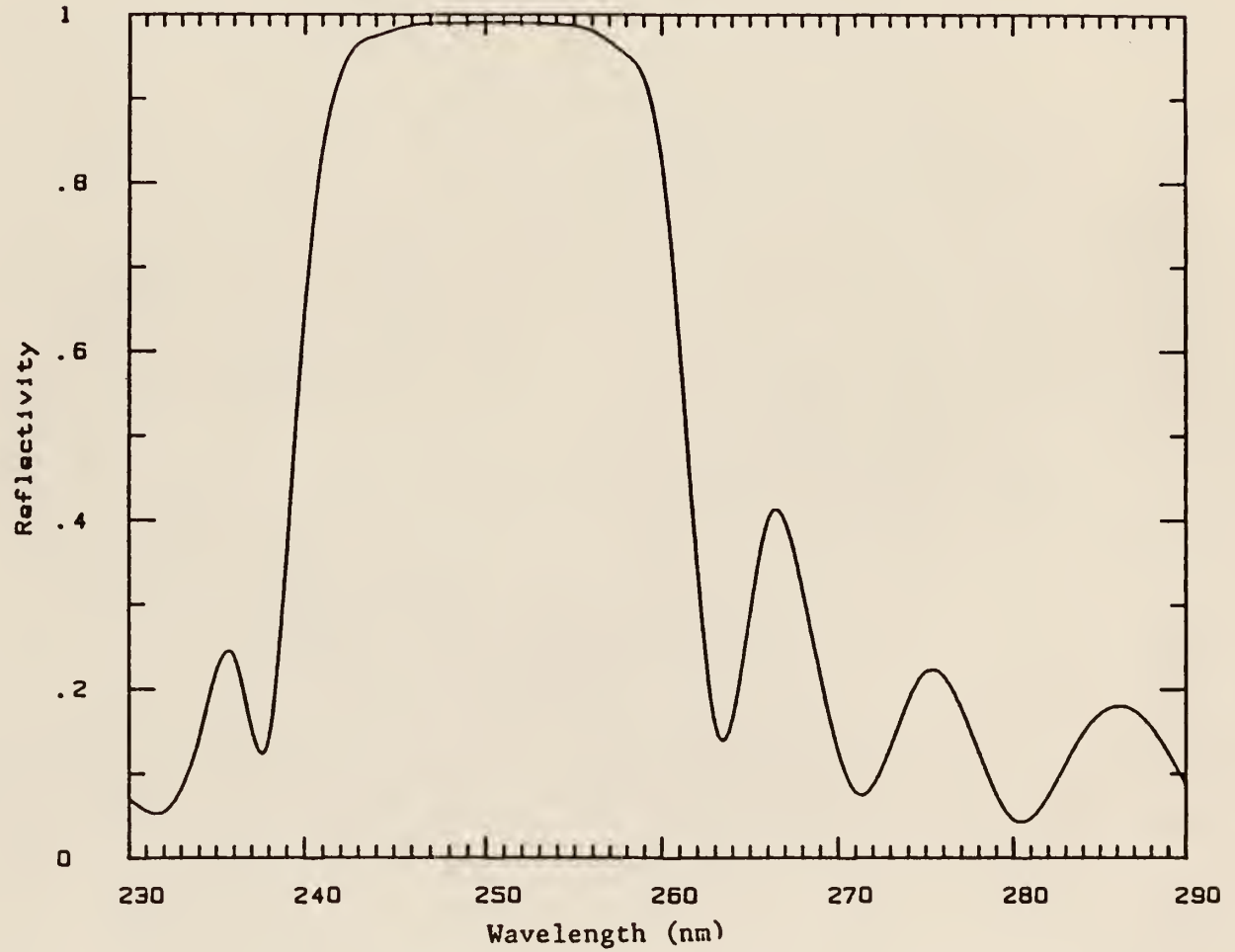

Fig. 5.6 Pre- and post-irradiation reflectivity profiles for dielectric mirror # 4.

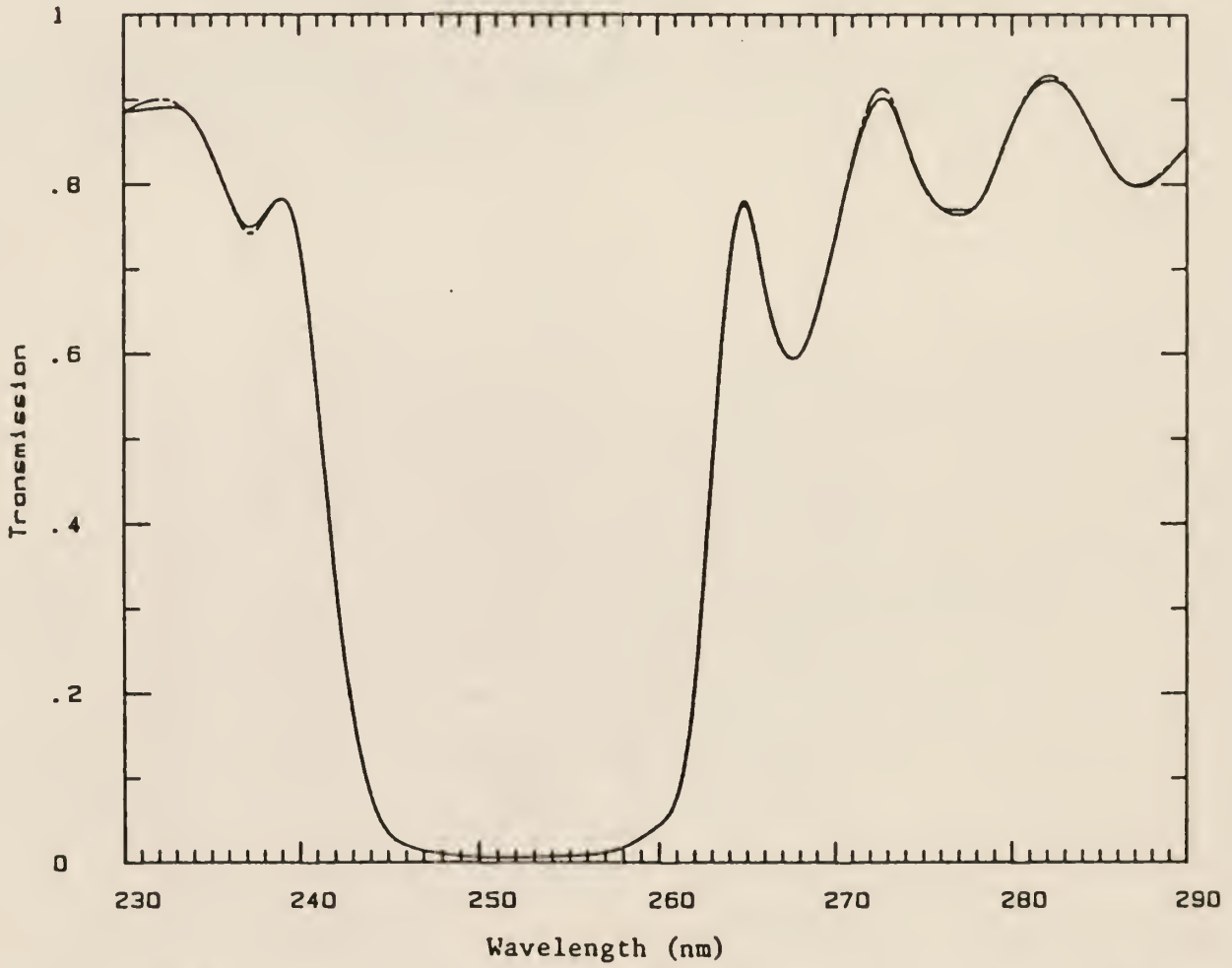

Fig. 5.7 Pre- and post-irradiation transmission profiles for dielectric mirror # 4.

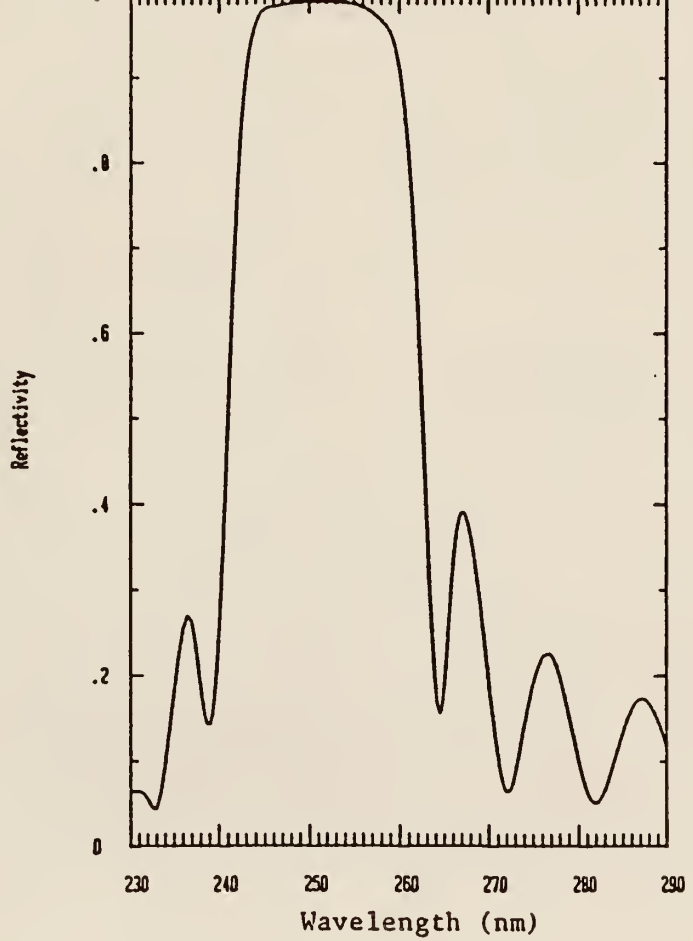

Fig. 5.8 Pre- and post-irradiation reflectivity profiles for dielectric mirror # 5.

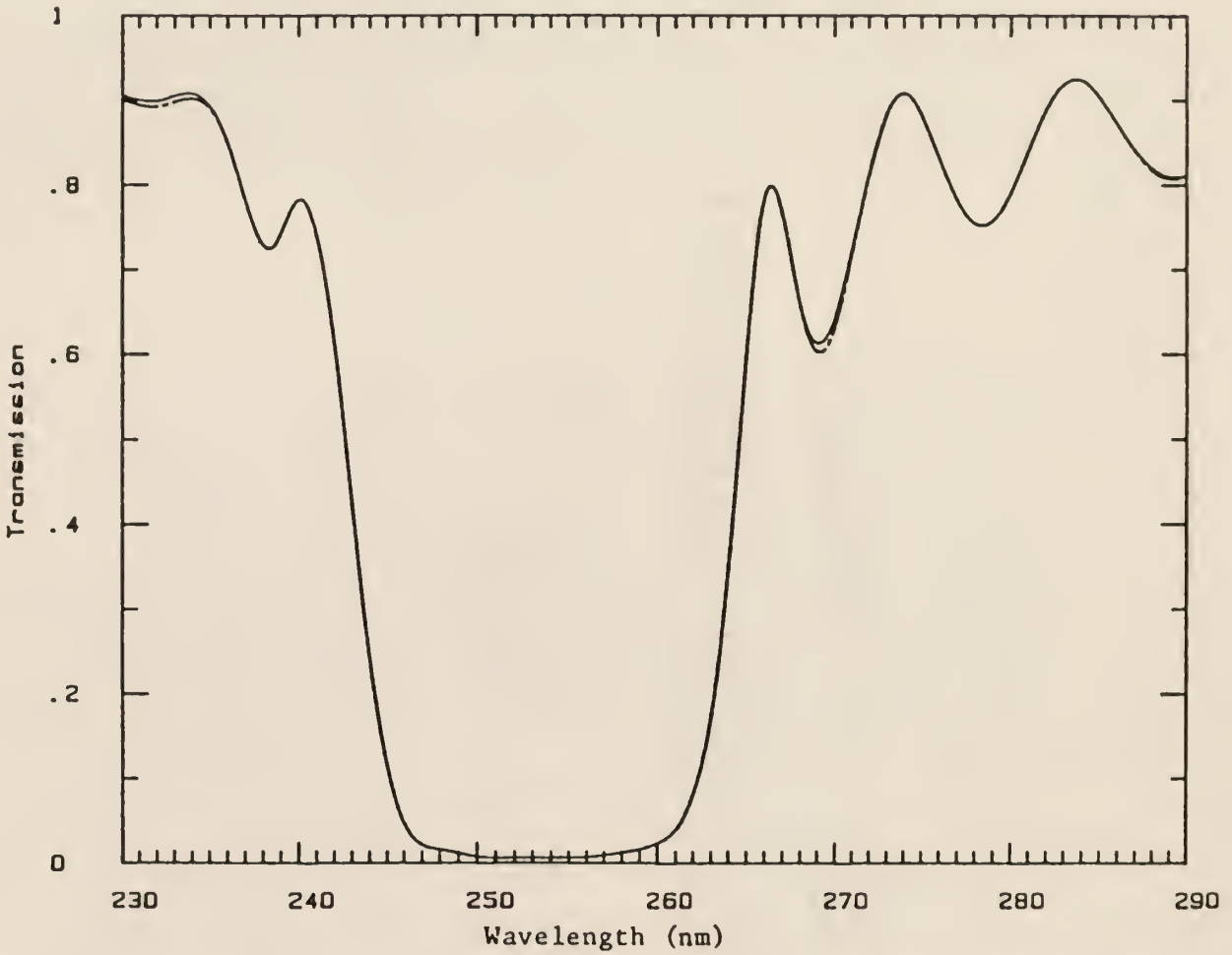

Fig. 5.9 Pre- and post-irradiation transmission profiles for dielectric mirror # 5.

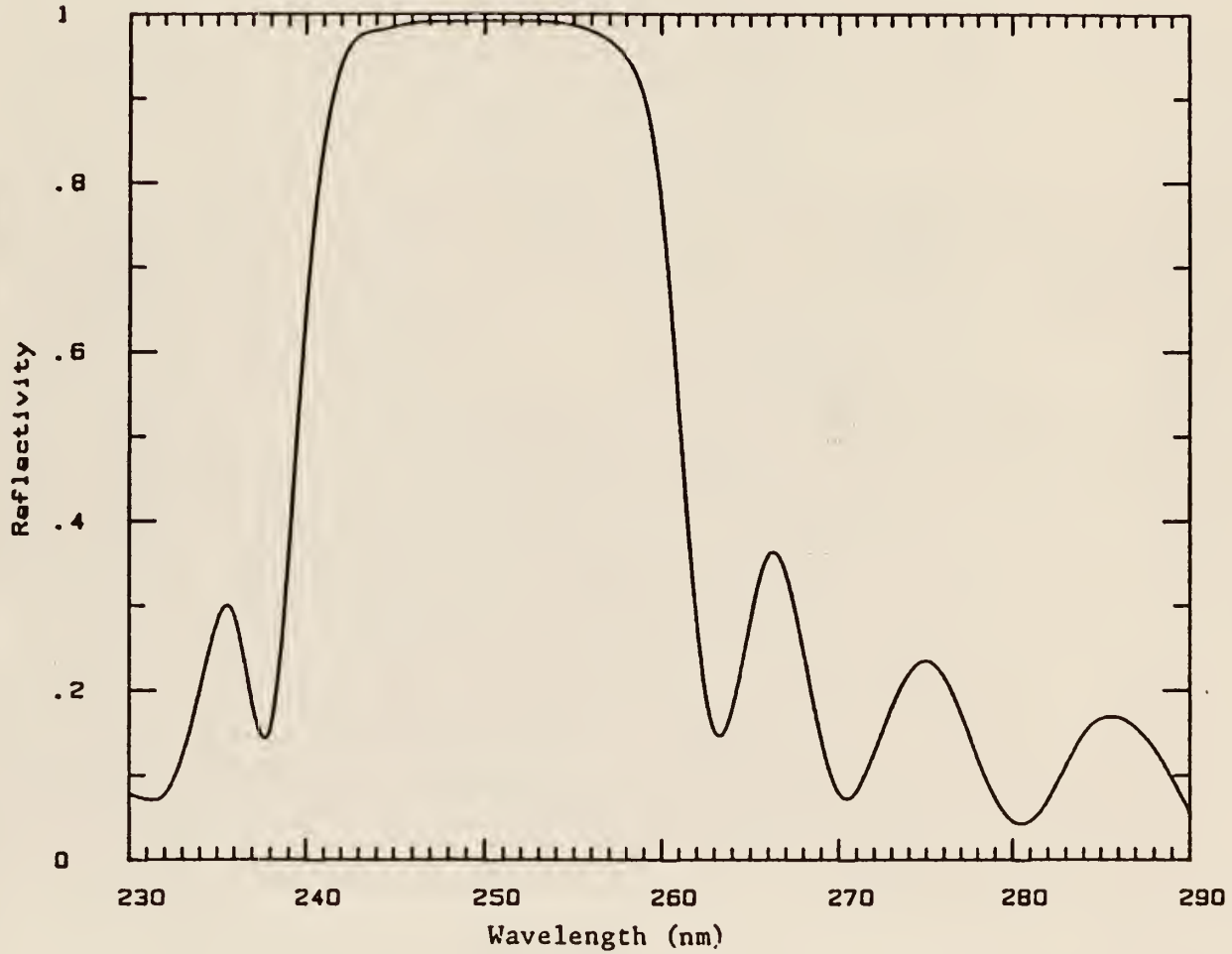

Fig. 5.10 Pre- and post-irradiation reflectivity profiles for dielectric mirror #6.

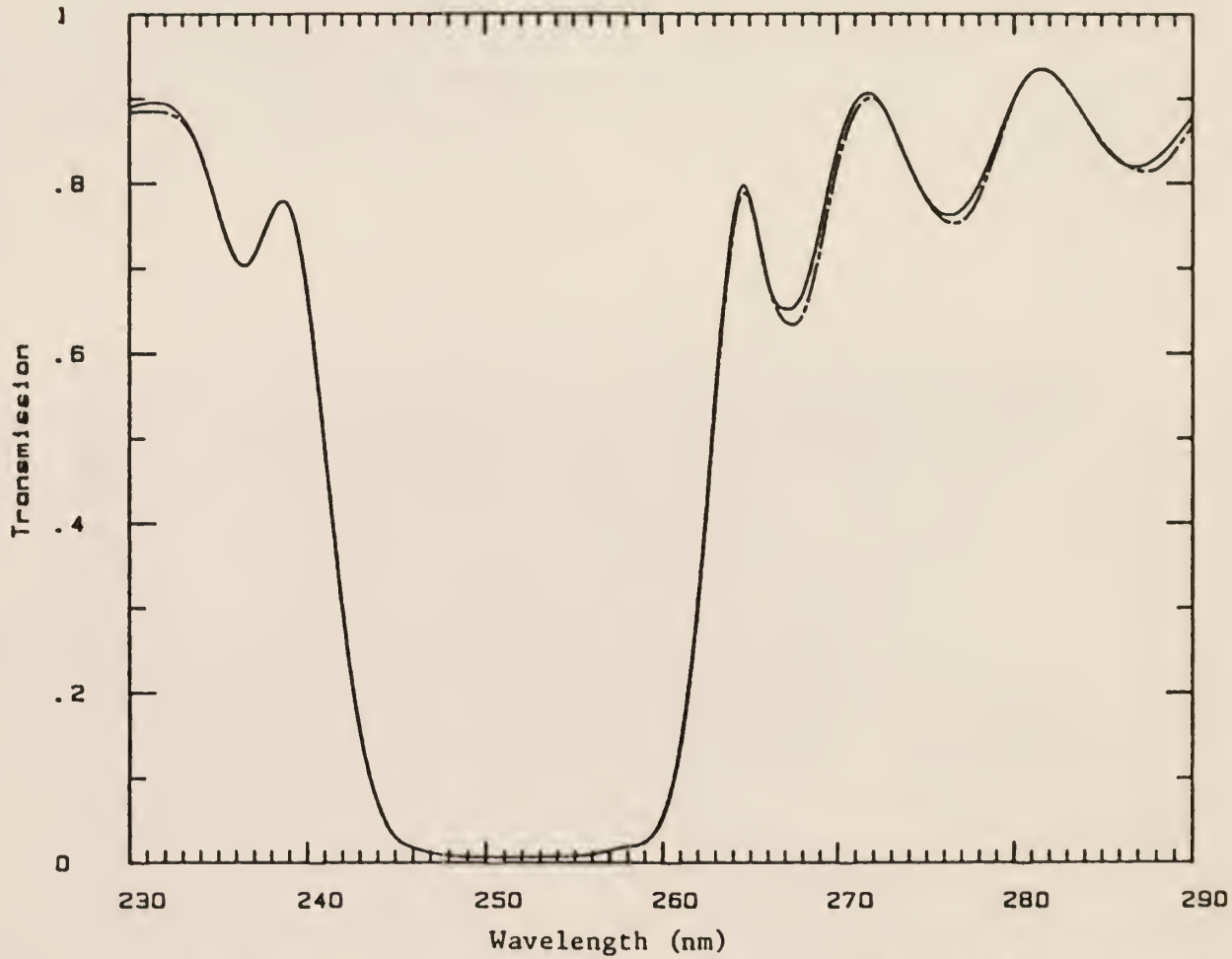

Fig. 5.11 Pre- and post-irradiation transmission profiles for dielectric mirror #6.

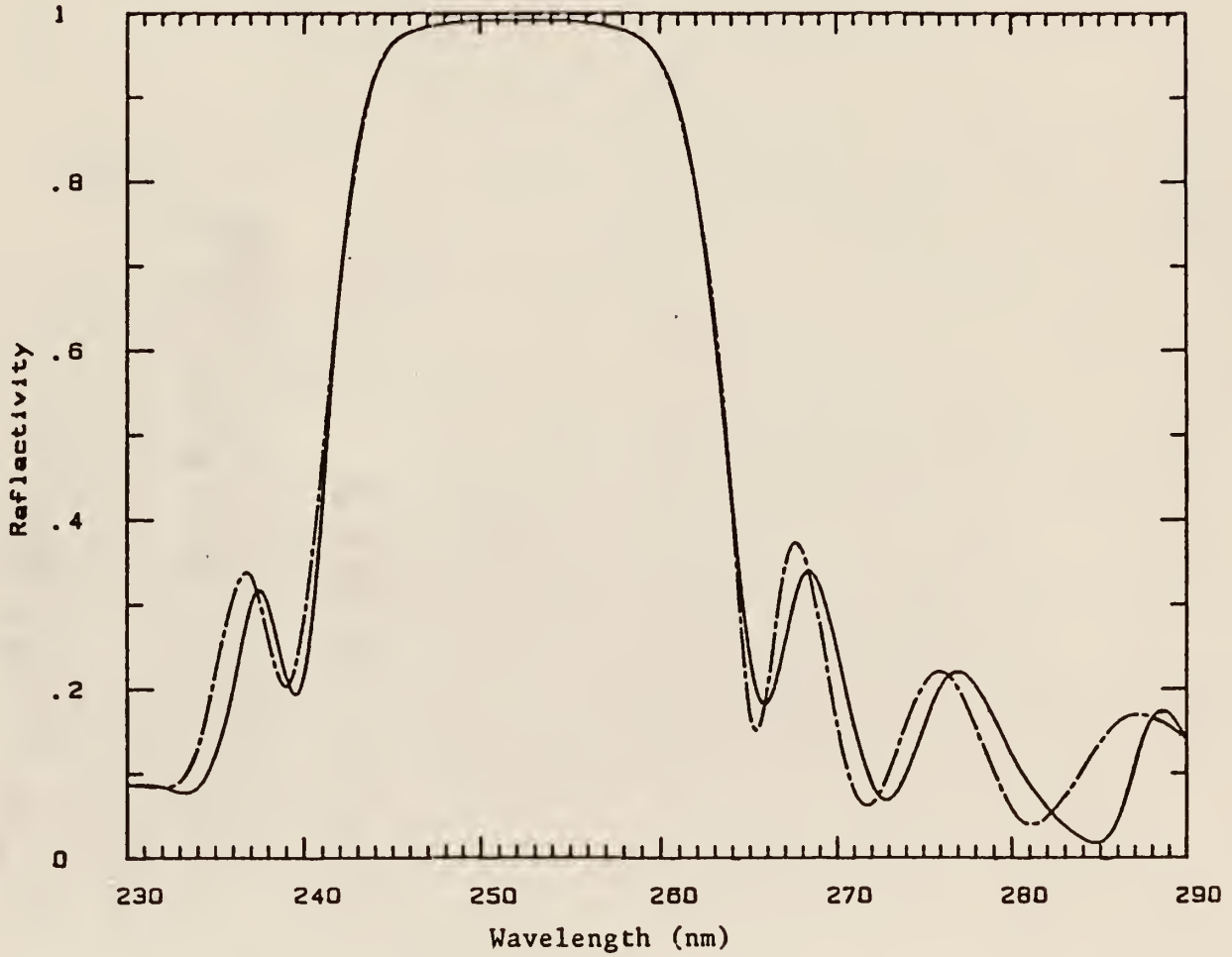

Fig. 5.12 Pre- and post-irradiation reflectivity profiles for dielectric mirror # 7.

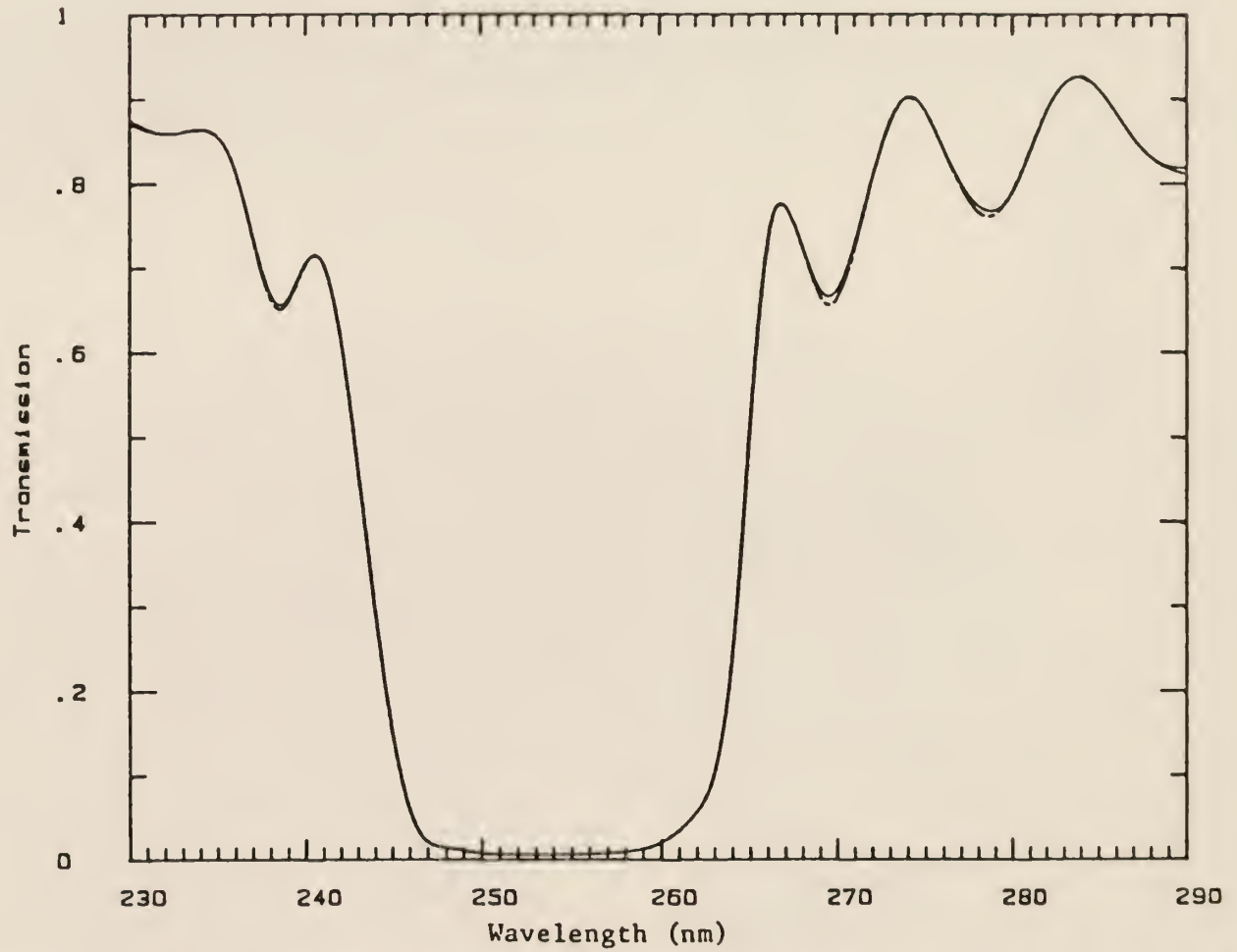

Fig. 5.13 Pre- and post-irradiation transmission profiles for dielectric mirror # 7.

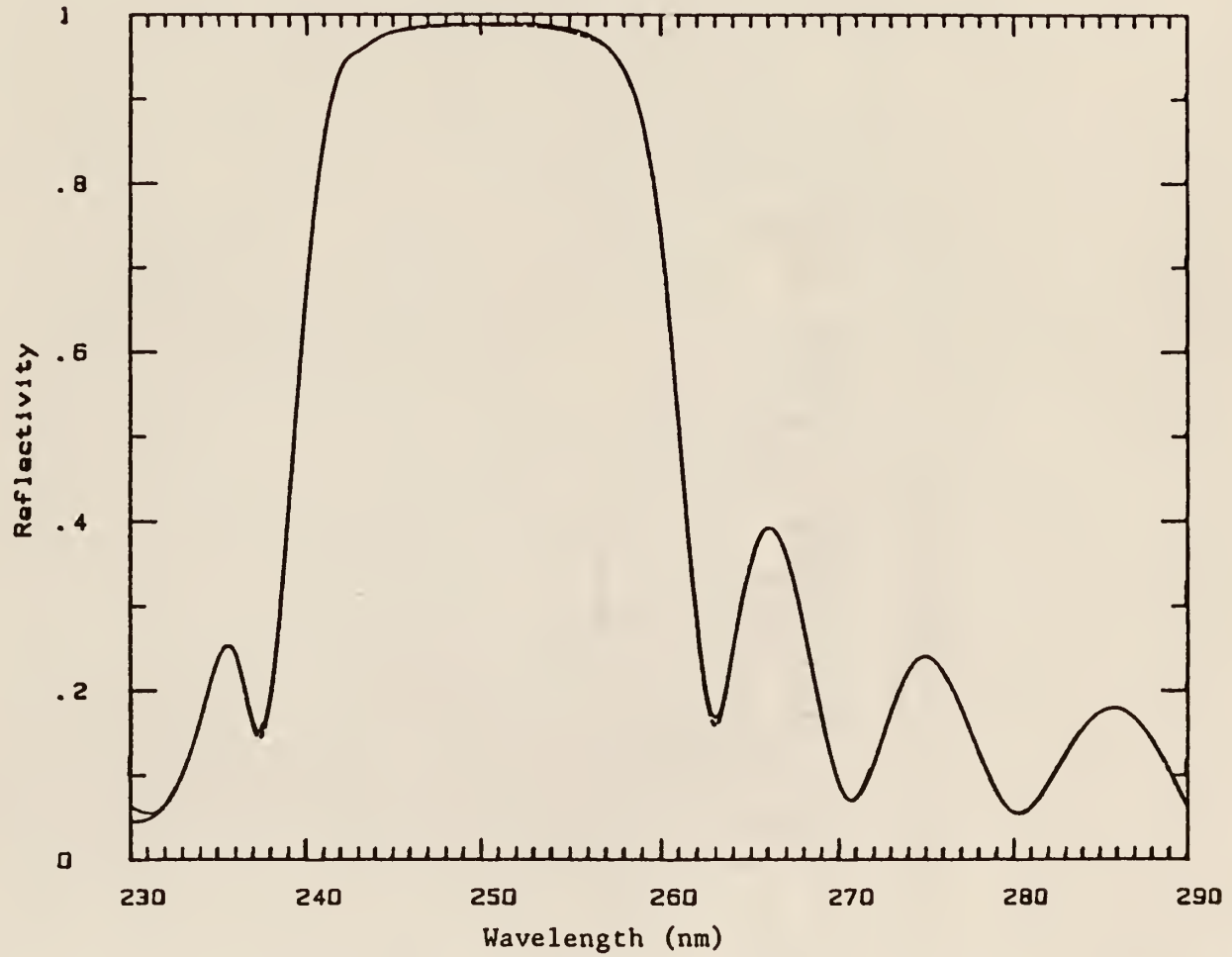

Fig. 5.14 Pre- and post-irradiation reflectivity profiles for dielectric mirror # 8.

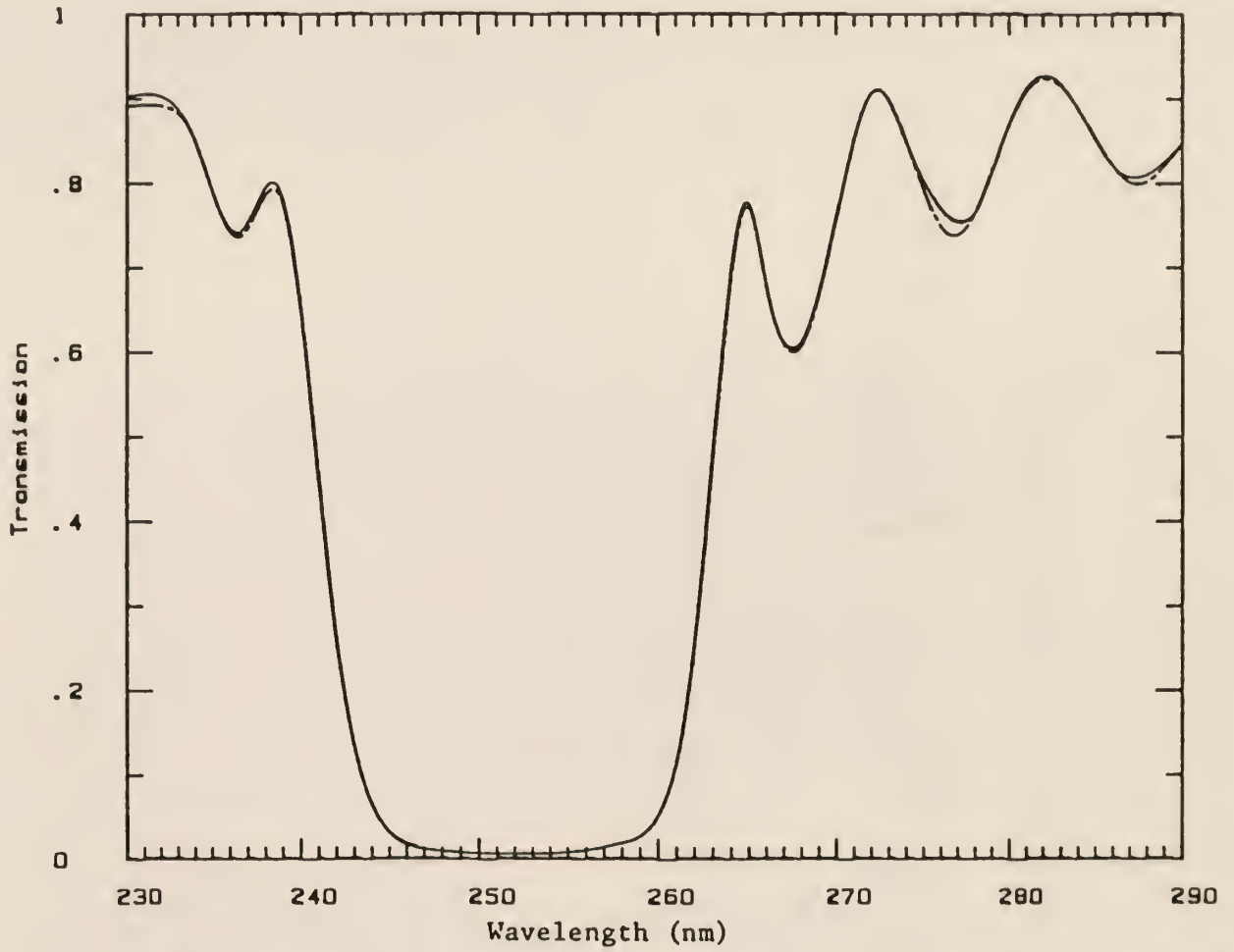

Fig. 5.15 Pre- and post-irradiation transmission profiles for dielectric mirror # 8.

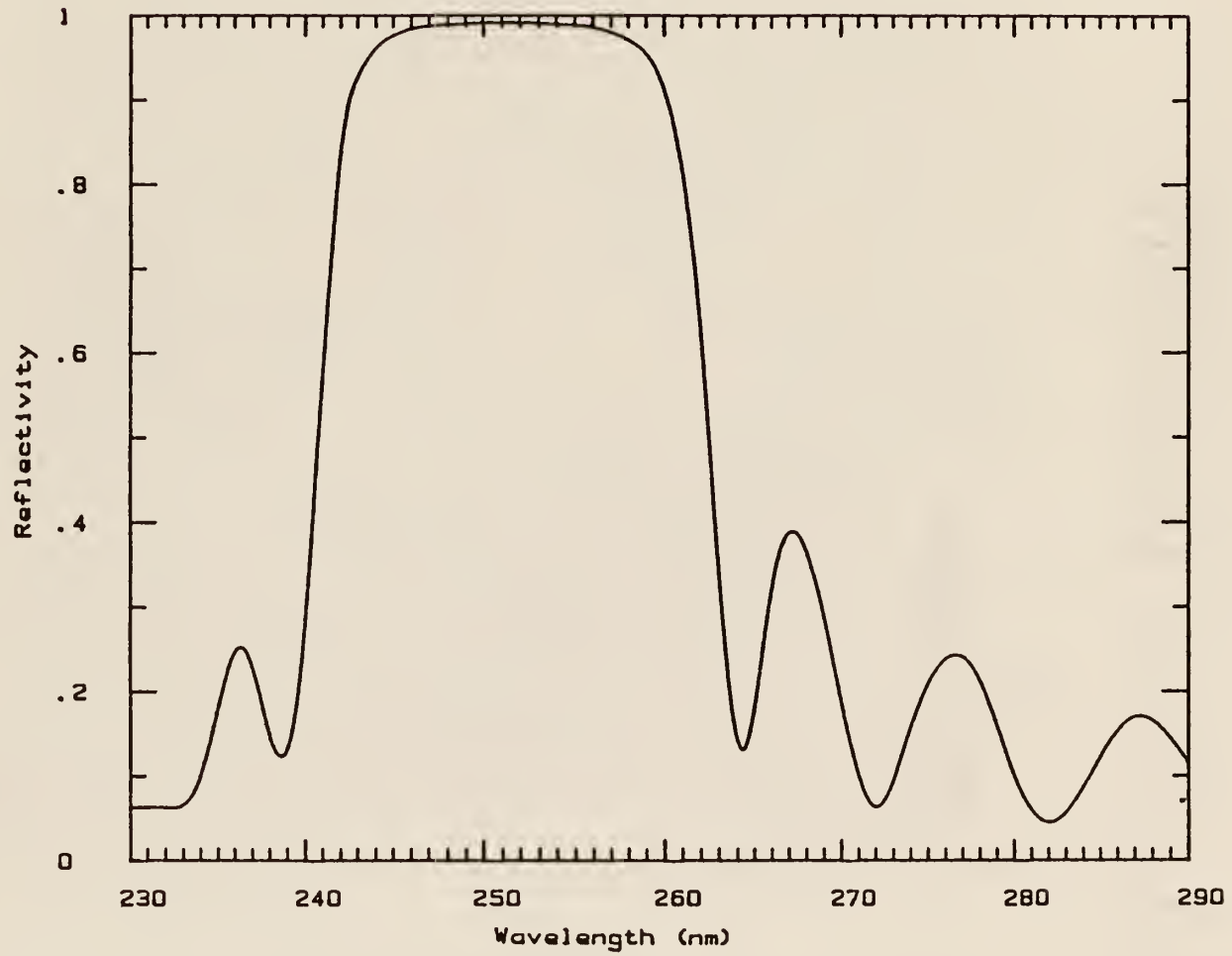

Fig. 5.16 Pre- and post-irradiation reflectivity profiles for dielectric mirror # 9.

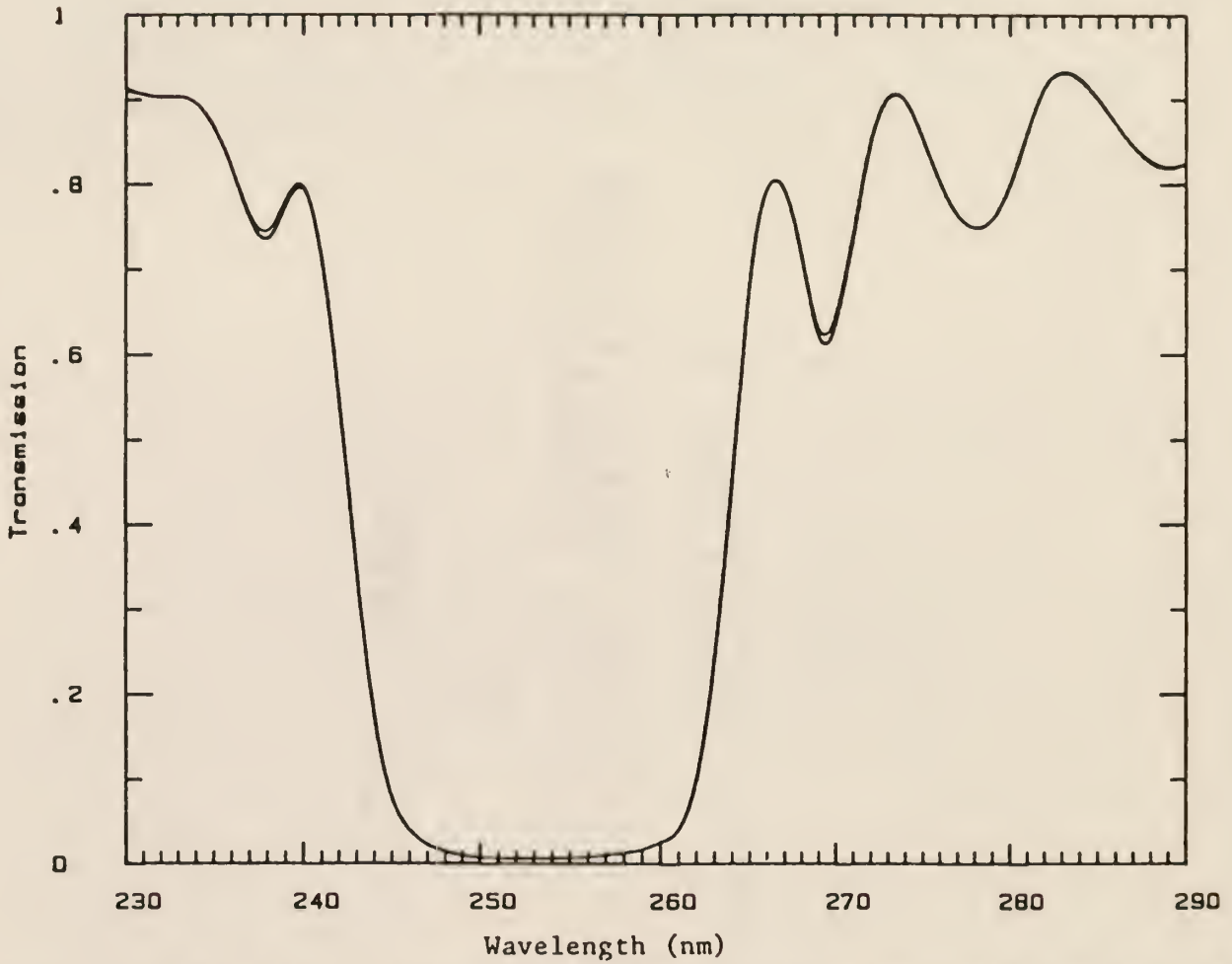

Fig. 5.17 Pre- and post-irradiation transmission profiles for dielectric mirror # 9.

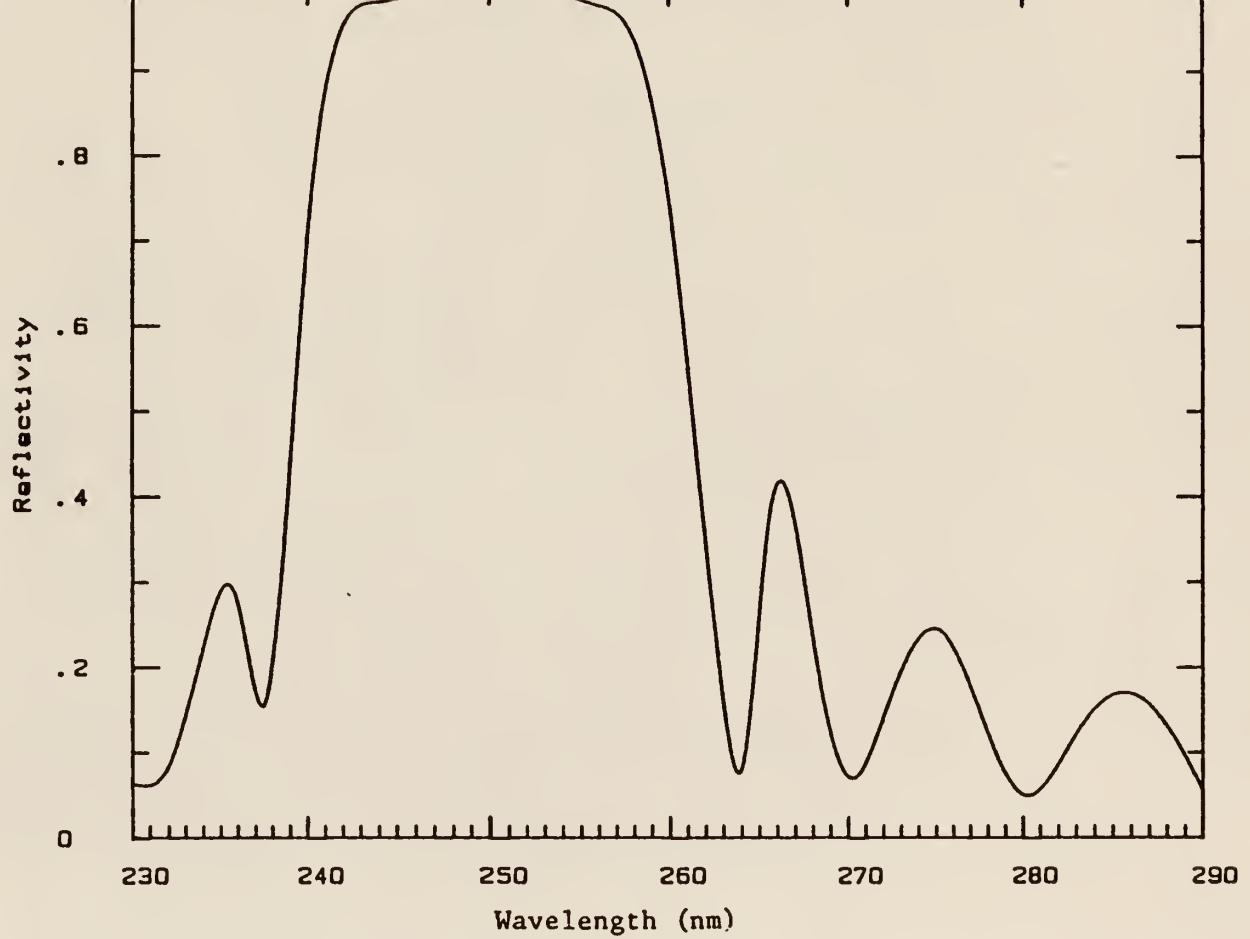

Fig. 5.18 Pre- and post-irradiation reflectivity profiles for dielectric mirror # 10.

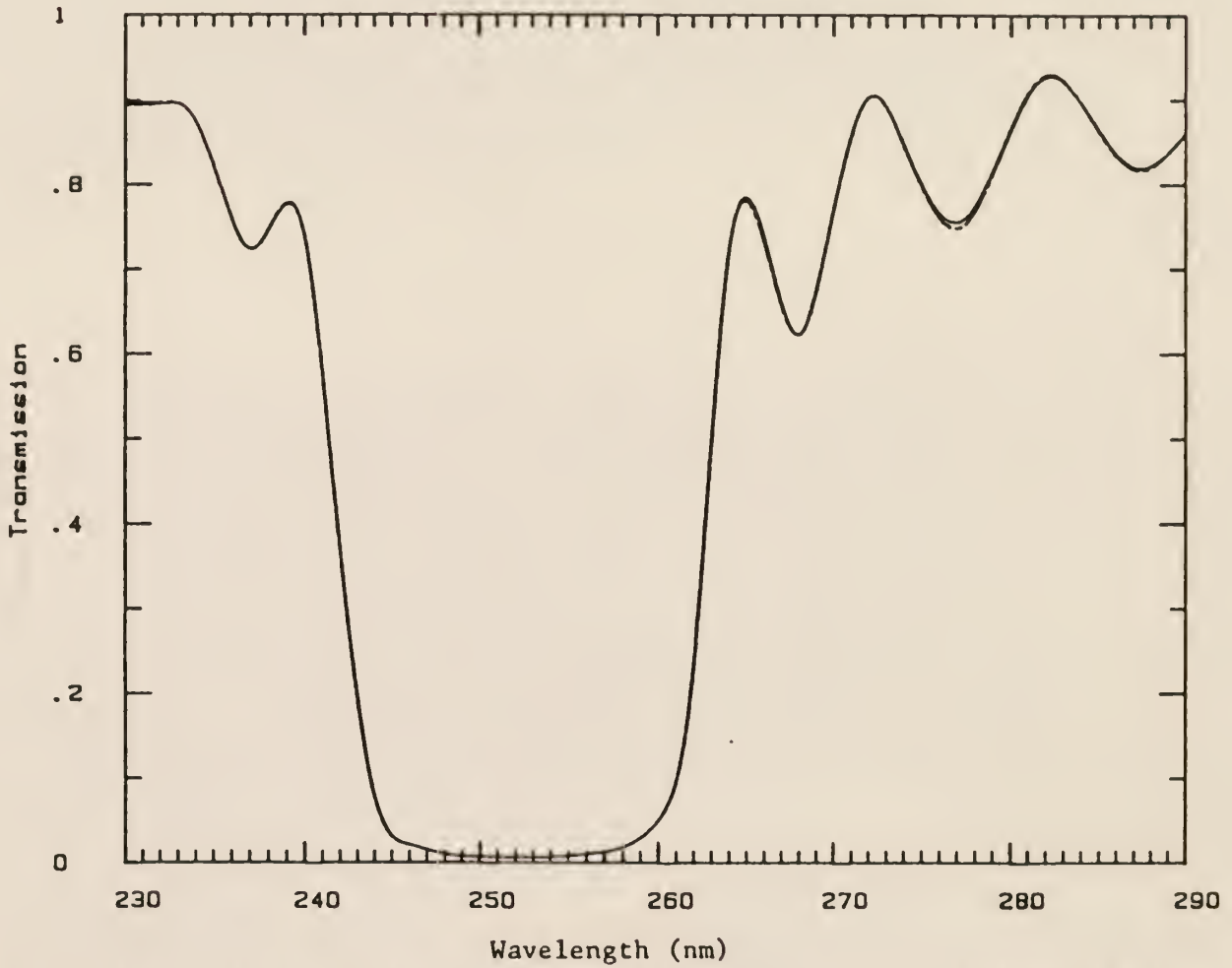

Fig. 5.19 Pre- and post-irradiation transmission profiles for dielectric mirror # 10.

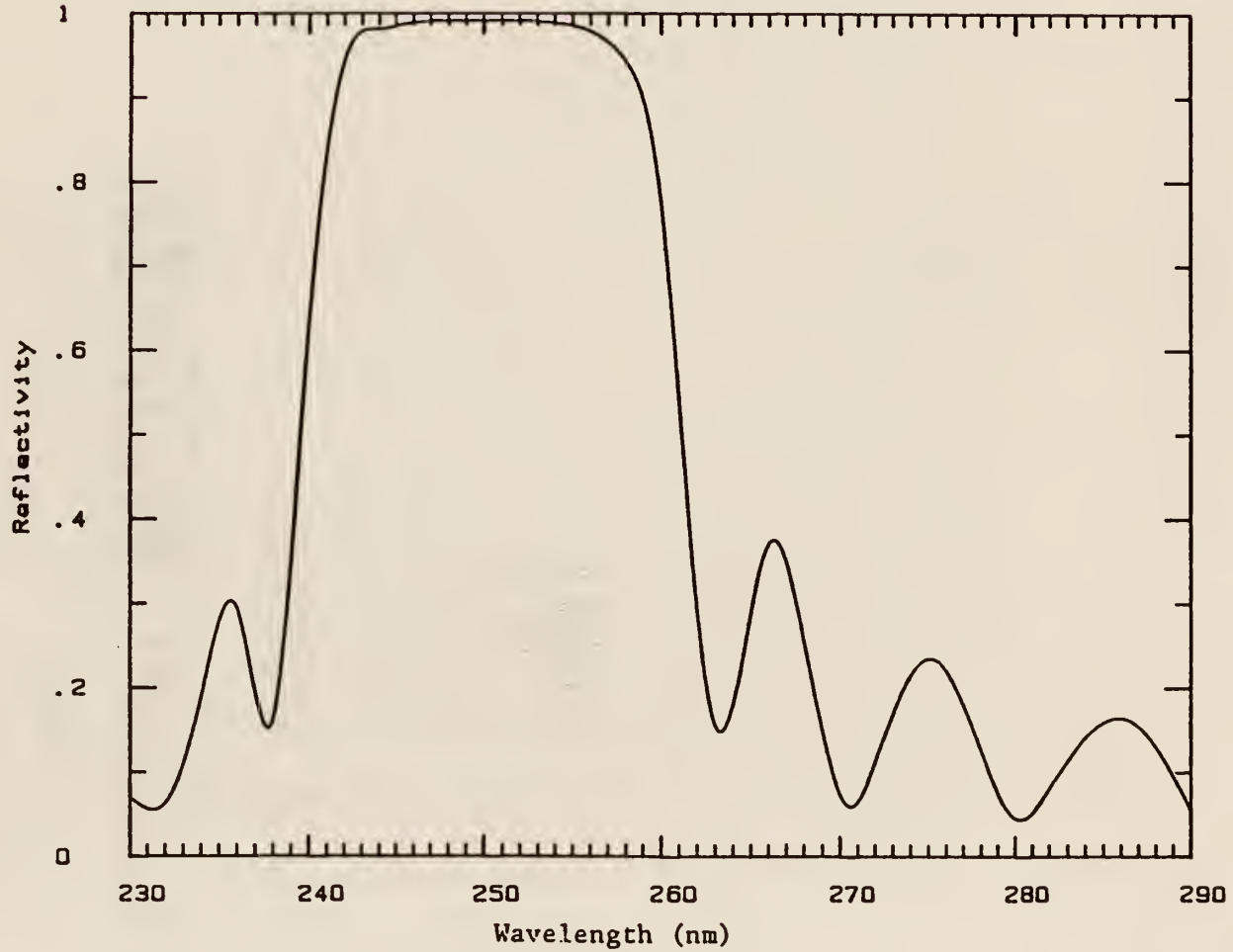

Fig. 5.20 Pre- and post-irradiation reflectivity profiles for dielectric mirror # 11.

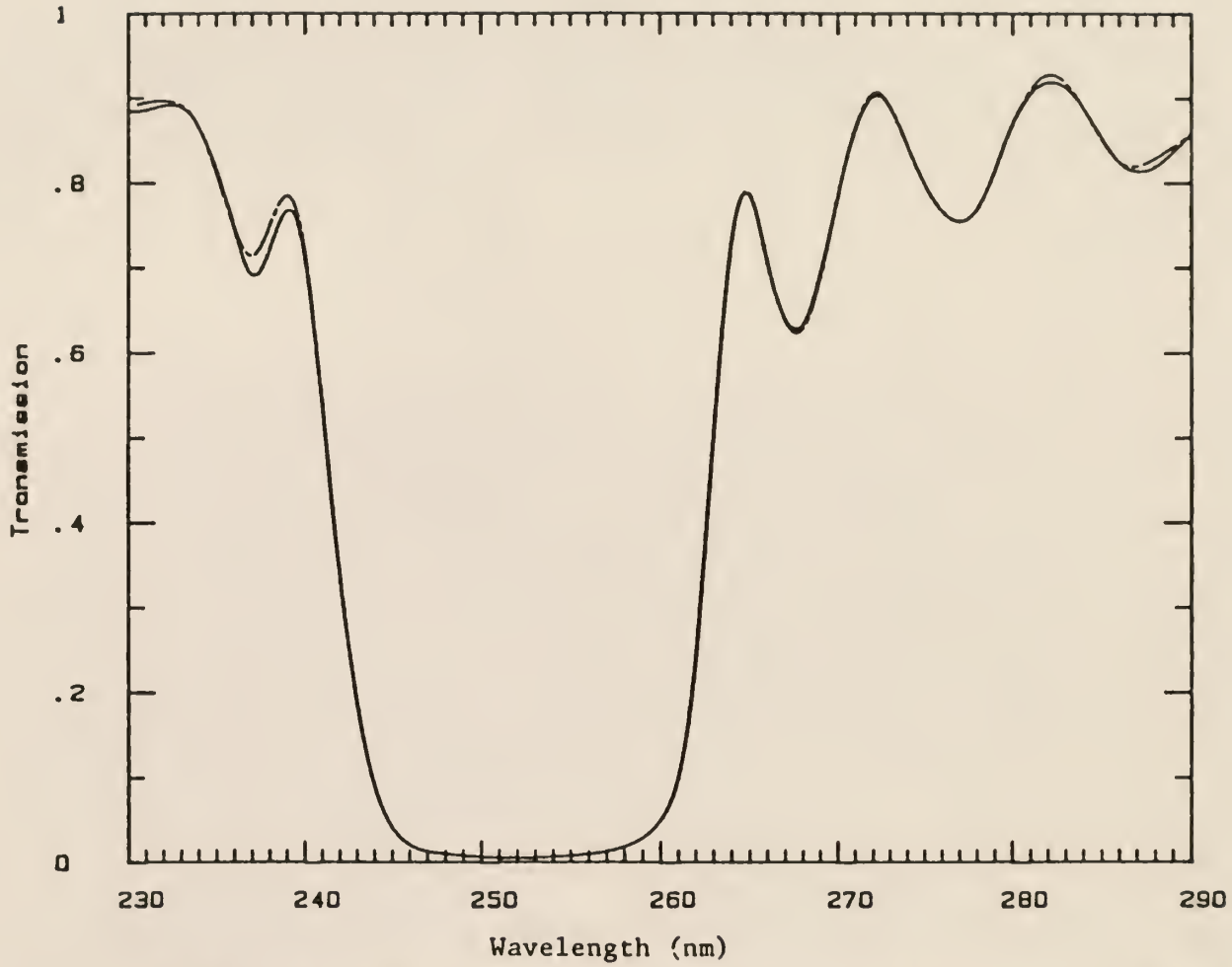

Fig. 5.21 Pre- and post-irradiation transmission profiles for dielectric mirror # 11.

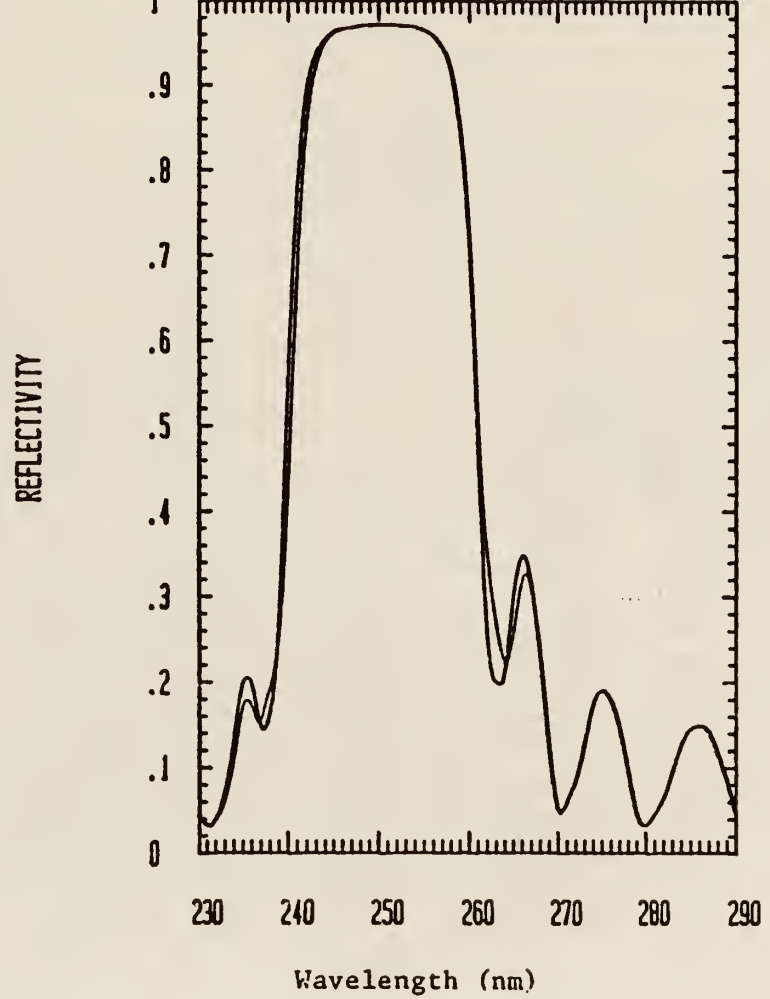

Fig. 5.22 Pre- and post-irradiation reflectivity profiles for dielectric mirror # 12.

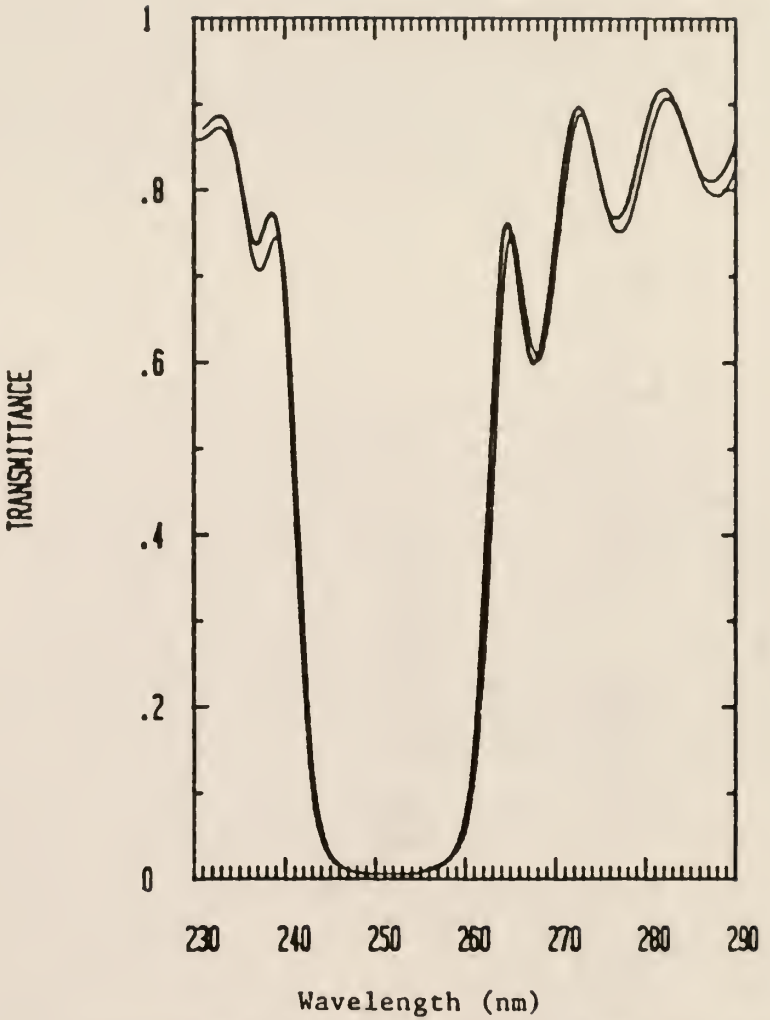

Fig. 5.23 Pre- and post-irradiation transmission profiles for dielectric mirror # 12.

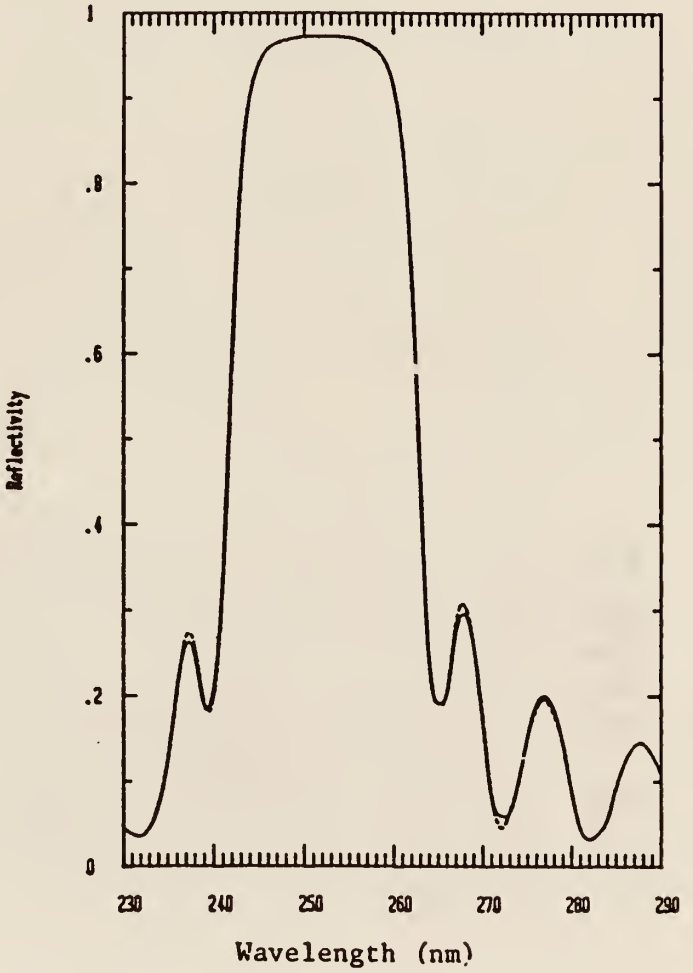

Fig. 5.24 Pre- and post-irradiation reflectivity profiles for dielectric mirror # 13.

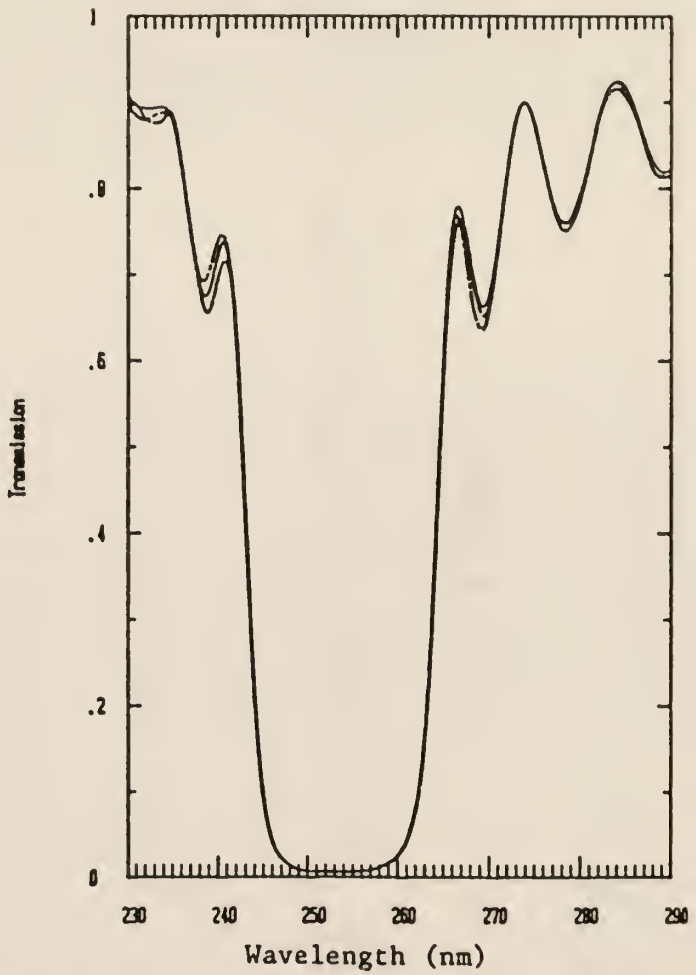

Fig. 5.25 Pre- and post-irradiation transmission profiles for dielectric mirror # 13.

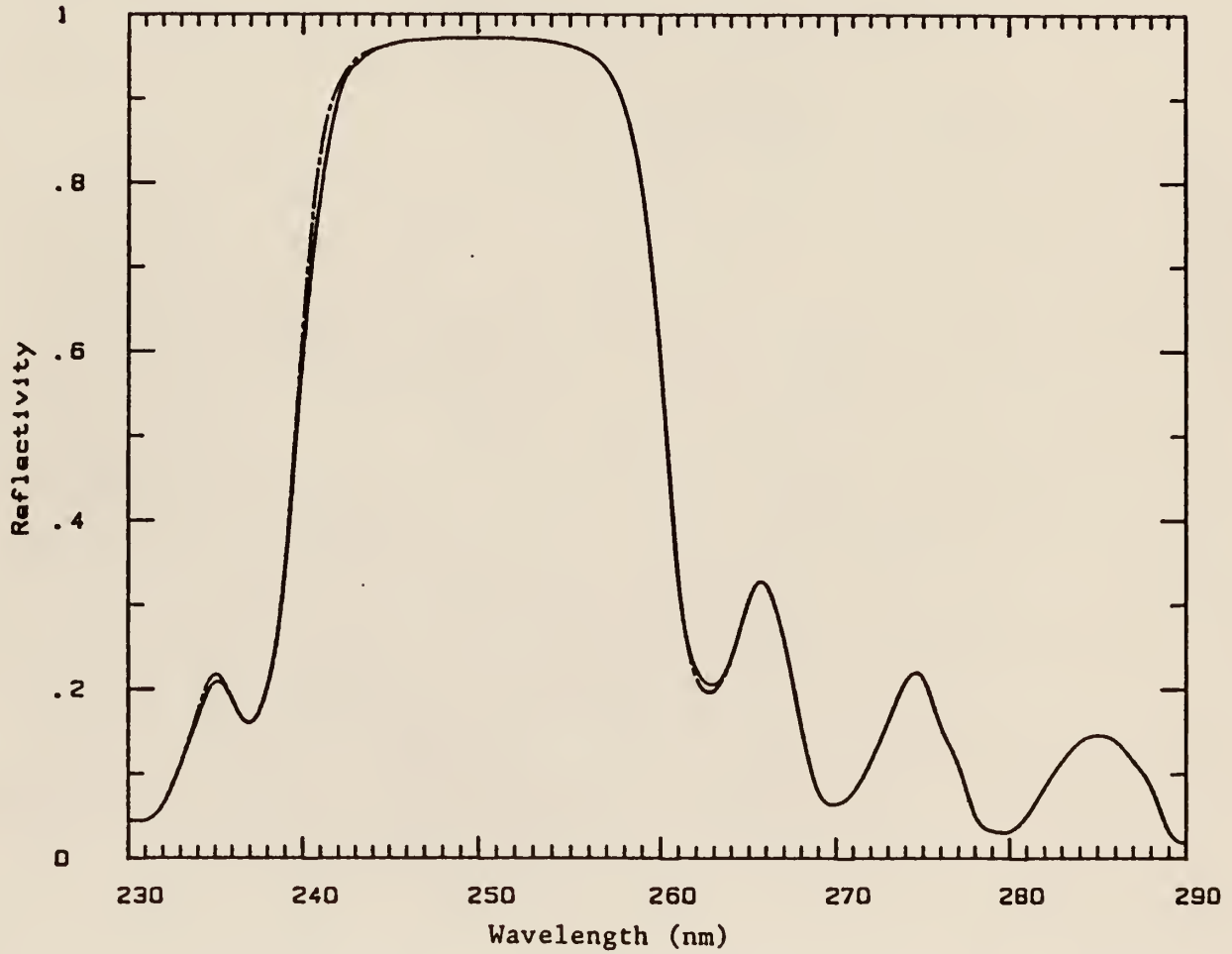

Fig. 5.26 Pre- and post-irradiation reflectivity profiles for dielectric mirror # 14.

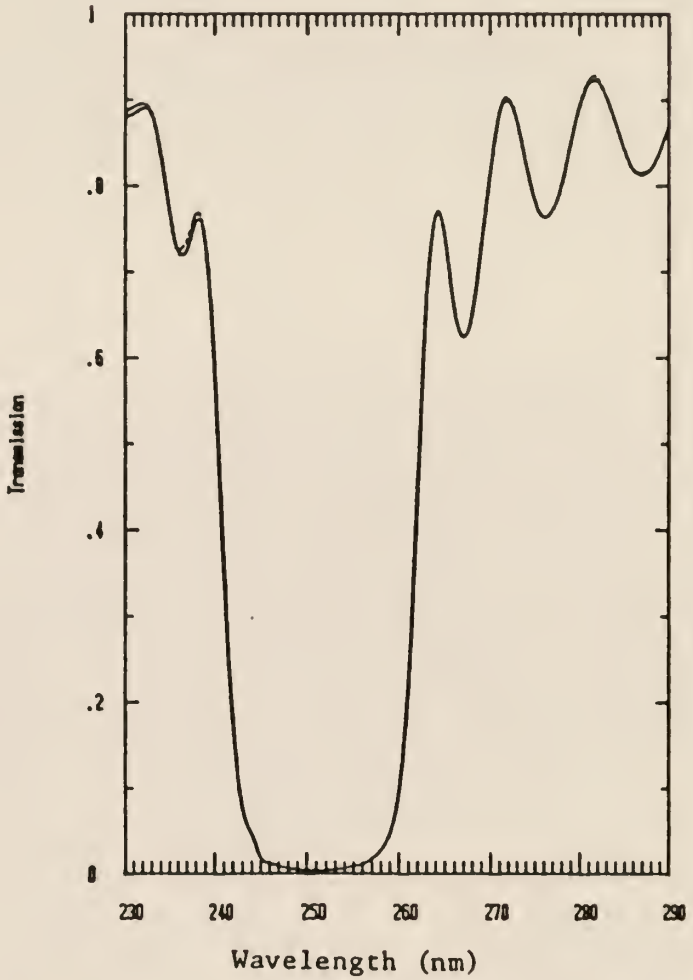

Fig. 5.27 Pre- and post-irradiation transmission profiles for dielectric mirror # 14.

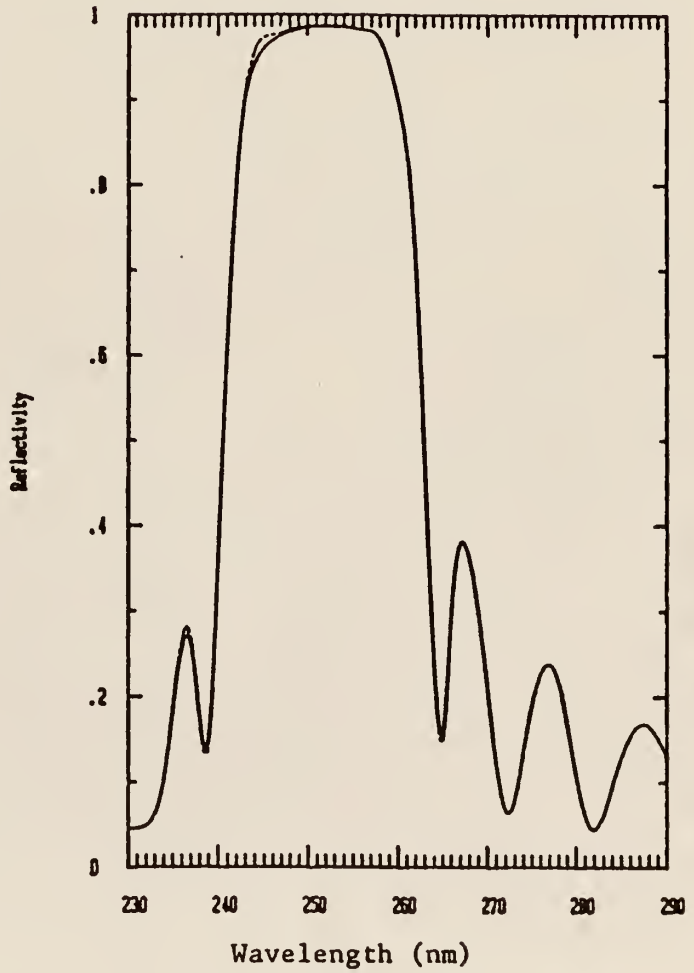

Fig. 5.28 Pre- and post-irradiation reflectivity profiles for dielectric mirror # 26.

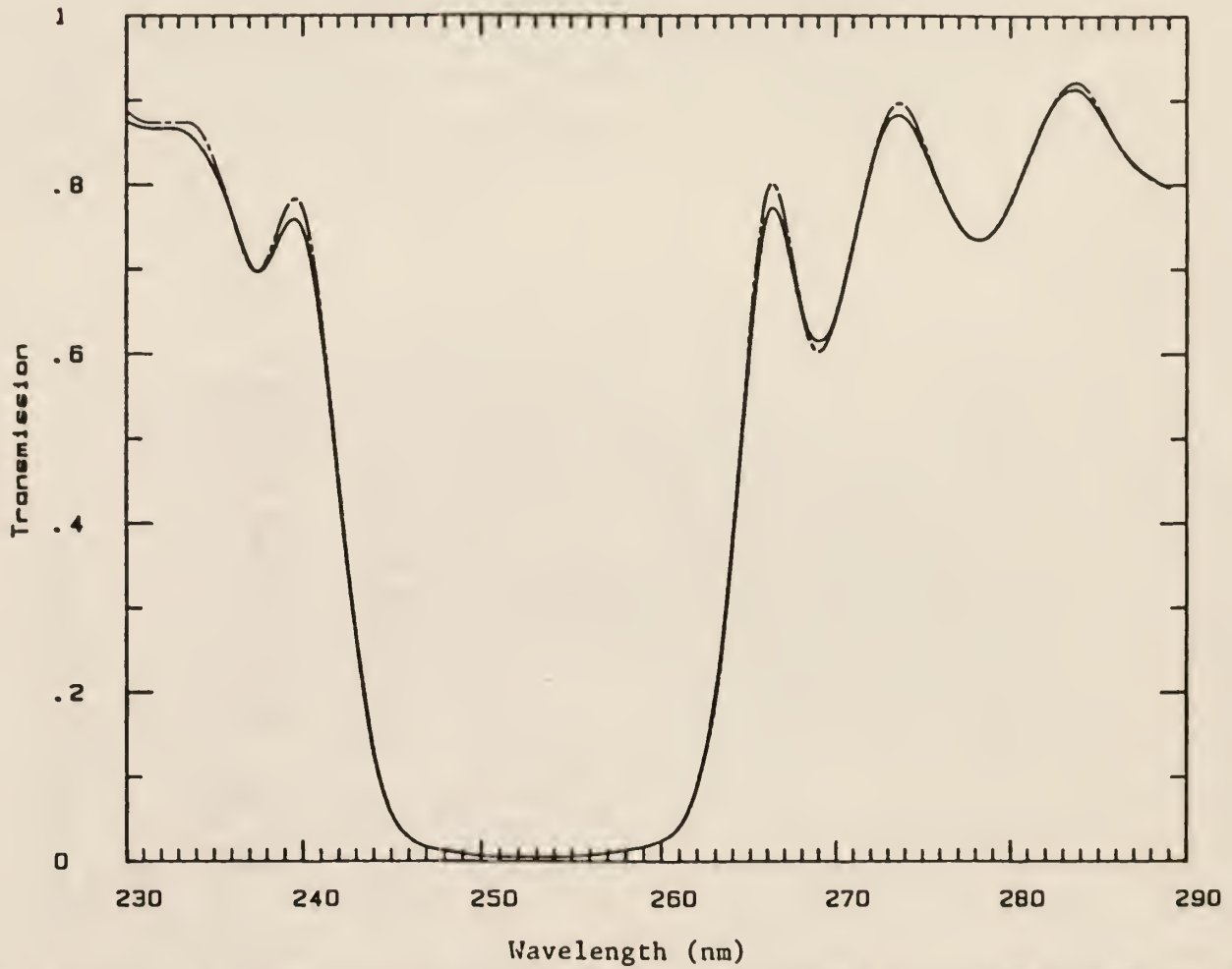

Fig. 5.29 Pre- and post-irradiation transmission profiles for dielectric mirror # 26.

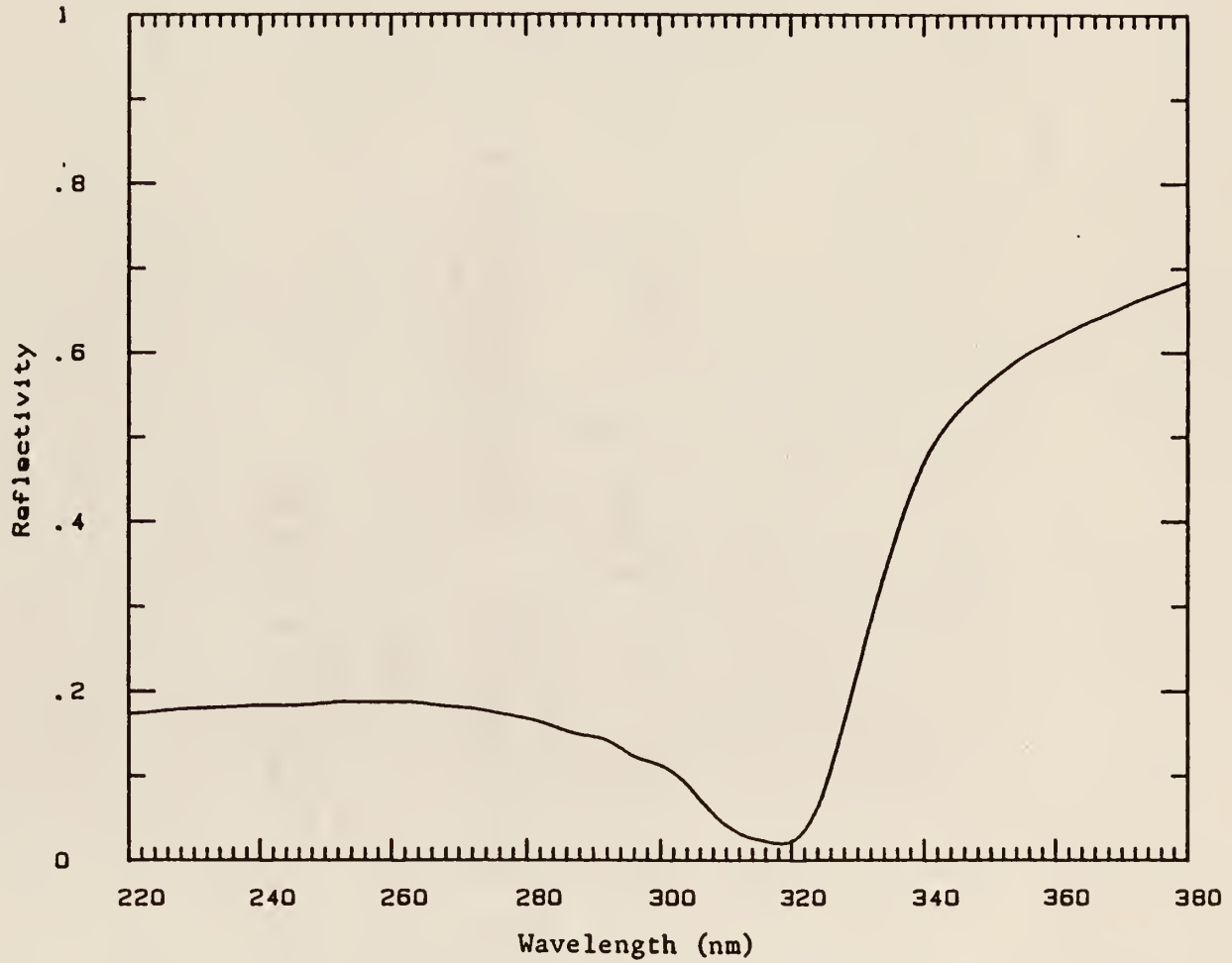

Fig. 5.30 Pre- and post-irradiation reflectivity profiles for metal-coated mirror #1L.

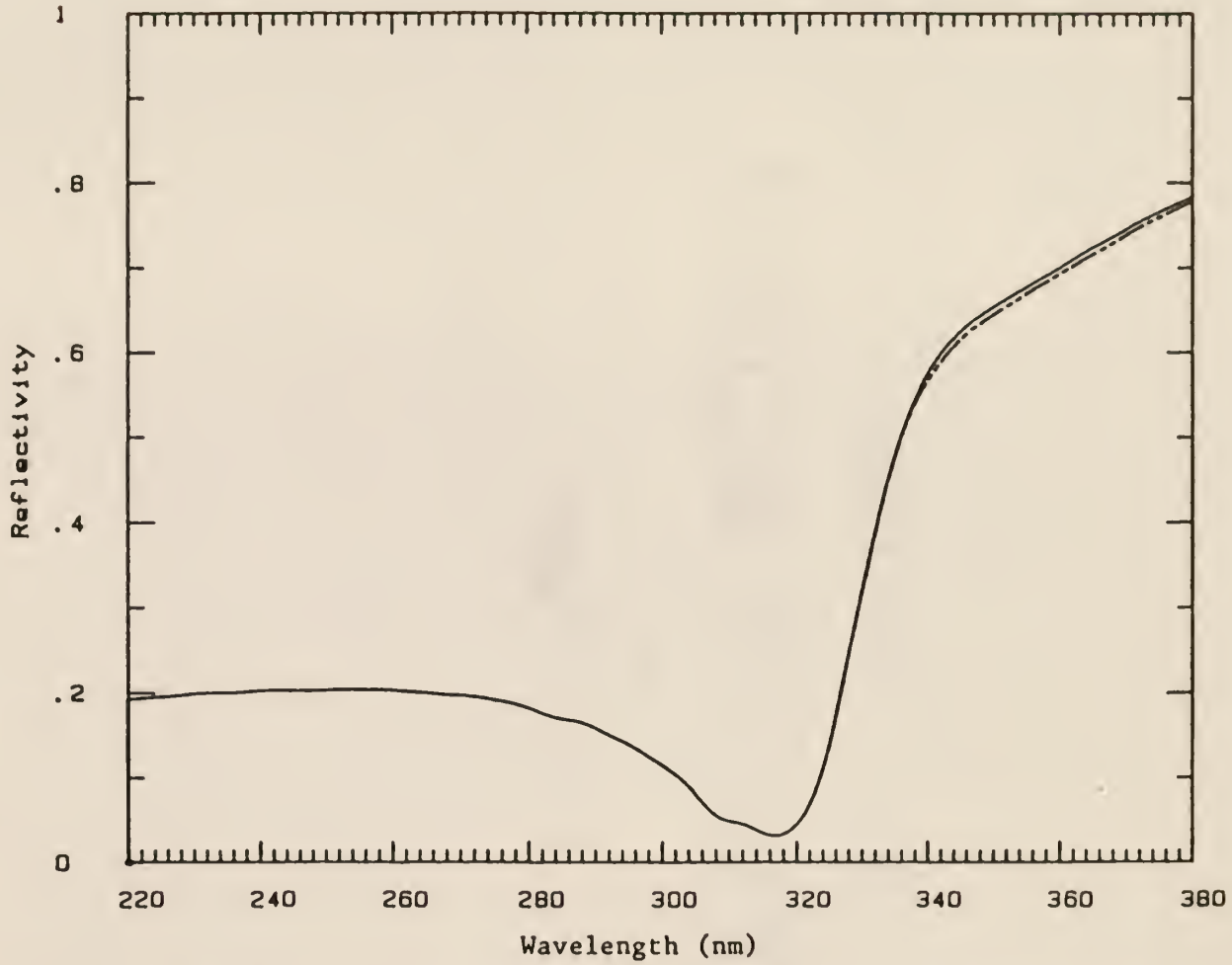

Fig. 5.31 Pre- and post-irradiation reflectivity profiles for metal-coated mirror #2L.

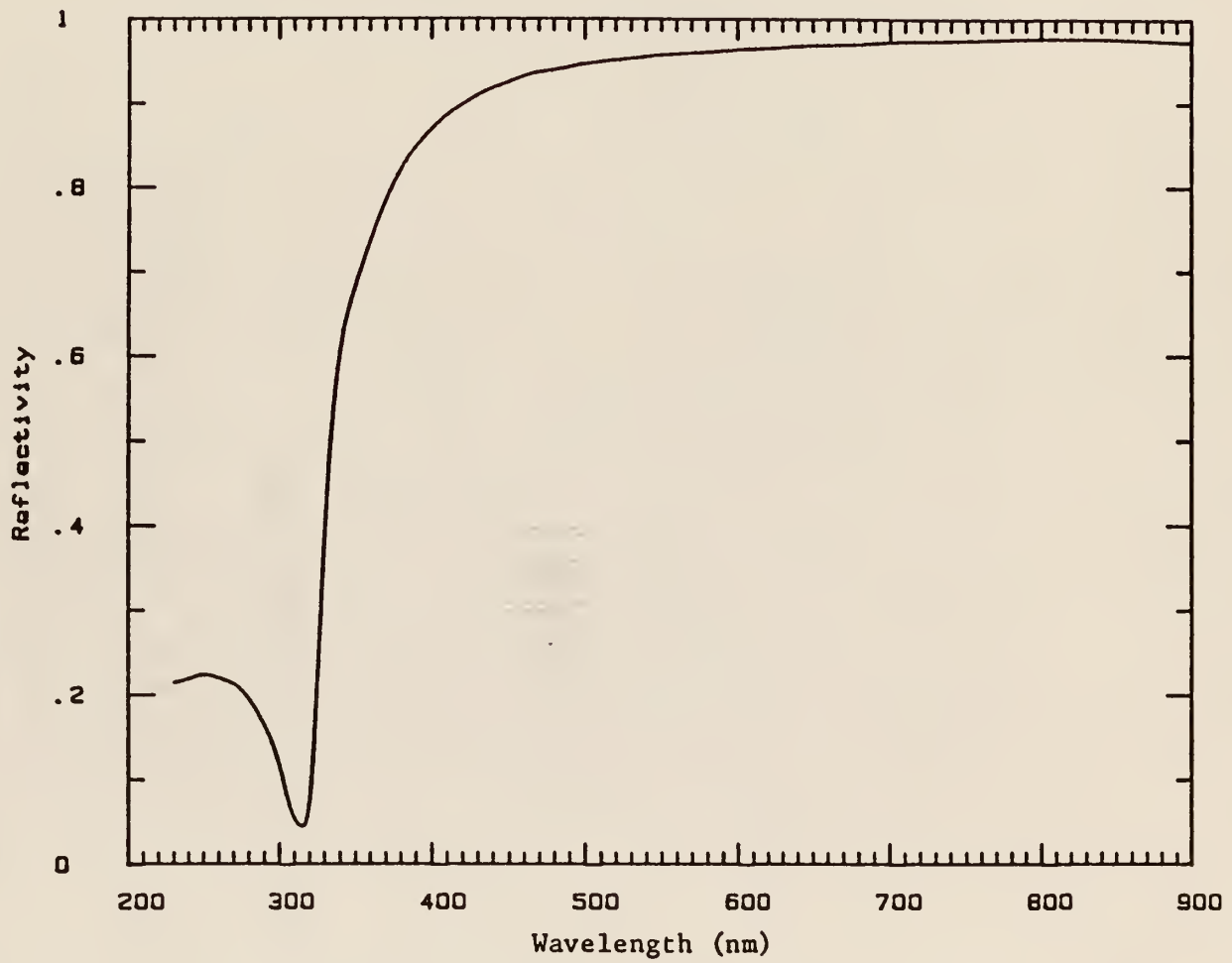

Fig. 5.32 Pre- and post-irradiation reflectivity profiles for metal-coated mirror #3L.

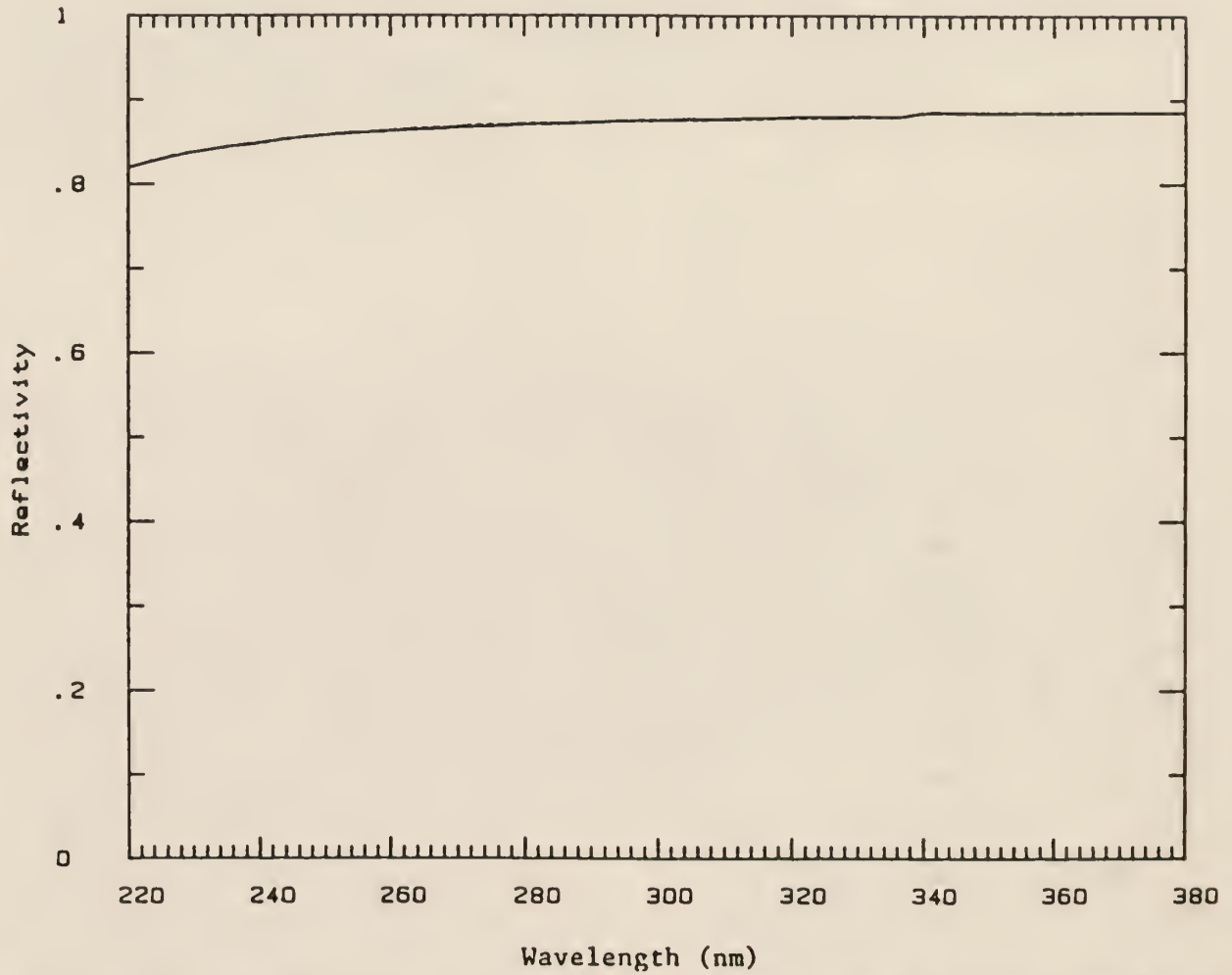

Fig. 5.33 Pre- and post-irradiation reflectivity profiles for metal-coated mirror #6L.

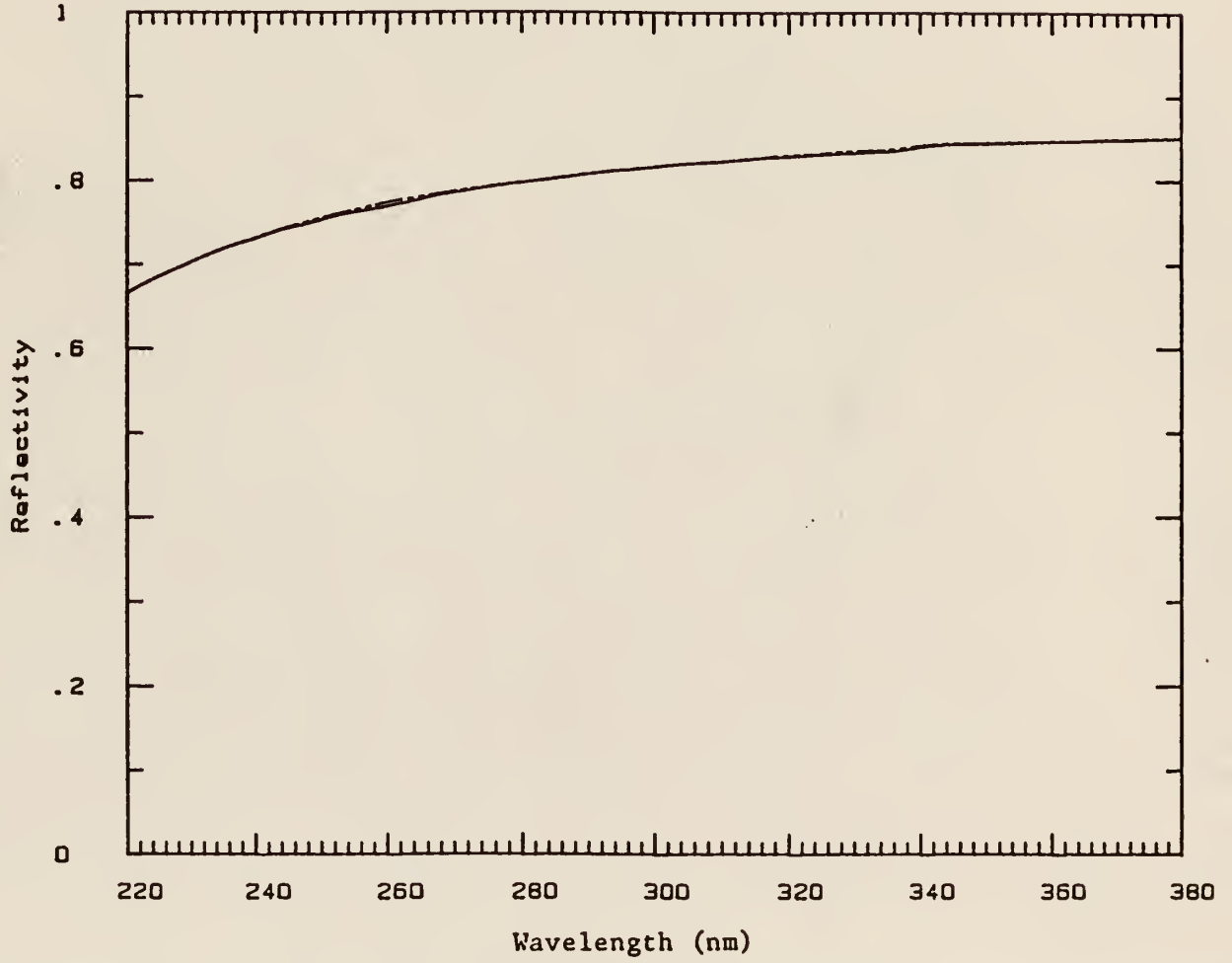

Fig. 5.34 Pre- and post-irradiation reflectivity profiles for metal-coated mirror #7L.

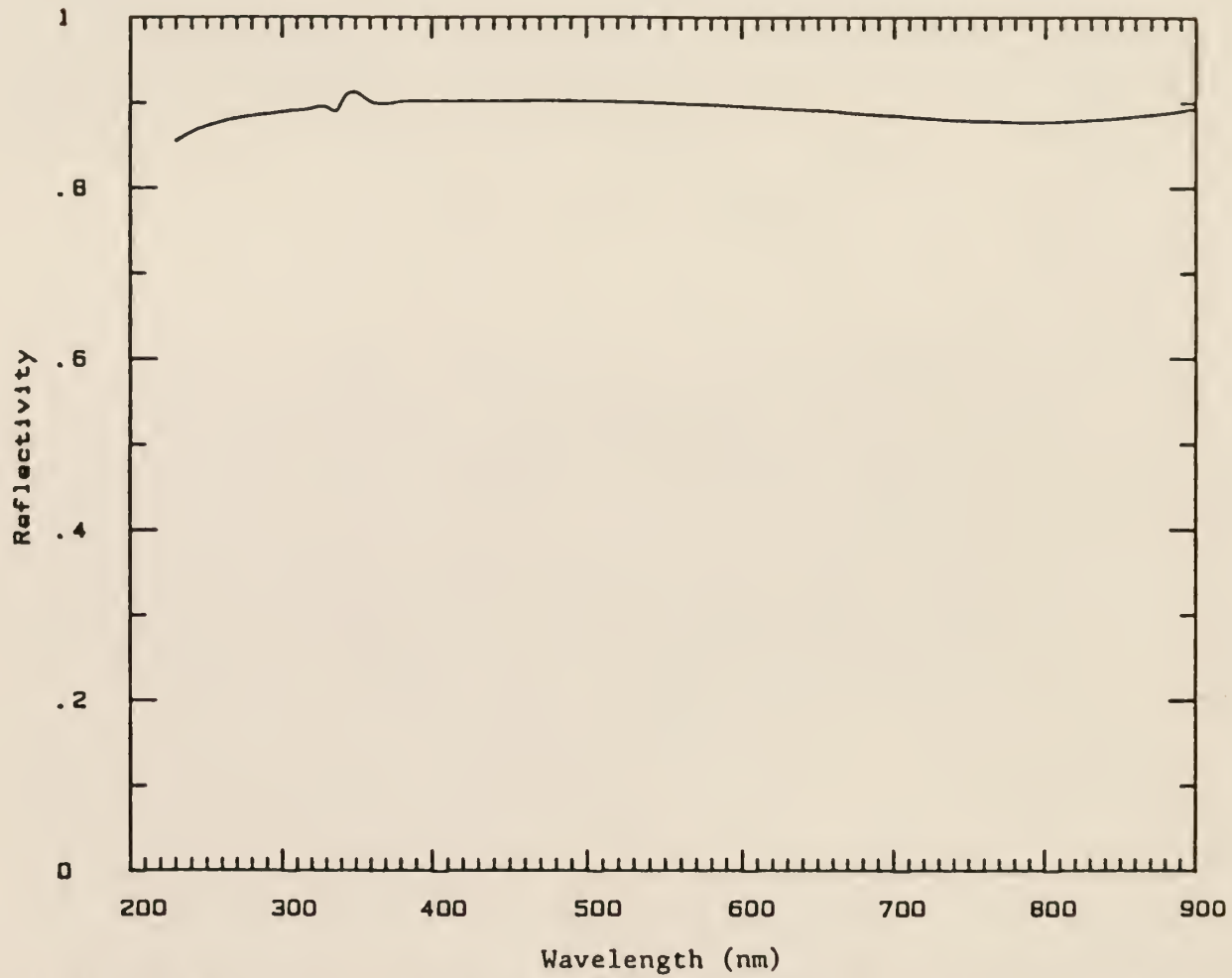

Fig. 5.35 Pre- and post-irradiation reflectivity profiles for metal-coated mirror #8L.

6. DISCUSSION AND CONCLUSIONS

6.1 Discussion of Previous Work:

As was mentioned before, this study showed no damage to the mirrors investigated from the irradiation done in this experiment. While there is not work previously done with the specific mirrors studied here, there are some studies from the same field of study which may provide some insight on what might have been expected if damage had been shown.

The expected damage mechanism for the dielectric materials is the production of absorption centers (F-centers, etc.). The process by which the thermoluminescent dosimeters correlate radiation exposure to their TL release is basically the same mechanism. In work done by Smarsh[12] it was found that the response of CaF_2:Mn TLD's could be fitted to variance of dose and dose rate using the following mathematical model:

$$R = R_{00} + R_{10}\, D + R_{01}\, \theta + R_{11}\, D\theta \ ,$$

where $D \equiv$ Dose,

$\theta \equiv$ Dose Rate, and

$R \equiv$ Response.

The study by Smarsh showed response to be a function of both dose and dose rate. The radiation source in that experiment was 15 MeV electrons from the Argonne National Laboratory LINAC. Similar results were obtained by Kaiseruddin[13] with LiF:Mg,Ti TLD's by

15 MeV electrons from the Argonne National Laboratory LINAC, showing the response to be also a function of both dose and dose rate.

Brannon, Morris, and Gerardo[14] at Sandia National Laboratories observed detectable absorption in 7940 Fused Silica at greater than about 20 krad total ionizing dose. The absorption coefficient was fitted as 3.3 cm^{-1}/Mrad at 257 nm. The same study also showed a dependence of the induced absorption coefficient with dose rate. This study used reactor radiation (primarily neutron and gamma), but there is evidence that the response for these kinds of materials is primarily dependent on the total ionizing dose resulting from all radiation. See Compton and Arnold's[15] results for 7940 fused silica at 215 nm for more information.

The author was unable to obtain information on work specific to Aluminum Oxide and unable to obtain work known to exist on damage to Silicon Oxide. It is reasonable to assume that the behavior of these materials would be similar to that of fused silica upon irradiation.

6.2 Conclusions:

There is one major conclusion that may be made about this work. That is the fact that exposure to doses of up to 140 krad at dose rates up to 3.5 krad/ns of 16.5 MeV electron causes no noticeable permanent change in the optical properties of the mirrors studied in this experiment. No damage threshold was able to be determined from

this study. The thinness of the reflecting stack is probably a major factor.

As a by-product of the radiation damage study the dielectric mirror properties were shown to conform well to theoretical predictions of those optical properties based on design criteria. The as-built metal mirror optical properties also conformed to expected behavior.

7. SUGGESTIONS FOR FUTURE WORK

Based on the results of this study, and on some of the difficulties found while carrying out this study, there are some suggestions to be made to improve work involving these specific mirrors and other work of this type.

1. To find the damage threshold of Al_2O_3+SiO_2 dielectric mirrors there is a need to increase the dose actually absorbed by the mirrors. This would require a new irradiation facility, because multiple LINAC pulses would allow for between-pulse relaxation effects, thus incorrect conclusions.
2. Studies with different types of radiation might provide greater insight as to the radiation dose resilancy of the mirrors.
3. Work with other types of mirrors for use at similar wavelength bands in laser systems should be done to allow for a broader base of information in this subject area. A central compilation of information by the parties responsible for government sponsored work in this area could produce a more efficient use of manpower on future studies of this type.
4. The author would also suggest that, since there is certain long running exposure to be expected in space-based applications, work should be done at lower dose rates for extended exposures to radiation.

This type of work will continue to be vital in the future in a number of applciations and should continue to be done to facilitate the growth of scientific knowledge in the radaition damage field.

8. ACKNOWLEDGEMENTS

The author would like to give his thanks to the Air Force Systems Command, the Air Force Office of Scientific Research, and to Universal Energy Systems, Inc., for giving him the opportunity to spend an enriching summer at the Frank J. Seiler Research Laboratory, USAF Academy, Colorado Springs, Colorado. He would like to acknowledge the Laboratory, the Lasers and Aerospace Mechanics Directorate, and particularly Lt. Colonel Albert J. Alexander and Major Terrence F. Deaton, and Ms. Leah Kelly for the assistance they provided.

In addition, he would like to thank the staff at EG&G in Goleta, California, who gave us such great help while we were using their LINAC facility: Dr. Paul A. Zagarino, Dr. Stephen S. Lutz, Dr. Steven G. Iverson, Mr. Steven A. Jones, Mr. Ron Sturges, and Mr. Paul E. Nash. Furthermore, the author wishes to express sincere appreciation to the following staff members of the Air Force Weapons Laboratory at Kirtland Air Force Base, New Mexico for their tremendous help: Captain Patricia Morse, Dr. William Kunzler, Dr. Wayne Wasson.

The author would also like to acknowledge the many hours on the computer that Mr. Roger Goerke donated. Thanks also go to Ms. Merna Brisbin for her help and to Ms. Connie Schmidt for typing this work.

Finally, he would like to thank Dr. Hermann Donnert for his help in getting started in this area of research and his continuing guidance. Thanks also go to Mr. Kevin Stroh and Mr. Mark Ferrel who provided the author with different points of view when they were needed.

9. LITERATURE CITED

1. Hermann. J. Donnert, "The Effects of Nuclear Radiation on the Optical Characteristics of (SiO_2+ZrO_2 on Si Substrate) Mirrors," Final Report, 1984, USAF-SCEEE.

2. Mark A. Ferrel, "The Effects of Nuclear Radiation on the Optical Characteristics of (SiO_2+ZrO_2 on Si Substrate) Mirrors," Final Report, 1984 USAF-SCEEE Graduate Student Seminar Support Program, 1984.

3. M. Born and E. Wolf, "Principles of Optics," 2nd edition, Pergammon Press, 1984.

4. Milton Abramowitz and Irene A. Stegun, "Handbook of Mathematical Functions," Dever Publications, Inc., 1964.

5. "American Institute of Physics Handbook," 3rd Edition, American Institute of Phycis, McGraw-Hill, Inc., 1972.

6. John McDonald, "Monographs on Applied Optics: No. 4 Metal-Dielectric Multilayers," Adam Hilger Ltd., 1971.

7. Eugene Hecht and Alfred Zajac, "OPTICS", Addison-Wesley Publishing Company, Inc. 1974.

8. Dr. Hugo Anders, "Thin Films in Optics," translated by J. N. Davidson, Focal Press Limited, English Edition, 1967.

9. Robert W. Hombeck, "Numerical Methods," Quantum Publishers, Inc., 1975.

10. L. V. Azaroff and J. J. Brophy, "Electronic Processes in Materials," McGraw-Hill, 1963.

11. C. Kittel, "Introduction to Solid State Physics," 5th Ed., John Wiley and Sons, Inc. 1976.

12. J. Smarsh, "Effects of Very High Dose Rates on the Response of Calcium Fluoride Thermoluminescent Dosimeters." M.S. Thesis, Kansas State University, 1971, pg. 58-59.

13. Kaiseruddin, M., "Effects of Very High Dose Rates on the Response of LiF Thermoluminescent Dosimeters," M.S. Thesis, Kansas State University, 1968.

14. P.J. Brannon, R. W. Morris, and J.B. Gerardo, "Nuclear-Radiation-Induced Absorption in Optical Materials," SPIE, Vol. 540, Southwest Conference on Optics, 1985.

15. W.D. Compton, and G.W. Arnold, Discuss. Faraday Soc., Vol. 31, 130, 1961.

APPENDIX A

A.1. Definition of Program Variables

T1 = θ_1, the incident angle

T2 = θ_2, the calculated angle of travel through low refractive index media

T3 = θ_3, the calculated angle for travel through high refractive index layers

TL = θ_ℓ, the calculated angle of travel through the substrate

N1 = refractive index of air

N2 = refractive index of low-index media (SiO_2)

N3 = refractive index of high-index media (Al_2O_3)

NL = refractive index of substrate (Fused-Silica)

H2 = thickness of low-index layers

H3 = thickness of high-index layers

R = reflectivity

T = transmissivity

T(I,J) = characteristic matrix for the complete mirror

LO = current wavelength in calculations

U(I) = value of i^{th} Chebychev Polynomial of the second kind

U1 = value of 23^{rd} Chebyshev Polynomial

U2 = value of 22^{nd} Chebyshev Polynomial

A.2 Use of Program

The program presented here was written in BASIC language for the Commodore 64 computer. See Table A.2 for listing. Use of the program is simple enough that it should be easy to convert it to another version of BASIC or to FORTRAN with little or no difficulty. Points of interest in the conversion of this program include:

a) The output section of the program in lines 2055-2065. Conversion to BASIC should require little change other than syntax and printer communication statements. Conversion to FORTRAN will require the addition of FORMAT statements and will require total rewriting of this section.

b) Comment statement may either be eliminated or left in the program. The user should check for syntax used to declare comment statements on his particular machine.

c) General command syntax should be confirmed. For instance, INPUT, DIM, GOSUB, and FOR...NEXT loops should be compared to see if changes are needed. In addition, the symbol π computes as the value of pi on the C64 and will likely need to have the numerical representation substituted into any expressions requiring this value.

Another helpful change for some uses involves calculations of R & T for intermediate mirror structures. Since the periodic characteristic matrix is computed then built upon to complete the structure, T(I,J) may be changed to any of the intermediate matrices in lines 2010 and 2011 to get Reflectivity and Transmission for these structures.

A.3 User Inputs

Due to the inability of the C64 to calculate inverse-sine functions the angles of transmission must be recalculated and

entered into the program, along with incident angle, in lines 710-740. These angles must be expressed in radians. Expressions for other angles in terms of incident angle may be found in Eq. (2.53) in Section 2.2

Line 1010 contains the values for the thickness (quarter-wave designed) of the high-index and low-index layers of dielectric material. The thicknesses are in units of nanometers. The thickness of the half-wave layer may either be entered here or just computed from the quarter-wave layer thickness as it is set up to do.

Lines 995-1000 contain the user derived expressions for index of refraction as a function of wavelength for the different materials. LO in this expression has units of nano-meters and the constants in these expressions should reflect this fact so that the index of refraction is unitless.

Lines 950 and 955 will prompt the user to enter the high and low wavelengths to be calculated over. These wavelengths are in nanometers.

A.4. Running A Profile Scan

Once the program is entered into the C64 from the keyboard, or from mass storage, the user types RUN and presses RETURN. This will clear the screen and prompt the user to enter first the starting wavelength and then the ending wavelength. Upon entry of the ending wavelength, the program will execute and compute the value of R & T

at each wavelength in the chosen range, printing to both the screen and printer. When the output is completed a prompt for starting wavelength will reappear. Entering a zero at this point will exit the program, or the user may enter a range for a new scan and continue. The program may also be exited during execution by depressing the RUN/STOP key. A sample program output is shown as Table A.1.

TABLE A. 1. A PROGRAM OUTPUT FOR THE COMPLETE MIRROR.

LAMDA	REFLECTIVITY	TRANSMISSION
230	.0836688689	.916331134
231	.0111048648	.988895134
232	.0211406936	.978859311
233	.142614429	.857385566
234	.276202264	.723797746
235	.336463141	.663536857
236	.283797101	.716202905
237	.0925868468	.907413153
238	.0592463468	.94075365
239	.543873981	.456126034
240	.827357848	.172642187
241	.92466469	.0753353011
242	.961151758	.0388482568
243	.977041528	.0229585112
244	.984856453	.0151435677
245	.98905563	.0109443714
246	.991443199	8.55685517E-03
247	.992825696	7.17430325E-03
248	.993588752	6.41127375E-03
249	.993918409	6.08162837E-03
250	.993892233	6.1078165E-03
251	.993513873	6.48615661E-03
252	.992717292	7.28273896E-03
253	.991343993	8.65601044E-03
254	.989081182	.0109188257
255	.985319699	.014680331
256	.978824275	.0211757568
257	.966914677	.0330853606
258	.943251889	.056748153
259	.891348592	.108651416
260	.765653491	.234346491
261	.465301401	.534698608
262	.0597930908	.940206894
263	.0527239413	.947276065
264	.227874979	.772125022
265	.323526482	.676473524
266	.334226832	.665773171
267	.281224461	.718775548
268	.183960199	.816039811
269	.0762733714	.923726638

TABLE A. 1. CONT'D.

LAMDA	REFLECTIVITY	TRANSMISSION
270	8.22321731E-03	.991776785
271	8.5725014E-03	.991427497
272	.0564421926	.943557806
273	.111409463	.888590536
274	.147385552	.85261445
275	.155660998	.844339
276	.137403661	.862596343
277	.0996225433	.900377463
278	.0544031701	.945596834
279	.0171160166	.982883986
280	5.43974363E-04	.999456031
281	7.84432089E-03	.992155683
282	.0314907958	.968509204
283	.0592550563	.940744943
284	.080741763	.919258239
285	.0900990419	.909900957
286	.0858301891	.914169811
287	.069895207	.930104795
288	.0469813573	.953018642
289	.0236217639	.97637824
290	6.54920107E-03	.993450799

TABLE A. 2. LISTING OF THE PROGRAM 'PROFILE'.

```
10 PRINT""
100 REM#########################################################################
101 REM# PROFILE!: A PROGRAM TO CALCULATE THE REFLECTIVITY AND TRANSMISSION #
102 REM# PROFILES FOR A PERIODIC MULTILAYERED DIELECTRIC MIRROR. WRITTEN IN #
103 REM# BASIC ON THE COMMODORE-64 BY GARY SCRONCE, BSNE 1984, KSU.          #
104 REM#########################################################################
105 REM
700 REM??????????????????????????????????????????????????????????????????????
701 REM?? IN LINES 710,720,730 ENTER THE PROPER ANGLES. T1= INCIDENT ANGLE  ??
702 REM?? AND THE OTHERS ARE RELATED TO IT BY SNELL'S LAW. ANGLES IN RADIANS??
703 REM??????????????????????????????????????????????????????????????????????
710 T1=.17453293:PRINT"T1=";(180*T1/π);" DEGREES"
720 T2=.11921932:PRINT"T2=";(180*T2/π);" DEGREES"
730 T3=.10479906:PRINT"T3=";(180*T3/π);" DEGREES"
740 TL=.11731028:PRINT"TL=";(180*T3/π);" DEGREES"
900 DIM T(2,2),M(2,2),L(2,2),H(2,2),U(24)
940 PRINT" "
950 INPUT"ENTER FIRST WAVELENGTH DESIRED (NM)";LS
951 L0=LS
952 IF L0=0 THEN GOTO 3000
955 INPUT"ENTER LAST WAVELENGTH DESIRED (NM)";LF
960 REM
995 N3=1.8147-(L0*.0005675):REM>>> VARIABLE INDEX FOR AL2O3 <<<
996 NL=1.6344335-.0005039218*L0:REM>>> VARIABLE INDEX FOR FUSED SILICA <<<
997 N2=1.6094335-.0005039218*L0:REM>>> VARIABLE INDEX FOR SIO2 <<<
1000 N1=1:REM>>> REFRACTIVE INDEX OF AIR <<<
1001 PRINT NL;N3;N2
1005 P1=N1*COS(T1):P2=N2*COS(T2):P3=N3*COS(T3):PL=P2
1010 H2=42.4657534:H3=37.3493976:HL=2*H2
1100 B2=2*π*N2*H2*COS(T2)/L0
1110 B3=2*π*N3*H3*COS(T3)/L0
1120 C2=COS(B2):C3=COS(B3)
1130 S2=SIN(B2):S3=SIN(B3)
1200 M(1,1)=C2*C3-P3*S2*S3/P2
1210 M(1,2)=-(C2*S3/P3+S2*C3/P2)
1220 M(2,1)=-(P2*S2*C3+P3*C2*S3)
1230 M(2,2)=C2*C3-P2*S2*S3/P3
1300 A=(M(1,1)+M(2,2))/2
1350 GOSUB 5000
1400 REM
1401 REM*** CALCULATE CHARACTERISTIC MATRIX FOR PERIODIC (HL)↑24 LAYERS ***
1402 REM
1410 M(1,1)=M(1,1)*U1-U2
1420 M(1,2)=M(1,2)*U1
1430 M(2,1)=M(2,1)*U1
1440 M(2,2)=M(2,2)*U1-U2


READY.
```

TABLE A. 2. LISTING OF THE PROGRAM 'PROFILE' CONTINUED. .

```
1500 REM
1501 REM*** CALCULATE CHARACTERISTIC MATRIX FOR 1/2 WAVE L-LAYER ***
1502 REM
1510 L(1,1)=C2*C2-S2*S2
1520 L(1,2)=-2*S2*C2/P2
1530 L(2,1)=-2*P2*S2*C2
1540 L(2,2)=C2*C2-S2*S2
1600 REM
1601 REM*** CALCULATE CHARACTERISTIC MATRIX FOR 1/4 WAVE H-LAYER ***
1602 REM
1610 H(1,1)=C3
1620 H(1,2)=-S3/P3
1630 H(2,1)=-P3*S3
1640 H(2,2)=C3
1700 REM
1701 REM*** CALCULATE MATRIX ELEMENTS FOR THE PERIODIC PLUS HIGH LAYER ***
1702 REM
1710 Z(1,1)=H(1,1)*M(1,1)-H(1,2)*M(2,1)
1720 Z(1,2)=M(1,2)*H(1,1)+H(1,2)*M(2,2)
1730 Z(2,1)=H(2,1)*M(1,1)+H(2,2)*M(2,1)
1740 Z(2,2)=M(2,2)*H(2,2)-H(2,1)*M(1,2)
1790 REM
1791 REM*** CALCULATE MATRIX ELEMENTS FOR THE COMPLETE MIRROR ***
1792 REM
1800 T(1,1)=L(1,1)*Z(1,1)-L(1,2)*Z(2,1)
1810 T(1,2)=L(1,1)*Z(1,2)+L(1,2)*Z(2,2)
1820 T(2,1)=L(2,1)*Z(1,1)+L(2,2)*Z(2,1)
1830 T(2,2)=L(2,2)*Z(2,2)-L(2,1)*Z(1,2)
2000 REM
2001 REM*************************************************************************
2002 REM*** CALCULATE THE REFLECTIVITY AND TRANSMISSION FOR WAVELENGTH L0  ***
2003 REM*************************************************************************
2004 REM
2010 RT=(P1*T(1,1)-PL*T(2,2))↑2+(T(1,2)*PL*P1-T(2,1))↑2
2011 RB=(P1*T(1,1)+PL*T(2,2))↑2+(T(1,2)*PL*P1+T(2,1))↑2
2020 R=RT/RB
2050 T=4*P1*PL/RB
2055 OPEN 4,4
2058 IF L0<>LS GOTO 2063
2059 REM************** MAIN OUTPUT ROUTINE TO PRINTER AND SCREEN **************
2060 PRINT#4,SPC(17);"LAMDA";SPC(8);"REFLECTIVITY";SPC(8);"TRANSMISSION"
2061 PRINT#4,SPC(15);"-------------------------------------------------"
2062 PRINT#4," "
2063 PRINT#4,SPC(17);L0;SPC(7);R;SPC(8);T
2064 PRINT"   ";L0;"   ";R;"   ";T
2065 CLOSE 4,4
2900 IF L0=LF THEN GOTO 2950
2905 L0=L0+1
2910 GOTO 960
2950 GOSUB 6000
2960 GOTO 940
3000 END

READY.
```

TABLE A. 2. LISTING OF THE PROGRAM 'PROFILE' CONTINUED..

```
5000 REM
5001 REM*************************************************************
5002 REM*** SUBROUTINE TO CALCULATE THE VALUE OF THE CHEBYCHEV POLYNOMIALS ***
5003 REM*** OF THE SECOND KIND FOR USE IN THE PERIODIC MATRIX ELEMENTS...  ***
5004 REM*************************************************************
5005 REM
5010 U(0)=1
5020 U(1)=2*A
5030 FOR I=2TO24
5040 U(I)=2*A*U(I-1)-U(I-2)
5050 NEXT I
5060 U1=U(23)
5070 U2=U(22)
5080 RETURN
5090 END
5091 REM
5999 REM********** FINISHING ROUTINE FOR OUTPUT TO PRINTER **********
6000 OPEN 4,4
6005 PRINT#4," "
6010 PRINT#4,SPC(15);"-------------------------------------------"
6020 CLOSE 4,4
6030 RETURN

READY.
```

EFFECTS OF NUCLEAR RADIATION ON THE OPTICAL PROPERTIES OF Al_2O_3+SiO_2 MIRRORS IN THE ULTRAVIOLET REGION

by

GARY WAYNE SCRONCE

B.S., Kansas State University, 1984

AN ABSTRACT OF A MASTER'S THESIS

submitted in partial fulfillment of the

requirements for the degree

MASTER OF SCIENCE

Department of Nuclear Engineering

KANSAS STATE UNIVERSITY
Manhattan, Kansas

1987

ABSTRACT

Three types of mirrors were examined in this study: Al_2O_3+SiO_2 multilayer dielectric mirrors, Al metal mirrors, and Cu+Ag metal mirrors. The dielectric mirrors were of primary importance as the metal mirrors reflect poorly in the UV-region. They were designed for use in KrF eximer lasers and to have a peak reflectivity band about 248 nm.

A theoretical model was developed and program written to predict the optial properties of the dielectric mirrors at varying wavelengths. The completed theoretical model compares well to the measured reflectivity and transmission profiles. A similar, less in depth comparison was made for both types of metal mirrors with similar results.

In the irradiation of the mirrors, 16.5 MeV electrons were used to simulate the effect of gamma rays. The irradiation was done at the LINAC facility owned by EG&G, Santa Barbara. Doses delivered ranged from 22.5 krad to 140 krad, at dose rates from 0.1125 krad/ns to 3.5 krad/ns. Post-irradiation measurements of the optical properties of all mirrors showed no definitive indication of damage.

A means of delivering greater doses will need to be used to find the optical damage threshold of the mirrors.